STUDY ON WIRELESS ENERGY HARVESTING IN COOPERATIVE COMMUNICATIONS WITH RELAY SELECTION AND PHYSICAL LAYER SECURITY

DISSERTATION

for the Degree of

DOCTOR OF PHILOSOPHY
(Electrical Engineering)

VAN PHU TUAN

MAY 2018

Study on wireless energy harvesting in cooperative communications with relay selection and physical layer security

DISSERTATION

for the Degree of

Doctor of Philosophy
(Electrical Engineering)

VAN PHU TUAN

May 2018

Study on wireless energy harvesting in cooperative communications with relay selection and physical layer security

DISSERTATION

Submitted in Partial Fulfillment
of the Requirements for the
Degree of

DOCTOR OF PHILOSOPHY
(Electrical Engineering)

at the

UNIVERSITY OF ULSAN

by

Van Phu Tuan
May 2018

Publication No._____

Study on wireless energy harvesting in cooperative communications with relay selection and physical layer security

Approved by Supervisory Committee:

Prof. Sungoh Kwon, *chair*

Prof. Sunghwan Kim

Prof. Sangjo Choi

Prof. Hyung Suk Chu

Prof. Hyung Yun Kong, *adviser*

May, 2018

VITA

Van Phu Tuan was born in Quang Nam Province, Vietnam on July 20, 1987. He received the B.E. degree (2010) and M.E. degree (2013) in Electrical Engineering from Ho Chi Minh City University of Technology (HCMUT), Vietnam.

In March 2015, he began working full time towards his Ph.D. at University of Ulsan, Korea under the guidance of Professor Hyung Yun Kong. Since then, he has conducted researches in cooperative communications, MIMO communications systems, physical layer security and energy harvesting.

Dedicated to my grateful family

for their love and support

ACKNOWLEDGMENTS

I would like to express my sincere gratitude to my dissertation advisor, Professor Hyung Yun Kong, for giving me the opportunity to be a part of his research group and for his guidance which helped me complete this work. I am greatly indebted to him for his full support, constant encouragement and advice both in technical and non-technical matters.

I would also like to thank the other members of my Ph.D. supervisory committee for many useful interactions and for contributing their broad perspective in redefining the ideas in this dissertation.

I am grateful to my friends, my group mates of wireless communication laboratory (WCOMM), University of Ulsan (UOU), for their friendship, enthusiastic help and cheerfulness during my stay in Korea.

The financial support of the BK21+ programs is also gratefully acknowledged.

Last, but certainly not the least, I would like to thank my family for their spirit support and encouragement during the course of my studies. Especially, my parents have always believed in me and have supported every endeavor of mine.

ABSTRACT

Study on wireless energy harvesting in cooperative communications with relay selection and physical layer security

by

Van Phu Tuan

Advisor: Prof. Hyung Yun Kong

Submitted in Partial Fulfillment of the Requirements for the Degree of Doctor of Philosophy (Electrical Engineering)

May 2018

Recently, Wireless Energy Harvesting (WEH), in which wireless nodes power their batteries by scavenging energy from ambient Radio Frequency (RF) signals, has become an promising solution to address the challenge of prolonging the lifetime of energy-constrained wireless networks and reducing the periodic recharging and replacement of batteries. Due to the great advantages mentioned above, the WEH technique finds important applications in both point-to-point communication and Cooperative Communication (CC), where energy-constrained relays harvest energy from wireless signals sent by the Access Points (APs) to assist the communication between the APs and their destinations. More recently, security in WEH has become an emerged research topic which has attracted a lot interest from researchers.

Because of the fact that the WEH nodes usually locate near the AP for harvesting much energy, they are capable of overhearing the confidential information from the AP. To overcome this problem, the Physical Layer Security (PLS) technique, which is capable of providing secure communication without using cipher codes, has become an effective solution. Motivated by above, in this thesis we focus on investigating two aspects of WEH in the cooperative relaying systems: relay selection and PLS. Moreover, we extend our studies by considering the effects of hardware impairment and imperfect channel on the (secrecy) performance of the WEH CC systems. The (secrecy) performance of all proposed systems is evaluated via mathematical analyses. The accuracy of the analytical results is verified by Monte Carlo simulations.

We first study the problem of K-th best relay selection in WEH system by analyzing a communication between a multiple-antennas source-destination pair via a K-th best relay of a single-antenna WEH relay network. Moreover, we propose deploying an energy beamforming technique known as Maximal Ratio Transmission (MRT) at the source and a combining technique known as Maximum Ratio Combining (MRC) at the destination for these such systems to improve the system performance.

Then, we extend our first study to the scenario of WEH CC system with non-ideal hardware. We assume that the RF impairments caused by the RF font-end hardware imperfections are not completely removed by using signal processing algorithms; hence, the Residual Transmit RF Impairment (RTRI) notably degrades the system performance. From the results in terms of the Outage Probability (OP) and capacity, we show that the influence of RTRI on the system performance can be effectively mitigated by using more antennas and/or more relays.

Next, we focus on investigating PLS in WEH CC systems. Different with most studies on PLS in CC, where external eavesdroppers create security risk, our studies deal with the problem of PLS in WEH CC using untrusted relays. In this investigation, we focus on studying the effects of imperfect channels and transmit-antenna techniques, i.e., MRT, Transmit Antenna Selection (TAS) and Random Antenna Selection (RAS), on the secure communication of the proposed system.

After that, we study the secure communication of a CC system via an untrusted WEH relay in the presence of an external eavesdropper. The secure communication can be overhear by both the untrusted relay and the external eavesdropper. In this problem, we focus on investigating the effects of the locations and the transmit powers on the secrecy performance. The obtained results show that in the presence of the external eavesdropper, a reasonable location of the untrusted relay can yield a higher secrecy performance.

Finally, we study the problem of joint relay–selection and PLS in an untrusted relaying WEH system. We propose employing multiple antennas and the MRT technique at the source and destination. Then, we use the MRT–based relay–selection methods to select the relay for assisting the communication. These proposals allow us to boost the harvested energy at the selected relay; moreover, under the assumption that lacking global knowledge of Channel State Information (CSI) at the relays, they also allow us to eliminate the security risks from the non–selected relays.

Contents

Supervisory Committee ii
Vita iii
Dedication iv
Acknowledgments v
Abstract vi
List of Figures xiv
Nomenclature xvi
List of Symbols xvii

1 Introduction **1**
1.1 Related Works 3
1.2 Dissertation Outline 5
1.3 Background 8
1.3.1 Wireless Channel Model 8
1.3.2 Cooperative Communication Protocol 10
1.3.3 Relay Selection Methods 11
1.3.4 Residual RF Impairment Issue 13
1.3.5 Imperfect Channel Issue 14
1.3.6 Physical Layer Security 15
1.3.7 Energy Harvesting 16

2 Wireless Energy-Harvesting in K-th Best Relay Selection Systems with Energy Beamforming over Nakagami-m Fading Channels **19**
2.1 Introduction 19
2.2 System Model and Relaying Protocols 21
2.2.1 System Model 21
2.2.2 Time-Switching Relaying Protocol 23
2.2.3 Power-Splitting Relaying Protocol 24
2.3 Performance Analysis 25
2.3.1 Outage Probability 25
2.3.2 Throughput Analysis 26

Delay-Limited Transmission Mode 26
Delay-Tolerant Transmission Mode 28
2.4 Results and Discussion 31
2.5 Conclusions 37

3 Wireless energy harvesting in relay-selection systems with residual transmit RF impairments 39
3.1 Introduction 39
3.2 System Model and Preliminary Results 41
3.2.1 System Model 41
3.2.2 Partial relay selection scheme 42
3.2.3 Time-switching relaying protocol with RTRI 43
Energy harvesting and source-to-relay transmission 43
Relay-to-destination transmission and end-to-end SNR 43
3.2.4 Power-splitting relaying protocol with RTRI 44
Energy harvesting and source-to-relay transmission 45
Relay-to-destination transmission and SNR at destination . . 45
3.3 Performance Analysis 46
3.3.1 Outage probability 46
3.3.2 Throughput analysis 47
Delay-limited transmission mode 47
Delay-tolerant transmission mode 48
3.4 Results and Discussion 49
3.5 Conclusions 56

4 Secure communication via a wireless energy-harvesting untrusted relay with imperfect CSI 59
4.1 Introduction 59
4.2 System Model 61
4.2.1 Communication in the first time slot 63
4.2.2 Communication in the second time slot 64
4.3 Performance Analysis 65
4.3.1 Secrecy outage probability 65
4.3.2 Average secrecy capacity 67
4.4 Results and Discussion 70
4.5 Conclusion 77

5 Secure communication via a wireless energy-harvesting untrusted relay in the presence of an eavesdropper 81
5.1 Introduction 81
5.2 System Model 82
5.2.1 Communication in the first time slot 83

5.2.2 Communication in the second time slot 84
5.3 Performance analysis 85
5.3.1 Secrecy outage probability 85
5.3.2 High-power secrecy outage probability approximation 86
5.3.3 Average secrecy capacity 87
5.4 Simulation results 89
5.5 Conclusions 93

6 Secure communication in untrusted relay-selection network with wireless energy-harvesting 97
6.1 Introduction 97
6.2 System Model and Preliminary Results 98
6.2.1 System Model 98
6.2.2 Preliminary Results 99
6.3 Performance Analysis 102
6.3.1 Secrecy outage probability 102
6.3.2 High-power secrecy outage probability approximation 104
6.3.3 Average secrecy capacity 105
6.4 Simulation results 108
6.5 Conclusions 112

7 Summary of Contributions and Further Works 114
7.1 Introduction 114
7.2 Summary of Contributions 114
7.3 Future Research Directions 116

Publications 117

References 119

A Proofs in Chapter 2 134
A.1 Proof of Proposition 2.1 134
A.1.1 Outage probability for the KBFC scheme 135
A.1.2 Outage probability for the KBSC scheme 136
A.2 Proof of Proposition 2.2 136
A.2.1 Ergodic capacity for the KBFC scheme 136
Calculation for $\mathcal{C}_{\gamma_{r,[w]}}$ 136
Calculation for $\mathcal{C}_{\gamma_{d,[w]}}$ 137
Calculation for $\mathcal{C}^{\text{low}}_{\gamma_{t,[w]}}$ 138
A.2.2 Ergodic capacity for the KBSC scheme 138

B Proofs in Chapter 3 **140**
B.1 Proof of Proposition 3.1 . . . 140
B.1.1 Calculation of $\mathcal{P}_{out,low}^{w,1}$ . . . 140
B.1.2 Calculation of $\mathcal{P}_{out,low}^{w,2}$ . . . 141
B.2 Proof of Proposition 3.2 . . . 141

C Proofs in Chapter 4 **142**
C.1 Proof of Proposition 4.1 . . . 142
C.1.1 Calculation for $\mathrm{SOP}_{\mathrm{RAS}}$ . . . 143
C.1.2 Calculation for $\mathrm{SOP}_{\mathrm{TAS}}$ . . . 143
C.1.3 Calculation for $\mathrm{SOP}_{\mathrm{MRT}}$ . . . 143
C.2 Proof of Proposition 4.2 . . . 143
C.2.1 Calculation for case of perfect CSI ($\zeta = 1$) . . . 143
C.2.2 Calculation for case of perfect CSI ($0 < \zeta < 1$) . . . 144
Calculation for $\mathrm{SOP}_{\mathrm{RAS}}^{\infty}$ . . . 144
Calculation for $\mathrm{SOP}_{\mathrm{TAS}}^{\infty}$ . . . 145
Calculation for $\mathrm{SOP}_{\mathrm{MRT}}^{\infty}$ . . . 145
C.3 Proof of Proposition 4.3 . . . 145
C.3.1 Calculation for the RAS scheme . . . 145
C.3.2 Calculation for the TAS scheme . . . 146
C.3.3 Calculation for the MRT scheme . . . 146
C.4 Proof of Proposition 4.4 . . . 147
C.4.1 Calculation for the RAS scheme . . . 147
C.4.2 Calculation for the TAS scheme . . . 147
C.4.3 Calculation for the MRT scheme . . . 148

D Proofs in Chapter 5 **149**
D.1 Proof of Proposition 5.1 . . . 149
D.2 Proof of Proposition 5.2 . . . 150
D.2.1 High–power approximation for $P_{\mathrm{sec},1}$ . . . 151
D.2.2 High–power approximation for $P_{\mathrm{sec},2}$ . . . 151
D.3 Proof of Proposition 5.3 . . . 153

E Proofs in Chapter 6 **154**
E.1 Proof of Proposition 6.1 . . . 154
E.1.1 Calculation for $P_{\mathrm{out,low}}^{\mathrm{KBFC}}$ . . . 154
E.1.2 Calculation for $P_{\mathrm{out,low}}^{\mathrm{KBSC}}$ . . . 155
E.2 Proof of Proposition 6.2 . . . 155
E.2.1 Calculation for $P_{\mathrm{out,HPL}}^{\mathrm{KBFC}}$ . . . 156
E.2.2 Calculation for $P_{\mathrm{out,HPL}}^{\mathrm{KBSC}}$ . . . 156
E.3 Proof of Proposition 6.3 . . . 157
E.3.1 calculation for $F_{\gamma_r}^{\mathrm{KBFC}}(\gamma)$ . . . 157

E.3.2 Calculation for $\mathcal{C}_{\mathrm{erg,r}}^{\mathrm{KBFC}}$ 158
E.3.3 Calculation for $\mathcal{C}_{\mathrm{erg,d}}^{\mathrm{KBFC}}$ 158

List of Figures

1.1 Channel model of direct wireless transmission. 9
1.2 System model of cooperative communication. 11
1.3 Cooperative scheme in wireless communication. 12
1.4 Wireless communication system with residual hardware impairment. . 13
1.5 System model of direct transmission under physical layer security. . . 16
1.6 Block diagram of the power splitting receiver at a destination node D. 17
1.7 Block diagram of the time switching receiver at a destination node D. 18

2.1 Proposed system model. 22
2.2 The OP with respect to α_T for the TSR protocol and θ for the PSR protocol. Other parameters: $\rho = 10$ (dB), $\gamma = 3$ (dB), $L = 3$ and $K = 2$. 32
2.3 Outage probability with respect to the noise power. Other parameters: $\rho = 10$ (dB), $\gamma = 3$ (dB), $L = 3$ and $K = 2$. 33
2.4 The throughput with respect to the energy-harvesting ratio α_T (or θ) and R. Other parameters: $\rho = 10$ (dB), $L = 4$ and $K = 2$. 34
2.5 The optimal throughput with respect to the noise power. Other parameters: $\rho = 10$ (dB), $L = 4, K = 2$, and $R = 2$ (bits/s/Hz). 36
2.6 The optimal throughput with respect to ρ. Other parameters: $R = 2$ (bits/s/Hz) for the LODLT mode. 37

3.1 System model. 41
3.2 The outage probability versus κ_0^2 for the (a) TSR and (b) PSR protocols. Other parameters: $P_s/2\sigma_0^2 = 10(dB)$ and $\gamma = 5(dB)$. 51
3.3 The effects of α_T (TSR protocol) and θ (PSR protocol) on the throughput in the (a) Delay–Limited Transmission (DLT) and (b) Delay–Tolerant Transmission (DTT) modes. Other parameters: $R = 2(bits/s/Hz)$ and $P_s/2\sigma_0^2 = 10(dB)$. 52
3.4 The optimal throughput versus κ_0^2. Other parameters: $P_s/2\sigma_0^2 = 10(dB)$. 54
3.5 The optimal throughput versus K for the (a) DLT and (b) DTT modes. Other parameters: $P_s/2\sigma_0^2 = 10(dB)$, and $R = 1(bits/s/Hz)$. 55

3.6 The DLT throughput versus $R(bits/s/Hz)$ for the (a) TSR and (b) PSR protocols. Other parameters: $P_s/2\sigma_0^2 = 10(dB)$. 57

4.1 System model. 61
4.2 The effect of ρ on the SOP and its asymptote in the cases of a) $\zeta = 1$ and b) $\zeta = 0.9$. Other parameters: $d = 1$ and $\rho_s = \rho_d = \rho$. 71
4.3 The effect of θ on the SOP and ASC. Other parameters: $d = 1, \rho_s = \rho_d = 25(dB)$ and $R_s = 2(bits/sec/Hz)$. 73
4.4 The effect of ρ_s and ρ_d on the optimal SOP and optimal ASC. Other parameters: $d = 1$ and $R_{th} = 2(bits/sec/Hz)$. 75
4.5 The optimal SOP and optimal ASC in term of the trade-off between ρ_s and ρ_d ($\rho_s + \rho_d = \rho_\Sigma$). Other parameter: $d = 1$ and $\rho_\Sigma = 30(dB)$. . 76
4.6 The effect of ζ on the SOP and ASC. Other parameter: $d = 1, \rho_s = \rho_d = 25(dB)$ and $R_s = 2(bits/sec/Hz)$. 78
4.7 The effect of the relays location on the optimal SOP and optimal ASC. Other parameters: $\rho_s = \rho_d = 15(dB)$. 79

5.1 System model. 83
5.2 The effect of ρ on the SOP and its approximation. Other parameters: $d_r = d_e = 1$ and $\rho_s = \rho_d = \rho$. 90
5.3 The effect of θ on a) the SOP and b) the ASC. Other parameters: $d_r = d_e = 1$, $\rho_s = \rho_d = \rho$, and $R_{th} = 2$ bits/s/Hz. 92
5.4 The effect of ρ_s and ρ_d on a) the optimal SOP and b) the optimal ASC. Other parameters: $d_r = d_e = 1$ and $R_{th} = 2$ bits/s/Hz. 94
5.5 The effect of distances on a) the optimal SOP and b) the optimal ASC. 95

6.1 System model. 99
6.2 The secrecy outage probability versus ρ. Other parameters: $m_1 = m_2 = 1$. 109
6.3 The average secrecy capacity versus θ. Other parameters: $P_s = P_d = N_0\rho_0$. 110
6.4 The effect of the relay locations on the optimal ASC. Other parameters: $P_s = P_d = N_0\rho_0$. 111
6.5 The effect of the number of relays on the optimal ASC. Other parameters: $P_s = P_d = N_0\rho_0$ and $K = 1$. 112

Nomenclature

Notation	Description
AF	Amplify–and–Forward
AN	Artificial Noise
AP	Access Point
ASC	Average Secrecy Capacity
ASR	Achievable Secrecy Rate
AWGN	Additive White Gaussian Noise
CC	Cooperative Communication
CCI	Co–Channel Interference
CDF	Cumulative Distribution Function
CSI	Channel State Information
DF	Decode–and–Forward
DL	Downlink
DLT	Delay–Limited Transmission
DTT	Delay–Tolerant Transmission
ER	Energy Receiver
FD	Full Duplex
GSS	Golden Section Search
HD	Half Duplex
IR	Information Receiver
LoS	Line–of–Sight
MSE	Mean Square Error
MIMO	Multiple Input Multiple Output
MISO	Multiple Input Single Output
MRC	Maximum Ratio Combining
MRT	Maximal Ratio Transmission
NOMA	Non–Orthogonal Multiple Access
NNC	Nano–Network Communication
PDF	Probability Density Function
PLS	Physical Layer Security
PS	Power Splitting
QoS	Quality of Service
RF	Radio Frequency
RRI	Residual RF Impairment
RV	Random Variable
SINR	Signal to Interference plus Noise Ratio
SNR	Signal to Noise Ratio
TAS	Transmit Antenna Selection
TS	Time Switching
UL	Uplink
WEH	Wireless Energy Harvesting
WEH–CC	Wireless Energy Harvesting–based Cooperative Communication

List of Symbols

Symbol	Definition
$\mathbf{h}$	The bold lower letter $\mathbf{h}$ denotes the vector.
x	The lower case letter x denotes the scalar.
$\min(\cdot)$	The operator that returns the minimum element of an array.
$\max(\cdot)$	The operator that returns the maximum element of an array.
K–th $\arg\max(\cdot)$	The operator that returns the index of the K–th maximum element of an array.
$\lvert\cdot\rvert$	The absolute value (or modulus) of a real number.
$\lVert\cdot\rVert_1$	The ℓ_1 norm of a vector.
$\lVert\cdot\rVert_2$ (or $\lVert\cdot\rVert$)	The ℓ_2 norm of a vector.
$[\cdot]^\top$	The transpose operator.
$[\cdot]^\dagger$	The Hermitian transpose operator.
$[x]^+$	$\max(x, 0)$.
$\mathbb{E}\{\cdot\}$	The expectation of a random variable.
$\lim_{x \to a^+} g(x)$	The limit of $g(x)$ as x approaches a from the right.
$\mathbb{1}(c_1, \ldots, c_n)$	$\mathbb{1}(c_1, \ldots, c_n) = 1$ if all inputs are true, otherwise $\mathbb{1}(c_1, \ldots, c_n) = 0$.
$\mathcal{CN}(\mathbf{0}, \mathbf{\Omega})$	The complex Gaussian random vector with zero mean and variance $\mathbf{\Omega}$.
$\binom{n}{k}$	$\frac{n!}{n!(n-k)!}$.
$\binom{n}{\mathbf{p}}$	$\frac{u!}{p_1! \ldots p_n!}$ where $\mathbf{p} = [p_1, \ldots, p_n]$ consists of non–negative elements and satisfies the condition $p_1 + \ldots + p_n = n$.
$\Sigma_{\lVert\mathbf{p}\rVert_1 = n}$	The sum taken over all non–negative integer tuples of a vector $\mathbf{p} = [p_1, \ldots, p_n]$ that add up to n, i.e., $p_1 + \ldots + p_n = n$.

Chapter 1

Introduction

Prolonging the lifetime of a wireless network has received significant attention from the research community [1–3]. Though replacing or recharging batteries can solve this issue, it incurs a high cost and can be inconvenient or hazardous (e.g., in toxic environments), or highly undesirable (e.g., the sensors embedded in building structures or inside the human body) [4, 5]. In such scenarios, a safe and convenient option is to harvest the energy from the environment. The conventional energy harvesting techniques rely on the external natural resources, such as solar power, wind energy or thermoelectric effects, which can not guarantee the delivery of reliable and uninterrupted communication services due to their randomness and intermittent property. Recently, the researchers have proposed a new research direction of energy harvesting technique known as WEH in which energy–constrained nodes can scavenge energy from ambient RF signals to power up their batteries. Since RF signal can be under control, it is more reliable than external natural resources and is a promising technique to power the wireless devices.

The first application of WEH was found in point-to-point communication systems. In these such systems, the user terminals are assumed to be energy–constrained nodes and they harvest energy from RF signals sent by the AP [6,7] and/or sent by interference sources [8–10] to maintain their connections to the AP. Next, the applications of WEH were extended to the CC scenario where the relay nodes, that usually have limited battery reserves, incur great RF resource expense to assist the communication. In the Wireless Energy Harvesting–based Cooperative Communication (WEH–CC) model, the relay nodes can extract energy from the RF signals sent from wireless terminals and use this energy to forward information to the wireless terminals; hence, they can save much energy [11–15].

In the WEH networks, the energy–constrained devices are located near the AP to harvest much energy; hence, these nodes are able to decode information from the AP. This gives rise to an information security issue in WEH networks. To prevent illegitimate terminals from attacking the confidential information of the AP, the PLS technique, which is capable of providing secure communications without using cipher codes, has become an effective solution [16–18]. The PLS technique focuses on creating positive secrecy capacity, at which the eavesdropper is unable to decode any information, by exploiting the physical characteristics of the wireless channel [19–22]. Moreover, different technologies have been proposed to improve the secrecy capacity, including Artificial Noise (AN)-aided security, cooperative jamming, and beamforming [23, 24].

Motivated by above-mentioned developments, this dissertation studies two important issues of WEH–CC, relay selection and PLS. We propose and analyze five

WEH–CC models in which we study the benefit of Relay Selection Scheme (RSS) in improving the performance and investigate the secrecy performance of WEH networks. Moreover, we extend our studies to practical scenarios, e.g., the devices suffer from RF impairments, the obtained CSIs are imperfect, the best relay is unavailable due to its service and the relays are untrusted nodes, to make our studies more practical and useful.

1.1 Related Works

To realize the idea of WEH, the author of [25] designed two practical receiver architectures, namely, Time Switching (TS) and Power Splitting (PS). For the TS architecture, the WEH receiver spends some time for energy harvesting and the remaining time for information processing; whereas for the PS architecture, it uses a portion of the received power for energy harvesting and the remaining power for information processing. Since then, a number of studies in WEH with these practical receivers have appeared in the literature. In [26, 27], the rate–energy regions of the WEH systems with different energy–harvesting receivers were investigated. For multiuser WEH systems, the authors of [28] proposed a protocol to support the Full Duplex (FD) mode at the AP for broadcasting wireless energy to the users in the Downlink (DL) and receiving information from the users in the Uplink (UL). Next, the authors of [29] designed the precoders of the multiuser WEH system including an AP, Information Receivers (IRs) and Energy Receivers (ERs) to solve two optimal problems. In the first optimal problem, the precoders are designed to minimize the Mean Square Error (MSE) under source transmit power and harvested energy con-

straints, whereas in the second optimal problem, they are designed to maximize the total harvested energy at the EHs under source transmit power and MSE constraints.

For the WEH–CC scenarios, the authors of [30, 31] examined the performance of a basic WEH–CC model including a source, a destination and a relay. Under the presence of Co–Channel Interference (CCI), the works in [32,33] examined the impacts of the CCI on the WEH–CC system where the CCI is the cause of degradation in Quality of Service (QoS) but can be a desired energy source at the relay. The studies related to multiple-antenna WEH–CC system were studied in [34, 35]. In [34], the authors proposed equipping two antennas at the relay and using FD relaying mode which enables higher harvested energy and better performance at the relay. In [35], the influences of the CCI on a WEH–CC system via a multiple-antenna relay were studied. After that, another aspect of WEH–CC known as RSS in WEH–CC has gained much attention from the researchers [36, 37]. Although the use of multiple relays creates a significant improvement in QoS by exploiting the spatial diversity [38], it causes the high system complexity and spectral efficiency loss. To mitigate the disadvantages of using multiple relays while providing an acceptable improvement in QoS, the RSSs have been proposed [39]. The effects of RSS on WEH–CC were studied in [37, 40, 41]. In [37], the authors studied the OP of the WEH–CC system using multiple Decode–and–Forward (DF) relays. In [40], the authors proposed and evaluated both the OP and the throughput of a relay–selection WEH–CC system in the case that all relays are two–way FD nodes. Next, the authors of [41] analyzed the effect of Distributed Switch and Stay Combining (DSSC) technique and imperfect CSI in the WEH–CC system, where the communication between the source and the

destination is conducted through either the direct transmission or the best FD WEH relay selected by using Partial Relay Selection (PRS).

Recently, PLS in WEH networks has gained much attention from researcher community. In [42], the authors proposed using both AN and beamforming technique to address the security issue in a Multiple Input Single Output (MISO) WEH system containing a single IR and multiple ERs. An extension of [42] to a scenario containing multiple IRs was presented in [43]. Next, the authors of [44] studied the effect of AN on the secure transmission of a single–antenna WEH system, then determined the optimal solution for a transmit power allocated for the AN signal that minimize the Secrecy Outage Probability (SOP) and maximize the secrecy rate. In the presence the imperfect CSI, the work in [45] studied the effects of imperfect CSI on an MISO WEH system and proposed an optimal PS ratio to maximize the SOP. Recently, the authors of [46] investigated the secure communication of a WEH–CC system in which a relay is assumed to be an untrusted node that assists the source transmission and also overhears confidential information from the source; moreover, the work in [46] shows that the destination–assisted jamming can be efficiently exploited to enhance the secrecy capacity.

1.2 Dissertation Outline

The dissertation consists of seven chapters structured as follows:

In Chapter 1, we present the related works of WEH–CC, relay–selection techniques and PLS. Then, we present the outline of the dissertation and background knowledge relevant to our studies.

In Chapter 2, we study the effects of K–th best PRS method on system performance of an WEH–CC system by analyzing a communication between a multiple-antenna source–destination pair via a single–antenna WEH relays. We propose using MRT at the source for boosting harvested energy at the relays and MRC at the destination for improving QoS. We derive the mathematical results for three performance metrics, i.e., OP, DTT throughput and DLT throughput, of the proposed system. These results are derived for an general fading known as Nakagami–m. Then, based on the throughput expressions, we investigate the characteristics of optimal and sub-optimal throughputs for DLT mode and optimal throughput for DTT mode. Finally, the influences of key parameters of WEH and CC are studied in detail.

In Chapter 3, we extend the study of Chapter 2 to the practical scenario in which the transmit hardwares are imperfect. In this system, the transmit signals at the source and the selected relay are distorted by RTRI noises before transmitting them on antennas. We focus on analyzing the benefits of the K–th best PRS method in mitigating the influences of RTRI. The results in terms of the OP, DLT throughput and DTT throughput show that an increase in number of relays can reduce the influence of RTRI on the system performance. Moreover, the MRT technique also shows its advantage in boosting the desired signal power while keeping RTRI noise power at the receiver constant; hence, the influence of RTRI can be mitigated. Finally, the design insights on the choices of energy-harvesting receiver architectures and key parameters are provided.

In Chapter 4, we study the PLS problem in an WEH CC system with an untrusted Amplify–and–Forward (AF) relay. To create the positive secrecy capacity, the destina-

tion–assisted jamming signal, which can interfere the untrusted relays while decreasing a small QoS at the destination, is employed. This jamming signal can be exploited as an additional energy source at the relay. To enhance QoS, we propose equipping source with multiple antennas and deploying transmit-antenna techniques, namely, MRT and TAS. For secrecy performance comparison, RAS is examined. Specifically, the channels of the source–relay links are considered in both cases, perfect channel and imperfect channel. To access the secrecy performance, the mathematical results for the SOP and Average Secrecy Capacity (ASC) are derived. From the obtained results, we compare the secrecy performances of three transmit–antenna techniques and then provide useful design insights on the choices of transmit–antenna techniques under different system configurations.

In Chapter 5, we extend the study of Chapter 4 to the scenario of existing an external eavesdropper. Therefore, the secure communication faces with two security risks from the untrusted relay and the external eavesdropper. The destination–assisted jamming signal interferes both the untrusted relay and the eavesdropper for achieving the positive secrecy capacity. We also focus on analyzing two secrecy metrics, SOP and ASC. The results in terms of the SOP and ASC provide valuable insights into the effects of various key parameters of PLS, WEH and CC on the secrecy performance of the proposed system. Especially, these results show that the untrusted relay should be closed to the eavesdropper for creating the greatest secrecy performance.

In Chapter 6, we study the problem of joint relay–selection and PLS in an untrusted relaying WEH system. We equip the source and destination with multiple antennas; then, we deploy the MRT technique at these nodes. Additionally, we use

the MRT–based relay–selection methods to select the relay for assisting the communication. With these proposals, we can boost the harvested energy at the selected relay; moreover, under the assumption that lacking global knowledge of CSI at the relays, the security risks from the non–selected relays are eliminated. Moreover, we use the destination–assisted jamming signal to interferes the selected relay. The secrecy performance is evaluated via the SOP and ASC.

Finally, Chapter 7 concludes the dissertation with a summary and discussion of future research directions.

1.3 Background

In this section, we introduce the concepts about wireless channel model, CC protocol, relay selection method, hardware impairment issue, imperfect channel issue, PLS and energy harvesting.

1.3.1 Wireless Channel Model

Figure 1.1 presents a channel model of direct wireless transmission in which a source S transmits a signals x_S to a destination D through wireless environment. The received signal at the destination D is modeled as in [47, 48].

$$y_{S,D} = \sqrt{P} h_{S,D} x_S + n_D, \tag{1.1}$$

where x_S and P are transmit signal and transmit power of the source S, respectively, $h_{S,D}$ is wireless fading channel coefficient between the source S and the destination D, and n_D is Additive White Gaussian Noise (AWGN) at the destination D and is

modeled by a Gaussian-distributed Random Variable (RV) [49, 50] with zero-mean and variance of N_0.

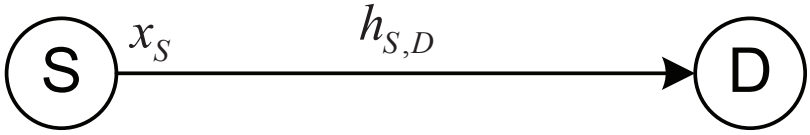

Figure 1.1: Channel model of direct wireless transmission.

In wireless environment, because of the constructive or destructive combination of scattered components of the radio signal, strength of arrived signals at the destination D is fluctuated or faded. In this thesis, we examine two fading channel models, namely, Rayleigh fading channel and Nakagami–m fading channel. In the Rayleigh and Nakagami–m fading models, the Line–of–Sight (LoS) component in the arrived signals does not exist. Let h_R and h_N be channel coefficients in Rayleigh and Nakagami–m fading channels, respectively. The channel gain $\mathcal{X} \triangleq |h_R|^2$ is exponential RV which has the Probability Density Function (PDF) and Cumulative Distribution Function (CDF) as follows [51].

$$f_{\mathcal{X}}(x;\lambda) = \lambda e^{-\lambda x}, \tag{1.2}$$

$$F_{\mathcal{X}}(x;\lambda) = 1 - e^{-\lambda x}, \tag{1.3}$$

where λ is a rate parameter (or inverse scale parameter).

The channel gain $\mathcal{Y} \triangleq |h_N|^2$ is gamma RV which has PDF and CDF as follows [52].

$$f_{\mathcal{Y}}(x;m,\lambda) = \frac{\lambda^m x^{m-1}}{\Gamma(m)} e^{-\lambda x}, \tag{1.4}$$

$$F_{\mathcal{Y}}(x;m,\lambda) = 1 - e^{-\lambda x} \sum_{n=0}^{m-1}, \frac{(\lambda x)^n}{n!} \tag{1.5}$$

where m is a shape parameter, $\Gamma(\alpha)$ and $\gamma(\alpha, x)$ are the gamma and lower incomplete gamma functions [53, Eq. (8.310.1) and Eq. (8.350.1)], respectively.

1.3.2 Cooperative Communication Protocol

Cooperative Communication is an efficient solution for mitigating the impact of channel fading, improving quality of service, and solving the coverage problem in wireless communication [54]. In the CC systems, the neighbouring nodes of the sources and destinations are employed as relay nodes that assist the sources in delivering packets to their destinations. The relays can apply the AF or DF protocols to process the received signals. In the AF protocol, the relay amplifies the received signals and forwards them to the destination. In the DF protocol, the relay first tries to decode the received signals; then the relay re–encodes and forwards these signals to the destination only if it successfully decodes the source's information [55, 56].

Figure 1.2 presents a simple system model of a CC system in which a cooperative relay R is ready to help the source S in forwarding the source signal x_S to the destination D. The operation principle in data transmission of this scheme can be split into two time slots. At the first time slot, the source S broadcasts the signal x_S to the relay R and the destination D. At the second time slot, the relay R processes (decodes or amplifies) the received signal and forwards the processed signal to the destination D. At the destination D, MRC technique in [57] can be applied to combines all received signals sent from the source S during the first time slot and sent from the relay R during the second time slot to enhance the system performance.

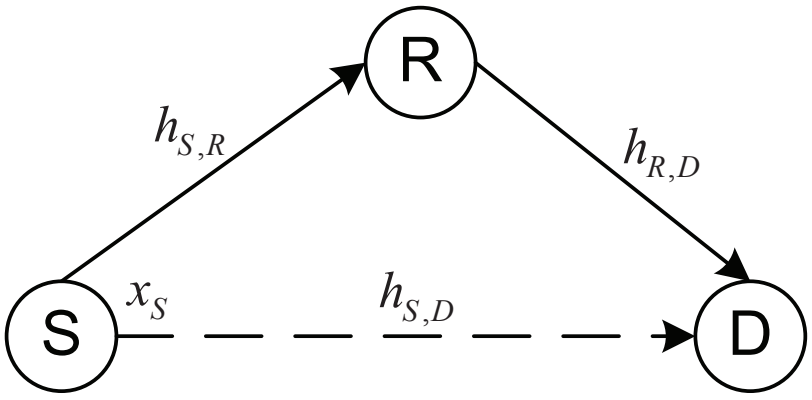

Figure 1.2: System model of cooperative communication.

1.3.3 Relay Selection Methods

Beside benefits providing by CC mentioned previously, the CC systems can also achieve the spatial diversity, which can enhance the system performance, by using multiple relays for assisting the overall communication. However, this method can increase scheme complexity and spectral efficiency loss. To reduce the disadvantages caused by using multiple relays while providing an acceptable improvement in QoS, various RSS have been well studied in the literature. Most RSSs include the assumption that the central entity has full knowledge about CSIs of all links; therefore, they can achieve full diversity order. However, the implementation of these strategies involves solving various issues, such as time synchronization, continuous channel feedback, and high power consumption [58]. For these reasons, the authors of [59, 60] proposed PRS, which requires one of the first–hop CSI and second–hop CSI, to perform the relay selection process.

In Figure 1.3, we present a cooperative scheme in wireless communication with

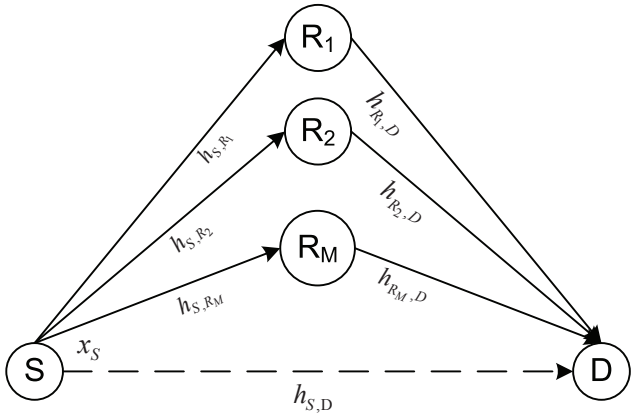

Figure 1.3: Cooperative scheme in wireless communication.

N relays, i.e., $R_1, R_2, ..., R_N$. The strategy of PRS for the case of using the first–hop CSI is given by

$$R_b = \underset{i=1,...,N}{\arg\max} \left(|h_{SR_i}|^2\right), \tag{1.6}$$

and the strategy of PRS for the case of using the second–hop CSI is given by

$$R_b = \underset{i=1,...,N}{\arg\max} \left(|h_{R_iD}|^2\right), \tag{1.7}$$

where R_b is denoted as the best relay; h_{SR_i} and h_{R_iD} are the channel coefficients of the S–R_i and R_i–D links, respectively.

In practical CC systems, the best relay may be unavailable or occupied by other service, a possible solution is to use the K–th best relay in order to avoid service interruption. An extension of PRS for the K–th best relaying scenario is called as K–th PRS. The strategy of K–th PRS for the case of using the first–hop CSI is given by

$$R^{(K)} = K\text{–th} \ \underset{i=1,...,N}{\arg\max} \left(|h_{SR_i}|^2\right), \tag{1.8}$$

and the strategy of K-th PRS for the case of using the second–hop CSI is given by

$$R^{(K)} = K\text{–th} \underset{i=1,\ldots,N}{\arg\max} \left(|h_{R_i D}|^2\right), \tag{1.9}$$

where $R^{(K)}$ is denoted as the K–th best relay ($1 \leqslant K \leqslant N$); hence, R_b can be written as $R^{(1)}$.

1.3.4 Residual RF Impairment Issue

Most studies in wireless communication were investigated with the assumption of ideal RF hardware. However, in practical systems, the transmitters and receivers suffer from various RF impairments caused by the RF font–end hardware imperfections, such as high–power amplifier (HPA) nonlinearity, in–phase/quadrature–phase (I/Q) imbalance, and oscillator phase noise [61, 62]. Although most of these impairments can be mitigated by using analog and digital signal processing algorithms, Residual RF Impairment (RRI) always remains. In [63], the behavior of RRI was first investigated. The results of [63] show that the influence of RRI can be characterized as additive and independent Gaussian noises.

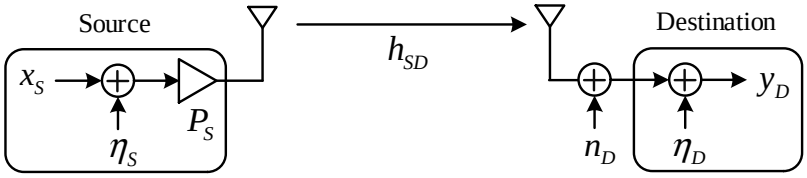

Figure 1.4: Wireless communication system with residual hardware impairment.

Figure 1.4 presents a communication of a wireless system in the presence of RRI. A source S sends a signal x_S to the destination D with transmit power P, where

$\mathbb{E}\{|x_S|^2\} = 1$. At the source, x_S is distorted by a RTRI noise $\eta_S \sim \mathcal{CN}(0, \kappa_S^2)$; and at the destination, the received signal of the destination D is also distorted by a Residual Receive RF Impairment (RRRI) noise $\eta_D \sim \mathcal{CN}(0, \kappa_D^2 P|h_{SD}|^2)$, where κ_S^2 is the RTRI level, κ_D^2 is the RRRI level, and $|h_{SD}|^2$ is channel coefficient of the S–D link. The signal used for information decoding at the destination D is expressed by

$$y_D(t) = \sqrt{P} h_{SD} \left(x_S(t) + \eta_S(t)\right) + n_D(t) + \eta_D(t). \tag{1.10}$$

According to [64], the distortions from transceiver impairments act as an additional noise source of variance $(\kappa_S^2 + \kappa_D^2)P|h_{SD}|^2$; therefore, (1.10) is rewritten as

$$y_D(t) = \sqrt{P} h_{SD} x_S(t) + n_D(t) + \eta_{SD}(t), \tag{1.11}$$

where $\eta_{SD} \sim \mathcal{CN}(0, (\kappa_S^2 + \kappa_D^2)P|h_{SD}|^2)$ represents the overall effects of η_S and η_D.

1.3.5 Imperfect Channel Issue

Another practical issue in wireless communication is imperfect channel issue where the transmitters and/or receivers use inaccurate CSI to process the desired signal. The imperfect channel occurs in two common scenarios, imperfect channel estimation and outdated CSI. In the imperfect channel estimation scenario, the estimated CSI values obtained from channel estimation process differ with the real CSI values due to the effects of noise or imperfect estimator. In the outdated CSI scenario, the CSI at the time of transmission may be outdated due to a delayed feedback since complexity in the transmission setup phase, such as, carrier synchronization, channel measurement and relay selection [65, 66].

Let h_{SD} be the channel coefficient between a source S and a destination D, and $\hat{h}_{SD}$ be the imperfect CSI version of h_{SD}. Mathematically, $\hat{h}_{SD}$ can be modeled as

$$\hat{h}_{SD} = \sqrt{\zeta} h_{SD} + \sqrt{1-\zeta} e, \tag{1.12}$$

where $\zeta \in [0, 1]$ is the channel correlation coefficient and $e \sim \mathcal{CN}(0, \bar{\gamma}_h)$ is a channel error with $\bar{\gamma}_h = \mathbb{E}\{|h_{SD}|^2\}$).

The value $\hat{h}_{SD}$ is closer to that of h_{SD} as ζ grows larger, and vice versa. Specifically, precise CSI can obtained when $\zeta = 1$, whereas $\hat{h}_{SD}$ is thoroughly independent of h_{SD} when $\zeta = 1$. According to [67], h_{SD} conditioned on $\hat{h}_{SD}$ follows a Gaussian distribution as

$$h_{SD}|\hat{h}_{SD} \sim \mathcal{CN}(\sqrt{\zeta}\hat{h}_{SD}, (1-\zeta)\bar{\gamma}_h). \tag{1.13}$$

1.3.6 Physical Layer Security

Nowadays, wireless communication becomes the most popular way to communicate. The broadcast nature of wireless medium makes wireless networks susceptible to eavesdropping. For that reason, security in wireless communication becomes a critical issue which gains a lot interest from the researchers [68–72]. The conventional solutions for creating secure communication rely on sophisticated algorithms with the assumption that eavesdroppers possess limited computational capabilities [73]. However, with the rapid development of computing devices, this assumption is not guaranteed. To overcome this challenge, PLS technology, which is capable of giving secure communications without using cipher codes, has introduced. In [74], Wyner showed that secure communication of a wireless system exists if the capacity of the

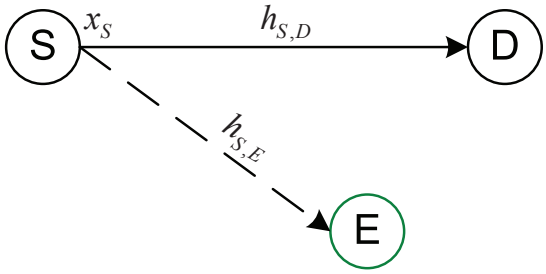

Figure 1.5: System model of direct transmission under physical layer security.

desired channel is greater than that of the eavesdropping channel. The secure capacity is evaluated through the Achievable Secrecy Rate (ASR) metric which determines the maximum secure information received at a destination.

Figure 1.5 presents a simple system model of a direct transmission under PLS in which a source S transmits its packets x_S to a destination D against wiretapping of an eavesdropper E. The ASR is defined as in [75] as

$$R_{\text{sec}} = [C_{S,D} - C_{S,E}]^+, \tag{1.14}$$

where R_{sec} is the ASR, $C_{S,D} \triangleq \log_2(1+P_s|h_{S,D}|^2/N_0)$ and $C_{S,E} \triangleq \log_2(1+P_s|h_{S,E}|^2/N_0)$ are achievable data rates of desired link, S–D, and wiretapped link, S–E, respectively, with P is a transmit power of the source S.

1.3.7 Energy Harvesting

Wireless energy harvesting, which allows wireless devices to power up their batteries by harvesting energy from ambient RF signals, has recently studied as an promising solution for prolonging the lifetime of wireless networks [76, 77]. To realize the idea of WEH, the authors of [25] designed two practical energy-harvesting receiver

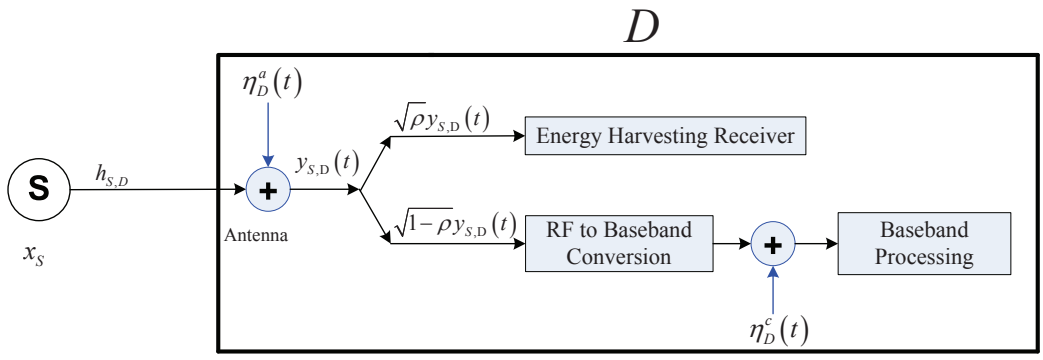

Figure 1.6: Block diagram of the power splitting receiver at a destination node D.

architectures, namely, TS, where the receiver switches in time between information decoding and energy harvesting, and PS, where the receiver uses a portion of the received signal strength for information decoding and the rest for energy harvesting.

Figure 1.6 presents a block diagram of the PS receiver as described in [30]. In Figure 1.6, a source S transmits a signal x_S to a destination D with a transmit power P, where $\mathbb{E}\{|x_S|^2\} = 1$. The received signal at the destination D is given as

$$y_{S,D}(t) = \sqrt{P}h_{S,D}x_S(t) + n_D^a(t), \tag{1.15}$$

where $h_{S,D}$ is the channel coefficient of the S–D link and $n_D^a(t)$ denotes the AWGN at the destination's antenna with variance N_0.

The destination D harvests the energy from a portion ρ of the received signal strength, $\sqrt{\rho}y_{S,D}(t)$, and uses the remaining part, $\sqrt{1-\rho}y_{S,D}(t)$, for information decoding, where $0 \leqslant \rho \leqslant 1$ is the PS ratio. Therefore, the harvested energy of the destination D during a total transmission time T is given by

$$E_{H,D}^{PS} = \rho P|h_{S,D}|^2\eta T, \tag{1.16}$$

where $0 < \eta < 1$ is the energy conversion efficiency at the destination D.

Figure 1.7 presents a block diagram of the TS receiver as described in [30]. In the TS policy, the destination D harvests energy from the received signal during the first interval time αT, $0 \leqslant \alpha \leqslant 1$, where α_T is the time-fraction coefficient or the TS ratio. The remaining time $(1-\alpha)T$ is used to process the source's information. Using (1.15), the harvested energy of the destination D during αT is given by

$$E_{H,D}^{TS} = P|h_{S,D}|^2 \eta \alpha T. \tag{1.17}$$

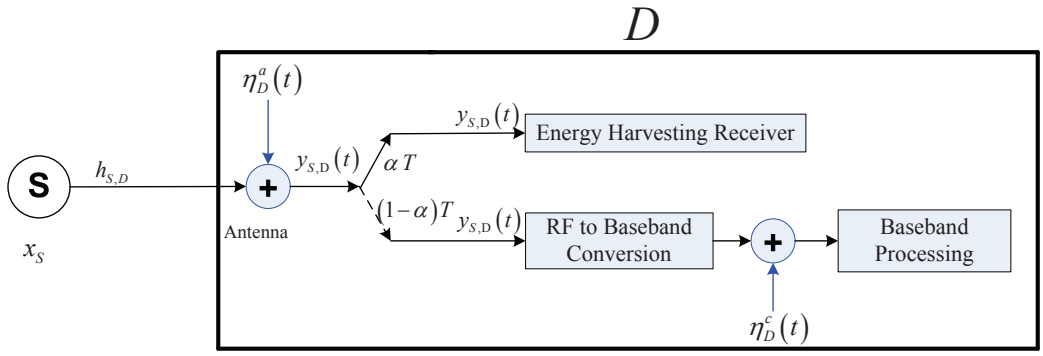

Figure 1.7: Block diagram of the time switching receiver at a destination node D.

Chapter 2

Wireless Energy-Harvesting in K-th Best Relay Selection Systems with Energy Beamforming over Nakagami-m Fading Channels[1]

2.1 Introduction

In this Chapter, we study the effects of the K–th PRS technique on the performance of WEH–CC systems via investigating a WEH–CC system consisting of a multi–antenna source, a multi–antenna destination and a single–antenna WEH relay network. The relay network chooses the K–th best relay using the PRS technique to help the communication between the source and the destination. This selected relay

[1]The study in this chapter was published in Wireless Personal Communications [78]

is chosen based on criteria such as the K–th Best First–Hop Channel–Gain (KBFC) and the K–th Best Second–Hop Channel–Gain (KBSC). The channel is modeled as the Nakagami–m fading. To maximize the harvested energy at the selected relay and enhance to QoS at the destination, MRT and MRC are applied at the source and destination, respectively. For performance evaluation, we derive the analytical expressions for the OP and ergodic capacity for both the Time–Switching Relaying (TSR) and Power–Splitting Relaying (PSR) protocols; then, the throughput for the DLT and DTT modes can be formulated. The analytical results are verified by the Monte Carlo simulations. After that, we use a numerical method, known as Golden Section Search (GSS) [79], to evaluate the optimal values of in the DLT and DTT modes. Moreover, the DLT mode is examined in two optimal cases: Global–Optimal Delay–Limited Transmission (GODLT) where the system operates at an optimal pair of values for the source rate and energy–harvesting ratio, and Local–Optimal Delay–Limited Transmission (LODLT) where the source rate is fixed and the throughput is maximized with the optimal energy–harvesting ratio. Finally, we use the Monte Carlo simulation to verify our analytical results.

The rest of this Chapter is organized as follows. The system model and relaying protocols are described in Section 2.2. The analytical expressions for the OP and throughput are derived in Section 2.3. The results and discussion are given in Section 2.4. Finally, the conclusions are presented in Section 2.5.

2.2 System Model and Relaying Protocols

2.2.1 System Model

We consider an AF relaying WEH–CC system illustrated in Figure 2.1, in which the communication of a multi-antenna source-destination pair is assisted by the K-th best relay $\mathcal{R}^{(K)}$ of a single-antenna WEH relay network $\mathcal{R}$ that includes L nodes ($\mathcal{R}_l$, for $l = 1, 2, \ldots, L$). The relays are located in a cluster and are close to each other relative to their distances d_1 to the source $\mathcal{S}$ and d_2 to the destination $\mathcal{D}$. $\mathcal{S}$ and $\mathcal{D}$ are equipped with N_1 and N_2 antennas, and they employ MRT and MRC, respectively. Both the TSR and PSR protocols are examined. The channel of each link undergoes Nakagami-m fading; hence, the channel gains are gamma RVs with the PDF given by (1.4) as

$$f_g(x; m, \lambda) = \frac{x^{m-1}}{\Gamma(m)\lambda^m} e^{-\frac{x}{\lambda}}, \tag{2.1}$$

where (m, λ) are the shape and scale parameters of the gamma RV. We assume that the channel coefficients are constants during a block time T and are identically and independently distributed (i.i.d.) between two different block times.

Let $\mathbf{h}_{1,l} = [h_{1,l,1}, \ldots, h_{1,l,N_1}]^\top$, $\mathbf{h}_{2,l} = [h_{2,l,1}, \ldots, h_{2,l,N_2}]^\top$, $\mathbf{h}_1^{(K)}$ and $\mathbf{h}_2^{(K)}$ denote the channel vectors of the $\mathcal{S}$–$\mathcal{R}_l$, $\mathcal{R}_l$–$\mathcal{D}$, $\mathcal{S}$–$\mathcal{R}^{(K)}$, and $\mathcal{R}^{(K)}$–$\mathcal{D}$ links, respectively, where $|h_{1,l,k_1}|^2$, $k_1 = 1, \ldots, N_1$, and $|h_{2,l,k_2}|^2$, $k_2 = 1, \ldots, N_2$, are gamma RVs with parameters $(m_1, \frac{\lambda_1}{m_1})$ and $(m_2, \frac{\lambda_2}{m_2})$, respectively. Therefore, $\|\mathbf{h}_{1,l}\|^2$ and $\|\mathbf{h}_{1,l}\|^2$ are gamma RVs with parameters $(N_1 m_1, \frac{\lambda_1}{m_1})$ and $(N_2 m_2, \frac{\lambda_2}{m_2})$, respectively. According to

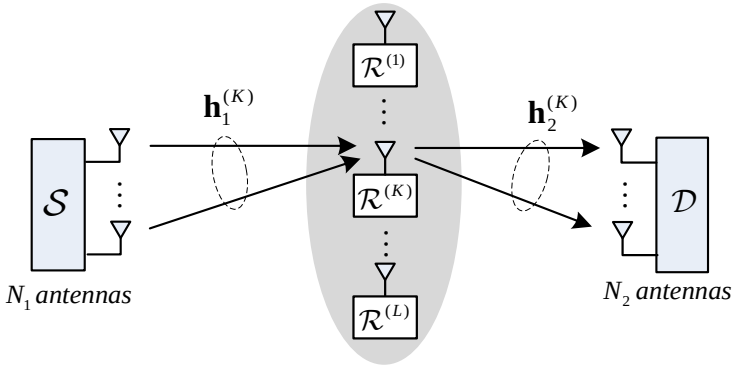

Figure 2.1: Proposed system model.

Section 1.3.3, the strategies of the KBFC and KBSC are described as follows:

$$\mathcal{R}^{(K)} = K\text{–th} \underset{1 \leqslant l \leqslant L}{\arg\max} \{\|\mathbf{h}_{1,l}\|^2\}, \qquad \text{(for KBFC scheme)} \tag{2.2a}$$

$$\mathcal{R}^{(K)} = K\text{–th} \underset{1 \leqslant l \leqslant L}{\arg\max} \{\|\mathbf{h}_{2,l}\|^2\}. \qquad \text{(for KBSC scheme)} \tag{2.2b}$$

After determining $\mathcal{R}^{(K)}$, a beamforming vector $\mathbf{w}_s = \frac{(\mathbf{h}_1^{(K)})^\dagger}{\|\mathbf{h}_1^{(K)}\|}$ is applied at $\mathcal{S}$ to maximize the harvested energy of $\mathcal{R}^{(K)}$. Therefore, the received signal of $\mathcal{R}^{(K)}$ can be expressed as

$$y_r(t) = \sqrt{\frac{P_s}{d_1^\tau}} \left\| \mathbf{h}_1^{(K)} \right\| x_s(t) + n_r^{[a]}(t), \tag{2.3}$$

where P_s is the transmit power of $\mathcal{S}$, $x_s(t)$ is the source information with $\mathbb{E}\{|x_s(t)|^2\} = 1$, τ is the path loss exponent, and $n_r^{[a]}(t) \sim \mathcal{CN}(0, \sigma^2_{n_r^{[a]}})$ is the antenna AWGN at $\mathcal{R}^{(K)}$.

2.2.2 Time-Switching Relaying Protocol

For the TSR protocol, each processing block time T is split into 3 intervals, $\alpha_T T$, $(1-\alpha_T)\frac{T}{2}$, and $(1-\alpha_T)\frac{T}{2}$, which are employed for the energy-harvesting, $\mathcal{S}$–$\mathcal{R}^{(K)}$ transmission and $\mathcal{R}^{(K)}$–$\mathcal{D}$ transmission phases, respectively, where $0<\alpha_T<1$ is the TS ratio. Using (1.17) and (2.3), the energy harvested by $\mathcal{R}^{(K)}$ during the interval $\alpha_T T$ is given as

$$E_{r,\mathrm{TS}} = \frac{\zeta P_s \left\|\mathbf{h}_1^{(K)}\right\|^2 \alpha_T T}{d_1^\tau}. \tag{2.4}$$

where $0<\zeta<1$ is the energy conversion efficiency.

According to [30], the sampled baseband signal at $\mathcal{R}^{(K)}$ is given by

$$y_{r,\mathrm{TS}}(k) = \sqrt{\frac{P_s}{d_1^\tau}}\left\|\mathbf{h}_1^{(K)}\right\| x_s(k) + n_r^{[a]}(k) + n_r^{[c]}(k), \tag{2.5}$$

where $n_r^{[c]}(k) \sim \mathcal{CN}(0, \sigma^2_{n_r^{[c]}})$ is the conversion AWGN at $\mathcal{R}^{(K)}$. It is possible to represent the effect of the two noise versions as $n_{r,\mathrm{TS}}(k) \sim \mathcal{CN}(0, \sigma^2_{n_{r,\mathrm{TS}}}) \triangleq n_r^{[a]}(k) + n_r^{[c]}(k)$ with $\sigma^2_{n_{r,\mathrm{TS}}} = \sigma^2_{n_r^{[a]}} + \sigma^2_{n_r^{[c]}}$.

During the $\mathcal{S} \to \mathcal{R}^{(K)}$ transmission phase, the transmit power of $\mathcal{R}^{(K)}$ can be computed as

$$P_{r,\mathrm{TS}} = \frac{2E_{r,\mathrm{TS}}}{(1-\alpha_T)T} = \frac{2\zeta P_s \left\|\mathbf{h}_1^{(K)}\right\|^2 \alpha_T}{d_1^\tau(1-\alpha_T)}, \tag{2.6}$$

and the sampled received signal of $\mathcal{D}$ can be expressed as

$$\mathbf{y}_{d,\mathrm{TS}}(k) = \sqrt{\frac{P_{r,\mathrm{TS}}}{d_2^\tau}}\mathbf{h}_2^{(K)} G_{r,\mathrm{TS}} y_{r,\mathrm{TS}}(k) + \mathbf{n}_d^{[a]}(k) + \mathbf{n}_d^{[c]}(k), \tag{2.7}$$

where $G_{r,\mathrm{TS}} = \left(\frac{P_s\|\mathbf{h}_1^{(K)}\|^2}{d_1^\tau} + \sigma^2_{n_{r,TS}}\right)^{-\frac{1}{2}}$ is a power constraint factor of $\mathcal{R}^{(K)}$, $\mathbf{n}_d^{[a]}(k) \sim \mathcal{CN}(\mathbf{0}, \sigma^2_{\mathbf{n}_d^{[a]}}\mathbf{I}_{N_2})$ and $\mathbf{n}_d^{[c]}(k) \sim \mathcal{CN}(\mathbf{0}, \sigma^2_{\mathbf{n}_d^{[c]}}\mathbf{I}_{N_2})$ are respectively the antenna and con-

version AWGNs at $\mathcal{D}$. The effect of $\mathbf{n}_d^{[a]}(k)$ and $\mathbf{n}_d^{[c]}(k)$ can be represented by $\mathbf{n}_d(k) \sim \mathcal{CN}(\mathbf{0}, \sigma^2_{\mathbf{n}_d}\mathbf{I}_{N_2}) \triangleq \mathbf{n}_d^{[a]}(k) + \mathbf{n}_d^{[c]}(k)$ with $\sigma^2_{\mathbf{n}_d} \triangleq \sigma^2_{\mathbf{n}_d^{[a]}} + \sigma^2_{\mathbf{n}_d^{[c]}}$.

2.2.3 Power-Splitting Relaying Protocol

For the PSR protocol, each processing block time T consists of two time slots $\frac{T}{2}$. During the first time slot, the received signal power is split into two streams with the PS ratio $0 < \theta < 1$, such that $\sqrt{\theta}y_r(t)$ for energy harvesting and $\sqrt{1-\theta}y_r(t)$ for information processing. Using (1.16) and (2.3), the energy harvested by $\mathcal{R}^{(K)}$ is given as

$$E_{r,\mathrm{PS}} = \frac{\zeta\theta P_s \left\|\mathbf{h}_1^{(K)}\right\|^2 T}{2d_1^\tau}, \tag{2.8}$$

and the sampled received signal of $\mathcal{R}^{(K)}$ can be expressed as

$$y_{r,\mathrm{PS}}(k) = \sqrt{\frac{(1-\theta)\,P_s}{d_1^\tau}}\left\|\mathbf{h}_1^{(K)}\right\| x_s(k) + \sqrt{(1-\theta)}n_r^{[a]}(k) + n_r^{[c]}(k). \tag{2.9}$$

It is possible to represent the effect of the two noise versions as $n_{r,\mathrm{PS}} \sim \mathcal{CN}(0, \sigma^2_{n_{r,\mathrm{PS}}}) \triangleq \sqrt{(1-\theta)}n_r^{[a]}(k) + n_r^{[c]}(k)$ with $\sigma^2_{n_{r,\mathrm{PS}}} \triangleq (1-\theta)\sigma^2_{n_r^{[a]}} + \sigma^2_{n_r^{[c]}}$. During the second time slot, the transmit power of $\mathcal{R}^{(K)}$ can be computed as

$$P_{r,\mathrm{PS}} = \frac{2E_{r,\mathrm{PS}}}{T} = \frac{\zeta\theta P_s \left\|\mathbf{h}_1^{(K)}\right\|^2}{d_1^\tau}, \tag{2.10}$$

and the sampled received signal of $\mathcal{D}$ can be expressed as

$$\mathbf{y}_{d,\mathrm{PS}}(k) = \sqrt{\frac{P_{r,\mathrm{PS}}}{d_2^\tau}}\mathbf{h}_2^{(K)}G_{r,\mathrm{PS}}y_{r,\mathrm{PS}}(k) + \mathbf{n}_d(k), \tag{2.11}$$

where $G_{r,\mathrm{PS}} = \left(\frac{(1-\theta)P_s\|\mathbf{h}_1^{(K)}\|^2}{d_1^\tau} + \sigma^2_{n_{r,\mathrm{PS}}}\right)^{-\frac{1}{2}}$.

2.3 Performance Analysis

2.3.1 Outage Probability

By definition, the OP is the probability that the instantaneous end-to-end Signal to Noise Ratio (SNR) falls below a predefined threshold γ. In this system, since the relays are fixed-gain AF nodes, the end-to-end SNR for the TSR and PSR protocols can be evaluated as

$$\gamma_{e2e,[w]} = \frac{\gamma_{r,[w]}\gamma_{d,[w]}}{\gamma_{r,[w]} + \gamma_{d,[w]} + 1}, \tag{2.12}$$

where $w = \{\text{TS,PS}\}$, $\gamma_{r,[w]} = \mathbb{a}_{[w]}\|\mathbf{h}_1^{(K)}\|^2$, and $\gamma_{d,[w]} = \mathbb{b}_{[w]}\|\mathbf{h}_1^{(K)}\|^2\|\mathbf{h}_2^{(K)}\|^2$ with $\mathbb{a}_{[\text{TS}]}, \mathbb{a}_{[\text{PS}]}, \mathbb{b}_{[\text{TS}]}$, and $\mathbb{b}_{[\text{PS}]}$ defined as $\frac{P_s}{d_1^\tau \sigma^2_{n_{r,\text{TS}}}}$, $\frac{(1-\theta)P_s}{d_1^\tau \sigma^2_{n_{r,\text{PS}}}}$, $\frac{2\zeta\alpha_T P_s}{(1-\alpha_T)d_1^\tau d_2^\tau \sigma^2_{n_d}}$, and $\frac{\zeta\theta P_s}{d_1^\tau d_2^\tau \sigma^2_{n_d}}$, respectively. Then, we can rewrite (2.12) as

$$\gamma_{\text{e2e},[w]} = \frac{\mathbb{a}_{[w]}\mathbb{b}_{[w]}\left\|\mathbf{h}_1^{(K)}\right\|^4\left\|\mathbf{h}_2^{(K)}\right\|^2}{\mathbb{a}_{[w]}\left\|\mathbf{h}_1^{(K)}\right\|^2 + \mathbb{b}_{[w]}\left\|\mathbf{h}_1^{(K)}\right\|_F^2\left\|\mathbf{h}_2^{(K)}\right\|^2 + 1}. \tag{2.13}$$

Because exact analysis appears to be difficult, a tight lower bound of the OP can be more easily analyzed using the upper bound of the end-to-end SNR given by

$$\gamma^{\text{up}}_{\text{e2e},[w]} = \frac{\mathbb{b}_{[w]}\left\|\mathbf{h}_1^{(K)}\right\|^2\left\|\mathbf{h}_2^{(K)}\right\|^2}{\frac{\mathbb{b}_{[w]}}{\mathbb{a}_{[w]}}\left\|\mathbf{h}_2^{(K)}\right\|^2 + 1}. \tag{2.14}$$

Proposition 2.1 The OP of the proposed system for the KBFC and KBSC schemes can be respectively bounded below by (2.15) and (2.16) as follows.

$$\mathcal{P}^{\text{low}}_{\text{KBFC},[w]}(\gamma) = 1 - \sum_{j=0}^{N_2m_2-1} \sum_{n=0}^{L-K} \sum_{\substack{N_1m_1-1 \\ \sum_{i=0} \\ p_i^{(1)}=K+n-1}} \sum_{q=0}^{N_1m_1+\omega_1-1} \frac{2L!(-1)^n}{j!\,(K-1)!\,(L-K)!}$$

$$\times \frac{\left(\frac{\lambda_2 \mathbb{b}_{[w]}}{m_2 \mathbb{a}_{[w]}}\right)^{N_1m_1+\omega_1-q-1}}{\Gamma(N_1m_1)(K+n)^{N_1m_1+\omega_1}} \binom{L-K}{n} \binom{K+n-1}{p_0^{(1)},\ldots,p_{N_1m_1-1}^{(1)}} \binom{N_1m_1+\omega_1-1}{q}$$

$$\times \left(\prod_{i=0}^{N_1m_1-1} \left(\frac{1}{i!}\right)^{p_i^{(1)}}\right) e^{-\frac{m_1(K+n)\gamma_{th}}{\lambda_1 \mathbb{a}_{[w]}}} \mu_{1,[w]}^{2N_1m_1+2\omega_1-q+j-1} K_{q-j+1}\left(2\mu_{1,[w]}\right), \tag{2.15}$$

$$\mathcal{P}^{\text{low}}_{\text{KBSC},[w]}(\gamma) = 1 + \sum_{i=0}^{N_1m_1-1} \sum_{t=0}^{K-1} \sum_{\substack{n=0 \\ t+n\neq 0}}^{L-t} \sum_{\substack{N_2m_2-1 \\ \sum_{j=0} \\ p_j^{(2)}=t+n}} \frac{2(-1)^n}{\Gamma(N_1m_1)} \binom{L}{t} \binom{L-t}{n}$$

$$\times \binom{N_1m_1-1}{i} \binom{t+n}{p_0^{(2)},\ldots,p_{N_2m_2-1}^{(2)}} \left(\prod_{j=0}^{N_2m_2-1} \left(\frac{1}{j!}\right)^{p_j^{(2)}}\right) \frac{\left(\frac{\lambda_2 \mathbb{b}_{[w]}}{m_2 \mathbb{a}_{[w]}}\right)^{N_1m_1-i-1}}{(t+n)^{N_1m_1+\omega_2-i-1}}$$

$$\times e^{-\frac{m_1\gamma}{\lambda_1 \mathbb{a}_{[w]}}} \mu_{2,[w]}^{2N_1m_1+\omega_2-i-1} K_{i-\omega_2+1}\left(2\mu_{2,[w]}\right). \tag{2.16}$$

where $K_\upsilon(\cdot)$ is the υ-*th* order modified Bessel function [53, Eq. (8.407.1)], $\mu_{1,[w]} = \sqrt{\frac{m_1m_2(K+n)\gamma}{\lambda_1\lambda_2\mathbb{b}_{[w]}}}$, $\mu_{2,[w]} = \sqrt{\frac{m_1m_2(t+n)\gamma}{\lambda_1\lambda_2\mathbb{b}_{[w]}}}$, $\omega_1 = \sum_{i=0}^{N_1m_1-1} ip_i^{(1)}$, and $\omega_2 = \sum_{j=0}^{N_2m_2-1} jp_j^{(2)}$.

Proof: See Appendix A.1

2.3.2 Throughput Analysis

Delay-Limited Transmission Mode

In the DLT mode, the throughput is determined by evaluating the OP at a threshold SNR $\gamma_{\text{th}} = 2^{2R} - 1$ and numbers of transmitted bits during an unit of time, where R (bits/s/Hz) is the transmission rate. For the TSR protocol, $\mathcal{S}$ spends an interval $(1-\alpha_T)\frac{T}{2}$ of each processing block time T to send its information; therefore, the

upper bound of the DLT throughput for the TSR protocol in both the KBFC and KBSC schemes can be expressed as

$$\mathcal{T}_{[k],\mathrm{TS}}^{R,\mathrm{up}} = \frac{1}{2}\left(1 - \mathcal{P}_{[k],\mathrm{TS}}^{\mathrm{low}}(\gamma_{\mathrm{th}})\right)(1-\alpha_T)\,R, \tag{2.17}$$

where $k = \{\mathrm{KBFC}, \mathrm{KBSC}\}$. For the PSR protocol, because $\mathcal{R}^{(K)}$ operates in a Half Duplex (HD) mode during each processing block time, the upper bound of the DLT throughput for the PSR protocol in both the KBFC and KBSC schemes can be expressed as

$$\mathcal{T}_{[k],\mathrm{PS}}^{R,\mathrm{up}} = \frac{1}{2}\big(1 - \mathcal{P}_{[k],\mathrm{PS}}^{\mathrm{low}}(\gamma_{\mathrm{th}}\,)\big)\,R. \tag{2.18}$$

With the outage expressions in (2.15) and (2.16), the optimal solution for throughput does not admit a closed-form solution; however, it can be efficiently solved via numerical evaluation using the GSS method. We consider the optimal throughput for the DLT mode in two cases: GODLT and LODLT. In the GODLT mode, the DLT throughput is maximized by an optimal pair of values for the energy-harvesting ratio and source rate, i.e., (α_T^*, R^*) for the TSR protocol and (θ^*, R^*) for the PSR protocol, with the strategies given by

$$\mathcal{T}^{*R,\mathrm{up}}_{[k],\mathrm{TS,GO}} = \max_{\substack{0<\alpha_T<1\\R>0}} \{\mathcal{T}^{R,\mathrm{up}}_{[k],\mathrm{TS}}\}, \qquad \text{(for TSR protocol)} \tag{2.19a}$$

$$\mathcal{T}^{*R,\mathrm{up}}_{[k],\mathrm{PS,GO}} = \max_{\substack{0<\theta<1\\R>0}} \{\mathcal{T}^{R,\mathrm{up}}_{[k],\mathrm{PS}}\}. \qquad \text{(for PSR protocol)} \tag{2.19b}$$

In the LODLT mode, R is fixed at a predetermined value; thus, the throughput is maximized by an optimal value of the energy-harvesting ratio with the strategies

given by

$$\mathcal{T}^{*R,\text{up}}_{[k],\text{TS,LO}} = \max_{\substack{0<\alpha_T<1 \\ R \text{ is predetermined}}} \{\mathcal{T}^{R,\text{up}}_{[k],\text{TS}}\}, \qquad \text{(for TSR protocol)} \tag{2.20a}$$

$$\mathcal{T}^{*R,\text{up}}_{[k],\text{PS,LO}} = \max_{\substack{0<\theta<1 \\ R \text{ is predetermined}}} \{\mathcal{T}^{R,\text{up}}_{[k],\text{PS}}\}. \qquad \text{(for PSR protocol)} \tag{2.20b}$$

Delay-Tolerant Transmission Mode

In the DTT mode, $\mathcal{S}$ is assumed to adapt the transmission rate to achieve the ergodic capacity $\mathcal{C}$, the absolute limit in error-free communication. According to [80], the ergodic capacity for the TSR and PSR protocols can be calculated as follows.

$$\mathcal{C}_{[w]} = \frac{1}{2}\mathbb{E}\left\{\log_2\left(1+\gamma_{\text{e2e},[w]}\right)\right\}. \tag{2.21}$$

Due to the complexity of the CDF of $\gamma_{\text{e2e},[w]}$, the ergodic capacity can be achieved using an alternative approach given by

$$\mathcal{C}_{[w]} = \frac{1}{2}\mathbb{E}\left\{\log_2\left(\frac{(1+\gamma_{r,[w]})(1+\gamma_{d,[w]})}{1+\gamma_{r,[w]}+\gamma_{d,[w]}}\right)\right\} = C_{\gamma_{r,[w]}} + C_{\gamma_{d,[w]}} - C_{\gamma_{t,[w]}}, \tag{2.22}$$

where $C_{\gamma_{r,[w]}} = \frac{1}{2}\mathbb{E}\{\log_2(1+\gamma_{r,[w]})\}$, $C_{\gamma_{d,[w]}} = \frac{1}{2}\mathbb{E}\{\log_2(1+\gamma_{d,[w]})\}$, and $C_{\gamma_{t,[w]}} = \frac{1}{2}\mathbb{E}\{\log_2(1+\gamma_{r,[w]}+\gamma_{d,[w]})\}$. Both $C_{\gamma_{r,[w]}}$ and $C_{\gamma_{r,[w]}}$ have closed-form solutions, whereas a closed-form solution for $C_{\gamma_{t,[w]}}$ is not possible. However, the lower bound of $C_{\gamma_{r,[w]}}$ can be obtained using Jensens inequality for a convex function $f(x,y) = \log_2(1+e^x+e^y)$ as follows:

$$C_{\gamma_{t,[w]}} \geqslant C^{\text{low}}_{\gamma_{t,[w]}} \triangleq \frac{1}{2}\log_2(1+e^{\mathbb{E}\{\gamma_{r,[w]}\}}+e^{\mathbb{E}\{\gamma_{d,[w]}\}}). \tag{2.23}$$

Proposition 2.2 The ergodic capacity of the proposed system for the KBFC and KBSC schemes can be respectively bounded above by (2.24) and (2.25) as follows.

$$\mathcal{C}^{\text{up}}_{\text{KBFC},[w]} = \frac{-1}{2\ln 2}\left(\sum_{t=0}^{K-1}\sum_{\substack{n=0\\ t+n\neq 0}}^{L-t}\sum_{\sum_{i=0}^{N_1m_1-1} p_i^{(1)}=t+n}(-1)^n\binom{L}{t}\binom{L-t}{n}\left(\frac{m_1}{\mathfrak{a}_{[w]}\lambda_1}\right)^{\omega_1}\right.$$
$$\times\binom{t+n}{p_0^{(1)},\ldots,p_{N_1m_1-1}^{(1)}}\left(\prod_{i=0}^{N_1m_1-1}\left(\frac{1}{i!}\right)^{p_i^{(1)}}\right)e^{\frac{m_1(t+n)}{\mathfrak{a}_{[w]}\lambda_1}}\Gamma\left(-\omega_1,\frac{m_1(t+n)}{\mathfrak{a}_{[w]}\lambda_1}\right)$$
$$\times\Gamma(\omega_1+1)-\sum_{n=0}^{L-K}\sum_{\sum_{i=0}^{N_1m_1-1} p_i^{(1)}=K+n-1}\frac{L!(-1)^n}{(L-K)!(K-1)!\Gamma(N_1m_1)\Gamma(N_2m_2)}$$
$$\times\frac{1}{(K+n)^{N_1m_1+\omega_1}}\binom{L-K}{n}\binom{K+n-1}{p_0^{(1)},\ldots,p_{N_1m_1-1}^{(1)}}\left(\prod_{i=0}^{N_1m_1-1}\left(\frac{1}{i!}\right)^{p_i^{(1)}}\right)$$
$$\left.\times G_{4,2}^{1,4}\left(\frac{\mathbb{b}_{[w]}\lambda_1\lambda_2}{m_1m_2(K+n)}\middle|\begin{matrix}-N_1m_1-\omega_1+1, & -N_2m_2+1, & 1, & 1\\ 1, & & 0 & \end{matrix}\right)\right)$$
$$-\frac{1}{2}\log_2\left(1+e^{(\ln(\mathfrak{a}_{[w]})+\mathcal{A})}+e^{\left(\ln(\mathbb{b}_{[w]})+\mathcal{A}+\psi(N_2m_2)-\ln\left(\frac{m_2}{\lambda_2}\right)\right)}\right), \tag{2.24}$$

$$\mathcal{C}^{\text{up}}_{\text{KBSC},[w]} = \frac{1}{2\ln 2}\left(\sum_{i=0}^{N_1m_1-1}\frac{1}{i!}\left(\frac{m_1}{\mathfrak{a}_{[w]}\lambda_1}\right)^i e^{\frac{m_1}{\mathfrak{a}_{[w]}\lambda_1}}\Gamma(i+1)\Gamma\left(-i,\frac{m_1}{\mathfrak{a}_{[w]}\lambda_1}\right)\right.$$
$$+\sum_{n=0}^{L-K}\sum_{\sum_{j=0}^{N_2m_2-1} p_j^{(2)}=K+n-1}\frac{(-1)^nL!}{(L-K)!(K-1)!\Gamma(N_1m_1)\Gamma(N_2m_2)(K+n)^{N_2m_2+\omega_2}}$$
$$\times\binom{K+n-1}{p_0^{(2)},\ldots,p_{N_2m_2-1}^{(2)}}G_{4,2}^{1,4}\left(\frac{\mathbb{b}_{[w]}\lambda_1\lambda_2}{m_1m_2(K+n)}\middle|\begin{matrix}-N_1m_1+1, & -N_2m_2-\omega_2+1, & 1, & 1\\ 1, & & 0 & \end{matrix}\right)$$
$$\left.\times\left(\prod_{j=0}^{N_2m_2-1}\left(\frac{1}{j!}\right)^{p_j^{(2)}}\right)\binom{L-K}{n}\right)-\frac{1}{2}\log_2\left(1+e^{\left(\ln(\mathfrak{a}_{[w]})+\psi(N_1m_1)-\ln\left(\frac{m_1}{\lambda_1}\right)\right)}\right.$$
$$\left.+e^{\left(\ln(\mathbb{b}_{[w]})+\psi(N_1m_1)-\ln\left(\frac{m_1}{\lambda_1}\right)+\mathcal{B}\right)}\right), \tag{2.25}$$

where $\mathcal{A}$ and $\mathcal{B}$ are respectively defined as (2.26) and (2.27).

$$\mathcal{A} = \sum_{n=0}^{L-K} \sum_{\sum_{i=0}^{N_1 m_1 - 1} p_i^{(1)} = K+n-1} \frac{L!(-1)^n \Gamma(N_1 m_1 + \omega_1)}{(L-K)!(K-1)!\Gamma(N_1 m_1)(K+n)^{N_1 m_1 + \omega_1}} \binom{L-K}{n} \times \binom{K+n-1}{p_0^{(1)}, \ldots, p_{N_1 m_1 - 1}^{(1)}} \left(\prod_{i=0}^{N_1 m_1 - 1} \left(\frac{1}{i!} \right)^{p_i^{(1)}} \right) \left(\psi(N_1 m_1 + \omega_1) - \ln\left(\frac{m_1 (K+n)}{\lambda_1} \right) \right), \tag{2.26}$$

$$\mathcal{B} = \sum_{n=0}^{L-K} \sum_{\sum_{j=0}^{N_2 m_2 - 1} p_j^{(2)} = K+n-1} \frac{L!(-1)^n \Gamma(N_2 m_2 + \omega_2)}{(K-1)!(L-K)!\Gamma(N_2 m_2)(K+n)^{N_2 m_2 + \omega_2}} \binom{L-K}{n} \times \binom{K+n-1}{p_0^{(2)}, \ldots, p_{N_2 m_2 - 1}^{(2)}} \left(\prod_{j=0}^{N_2 m_2 - 1} \left(\frac{1}{j!} \right)^{p_j^{(2)}} \right) \left(\psi(N_2 m_2 + \omega_2) - \ln\left(\frac{m_2 (K+n)}{\lambda_2} \right) \right). \tag{2.27}$$

where $\psi(x)$ is the Digamma function [53, Eq. (8.360.1)], $G_{p,q}^{m,n}(\cdot)$ is the Meijer G-function [53, Eq. (9.301)], and $\Gamma(s,x)$ is the upper incomplete gamma functions [53, Eq. (8.350.2)].

Proof: See Appendix A.2.

From the expressions of the ergodic capacity, the DTT throughput for the TSR protocol in both the KBFC and KBSC schemes has the upper bound given as

$$\mathcal{T}_{[k],\mathrm{TS}}^{\mathrm{erg,up}} = \frac{1}{2} (1 - \alpha_T) \mathcal{C}_{[k],\mathrm{TS}}^{\mathrm{up}}, \tag{2.28}$$

and the DLT throughput for the PSR protocol in both the KBFC and KBSC schemes has the upper bound given as

$$\mathcal{T}_{[k],\mathrm{PS}}^{\mathrm{erg,up}} = \frac{1}{2} \mathcal{C}_{[k],\mathrm{PS}}^{\mathrm{up}}. \tag{2.29}$$

Then, the optimal throughput of the DTT mode can be evaluated as

$$\mathcal{T}^{*\text{erg,up}}_{[k],\text{TS}} = \max_{0<\alpha_T<1}\{\mathcal{T}^{\text{erg,up}}_{[k],\text{TS}}\}, \qquad \text{(for TSR protocol)} \tag{2.30a}$$

$$\mathcal{T}^{*\text{erg,up}}_{[k],\text{PS}} = \max_{0<\theta<1}\{\mathcal{T}^{\text{erg,up}}_{[k],\text{PS}}\}. \qquad \text{(for PSR protocol)} \tag{2.30b}$$

2.4 Results and Discussion

In this section, we present the numerical results to validate the analytical expressions of the system performance presented in Section 2.3. Without loss of generality, we assume that $\sigma^2_{n_r^{[a]}} = \sigma^2_{\mathbf{n}_d^{[a]}} = \sigma^2_{n^{[a]}}$ and $\sigma^2_{n_r^{[c]}} = \sigma^2_{\mathbf{n}_d^{[c]}} = \sigma^2_{n^{[c]}}$, and the coordinates in the 2-dimensional plane of $\mathcal{S}, \mathcal{D}$ and $\mathcal{R}$ are respectively set at (0, 0), (1, 0) and $(0.5, 0.5)$. Unless otherwise specified, we set $\tau = 3, \zeta = 0.5, \alpha_T = 0.2, \theta = 0.5, \lambda_1 = \lambda_2 = 1, N_1 = N_2 = 2, m_1 = m_2 = 2, \sigma^2_{n^{[a]}} = \sigma^2_{n^{[c]}} = \sigma^2_0 = 0.5$, and $\rho \triangleq \frac{P_s}{\sigma^2_0} = 10$ (dB).

Figure 2.2 presents the OP with respect to α_T for the TSR protocol and θ for the PSR protocol. It can be observed that the OP for the TSR protocol is a decreasing function of α_T. This is because when α_T is set at high values, a higher transmit power of $\mathcal{R}^{(K)}$ produces a lower OP at $\mathcal{D}$. In contrast, the OP for the PSR protocol decreases as θ changes from zero to the optimal value, and it increases with further increase in θ. These results can be explained as follows. Low values of θ cause a low harvested energy of $\mathcal{R}^{(K)}$, and high values of θ cause low signal quality of $\mathcal{R}^{(K)}$; thus, an optimal value of θ balanced the harvested energy and signal quality of $\mathcal{R}^{(K)}$ gives the best OP. On the other hand, because the harvested energy depends on the quality of the first-hop links, the KBFC scheme provides better OP than the KBSC scheme. Moreover, the OP of the proposed system improves when the shape

parameters increase.

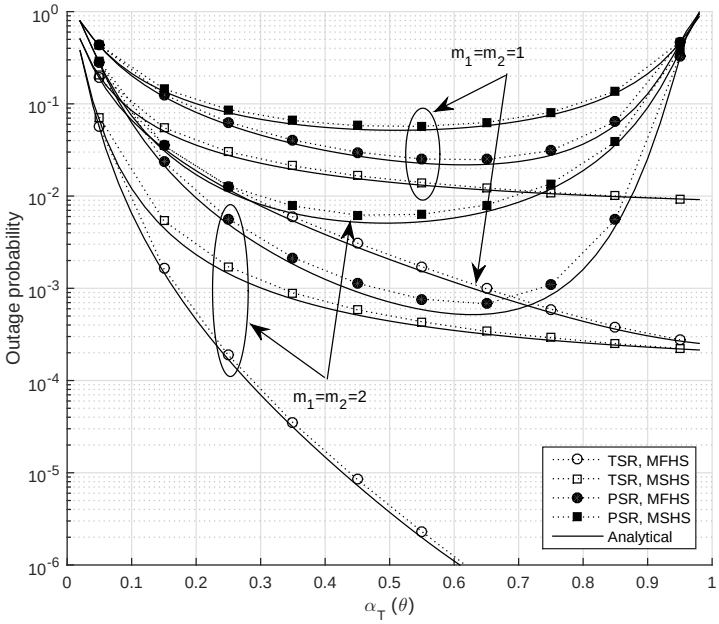

Figure 2.2: The OP with respect to α_T for the TSR protocol and θ for the PSR protocol. Other parameters: $\rho = 10$ (dB), $\gamma = 3$ (dB), $L = 3$ and $K = 2$.

In Figure 2.3, we show the OP of the proposed system in two cases: In one, we vary $0 < \sigma^2_{n^{[a]}} < 1$ with fixed $\sigma^2_{n^{[c]}} = 0.5$; and in the other case, we vary $0 < \sigma^2_{n^{[c]}} < 1$ with fixed $\sigma^2_{n^{[a]}} = 0.5$. The TSR protocol obtains the same OP in the two cases, whereas the PSR protocol gives different OPs in the two cases. These results can be explained as follows. For the TSR protocol, because $\sigma^2_{n^{[a]}}$ and $\sigma^2_{n^{[c]}}$ play the same role in the end-to-end SNR, the effects of these noise powers on the OP are identical. In contrast, for the PSR protocol, a portion of the received signal strength is employed for the signal-processing circuit (see equation (2.9)); thus, $\sigma^2_{n^{[c]}}$ exerts a greater influence than $\sigma^2_{n^{[a]}}$ on the source information. For that reason, the OP for the PSR protocol in the case of increasing $\sigma^2_{n^{[c]}}$ increases more rapid than that in the case of increasing $\sigma^2_{n^{[a]}}$.

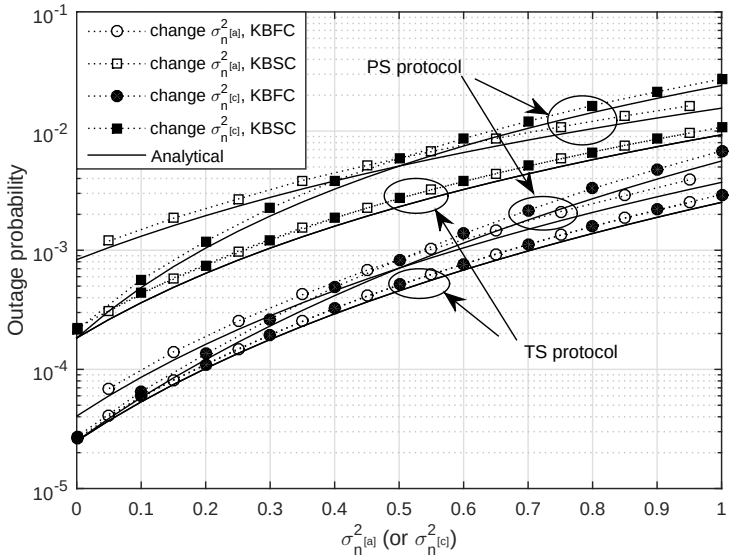

Figure 2.3: Outage probability with respect to the noise power. Other parameters: $\rho = 10$ (dB), $\gamma = 3$ (dB), $L = 3$ and $K = 2$.

Figure 2.4 presents the DLT throughput of the proposed system with respect to α_T, θ and R. As shown, the four sub-figures have similar shapes, i.e., concave-downward surfaces. To explain these results, we first investigate the effects of α_T and θ on the throughput. For the TSR protocol, the duration employed for the energy-harvesting and information-transmitting phase is determined by α_T. If the value of α_T is too small (i.e., $\alpha_T \to 0^+$), $\mathcal{R}^{(K)}$ forwards its received information with low transmit power; hence, a high OP at $\mathcal{D}$ causes low throughput. And if the value of α_T is too high (i.e., $\alpha_T \to 1^-$), $\mathcal{R}^{(K)}$ spends a short interval of each block time for assisting the source-to-destination communication; thus, the throughput becomes low. For the PSR protocol, the effect of θ on the throughput can be explained based on the characteristic of the OP presented in the discussion of Figure 2.2. Next, we consider the effect of R on the throughput. R influences both the transmission rate

and the SNR threshold γ_{th} of $\mathcal{D}$; therefore, if R is too low or too high, the throughput becomes low. As a result, an optimal pair of values for the energy-harvesting ratio and source rate, i.e., (α_T^*, R^*) for the TSR protocol and (θ^*, R^*) for the PSR protocol, can be determined.

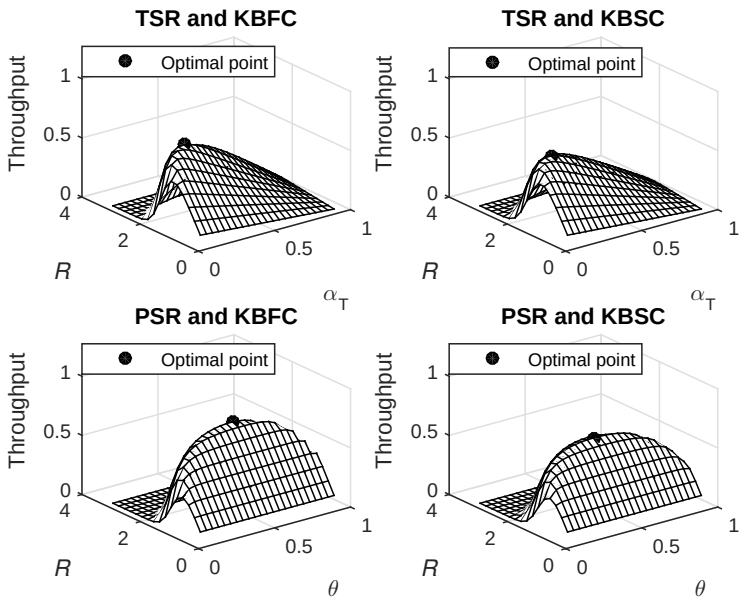

Figure 2.4: The throughput with respect to the energy-harvesting ratio α_T (or θ) and R. Other parameters: $\rho = 10$ (dB), $L = 4$ and $K = 2$.

In Figure 2.5, we consider the effects of $\sigma^2_{n^{[a]}}$ and $\sigma^2_{n^{[c]}}$ on the optimal throughput of the GODLT, LODLT and DTT modes. The value of $\sigma^2_{n^{[a]}}$ and $\sigma^2_{n^{[c]}}$ are configured similar to those in Figure 2.3. We can observe that, with the same system configuration, the optimal throughput of the DTT mode is superior to that of the GODLT mode, and the optimal throughput of the GODLT mode is higher than that of the LODLT mode. In the LODLT mode, when the noise powers increase, the optimal throughput of the PSR protocol is notably degraded; this means that the TSR proto-

col performs better than the PSR protocol at the low SNR regime. In contrast, in the GODLT and DTT modes, a crossover between the optimal throughput of the PSR and TSR protocols occurs only if $\sigma^2_{n^{[c]}}$ is very high (see Figure 2.5(b)). On the other hand, the optimal throughput for the TSR protocol is the same in the two cases of varying noise variances, whereas the optimal throughput for the PSR protocol shown in the two sub-figures is different. In particular, the optimal throughput in the case of increasing $\sigma^2_{n^{[c]}}$ (see Figure. 2.5(b)) decreases more significant than in the case of increasing $\sigma^2_{n^{[a]}}$ (see Figure 2.5(a)). These results can be explained based on the effects of $\sigma^2_{n^{[a]}}$ and $\sigma^2_{n^{[c]}}$ on the end-to-end SNR, which is described in the discussion of Figure 2.3.

Figure 2.6 presents the effect of ρ and the K-th best selection strategy on the optimal throughput. It can be observed that, the optimal throughput is increasing function of ρ and is decreasing function of K. Moreover, the optimal throughput of the DTT and GODLT modes is significantly increased as ρ increases whereas the optimal throughput of LODLT mode reaches the upper bound $R/2$ (bits/s/Hz) at high values of ρ. This is because the OP and α^*_T (for the TSR protocol) become small at high values of ρ. In the LODLT mode, at relatively low values of ρ, the KBSC scheme outperforms the KBFC scheme except for $K = 1$, and the TSR protocol performs better than the PSR protocol. In contrast, in the GODLT and DTT modes, the KBSC scheme is more efficient than the KBFC scheme only if K is set at high values, and the PSR protocol outperforms the TSR protocol. The effects of the KBFC and KBSC schemes from these assessments can be explained based on the influences of low quality links on the harvested energy at $\mathcal{R}^{(K)}$.

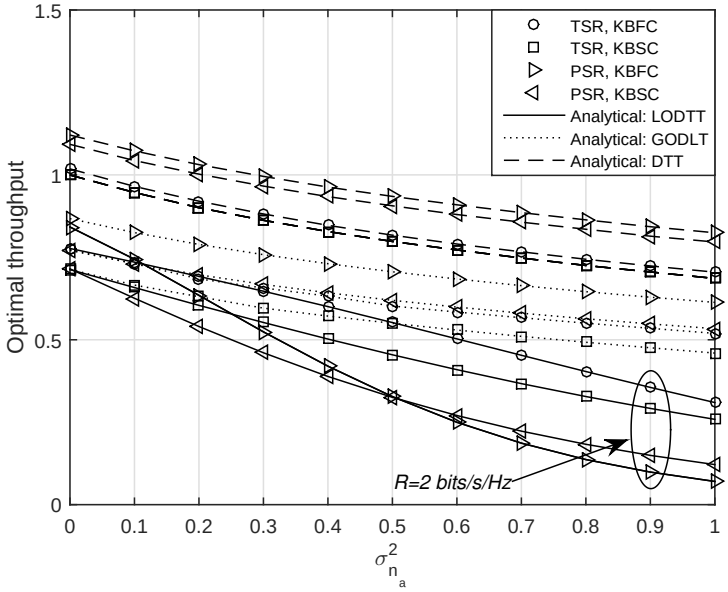

(a)

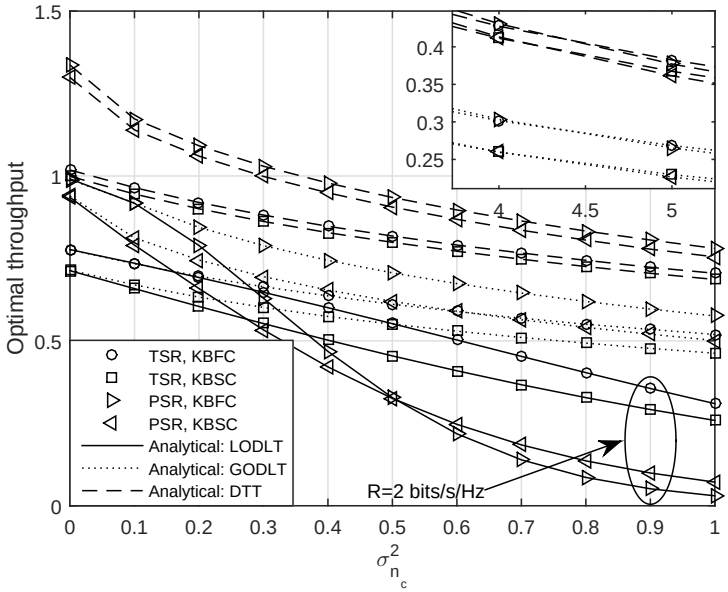

(b)

Figure 2.5: The optimal throughput with respect to the noise power. Other parameters: $\rho = 10$ (dB), $L = 4, K = 2$, and $R = 2$ (bits/s/Hz).

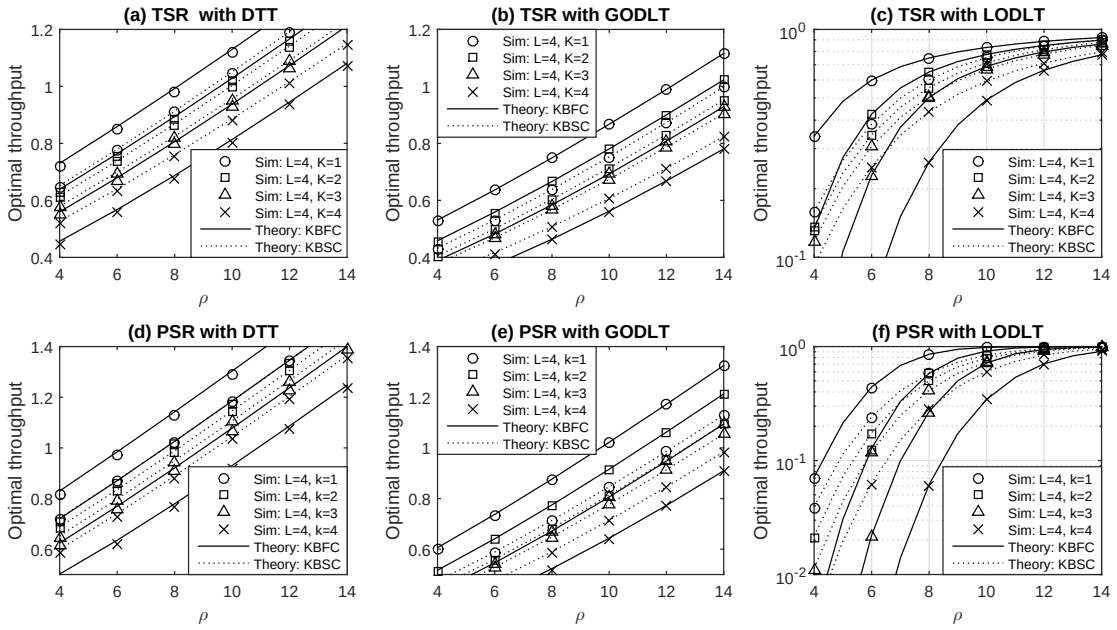

Figure 2.6: The optimal throughput with respect to ρ. Other parameters: $R = 2$ (bits/s/Hz) for the LODLT mode.

2.5 Conclusions

In this Chapter, we proposed and analyzed the AF relaying WEH–CC system with two K–th best PRS schemes, KBFC and KBSC. We derived the analytical expressions for Nakagami–m fading channel for three performance metrics, i.e., the OP, DLT throughput and DTT throughput for both the TSR and PSR protocols. Moreover, we examined the DLT throughput in two optimal cases, GODLT and LODLT. The results in terms of throughput show the following.

- The results of the DLT throughput in the LODLT case show that at relatively low SNRs, the KBSC scheme outperforms the KBFC scheme except at K=1, and the TSR protocol performs better than the PSR protocol.

- The results of the DLT throughput in the GODLT case and the DTT throughput show that the KBSC scheme is more efficient than the KBFC scheme at high values of K, and the PSR protocol outperforms the TSR protocol.

- When the signal quality increases, the DLT throughput in the GODLT case and the DTT throughput significantly enhance, whereas the DLT throughput in the LODLT case approximately reaches an upper limit.

- The system performance can be significantly improved by increasing the number of relays, device antennas, and the shape parameter of the Nakagami–m fading.

Finally, the effects of various system parameters, such as relay selection order, TS ratio, PS ratio, source rate, and transmit power, on the OP and throughput were investigated to provide useful insights.

Chapter 3

Wireless energy harvesting in relay-selection systems with residual transmit RF impairments [1]

3.1 Introduction

As mentioned in Chapter 1, the communication of the practical wireless systems suffers from the RRI caused by the imperfect RF hardwares and difficulty in designing ideal mitigation algorithms. Therefore, the studies on the behavior of the RRI are an essential research direction for the reality systems. The authors of [63] showed that the impacts of the RRI can be characterized as additive and independent Gaussian noises. Since then, a number of works studying the influences of the RRI on various wireless systems have been published. In [82], the impact of transceiver RF

[1] The study in this chapter was published in International Journal of Electronics [82]

impairments on relaying system was studied. The similar work regarding two–way relaying was investigated in [83]. Later, the authors of [84] quantified the impact of the RF impairments on an opportunistic relay–selection system. In other work, the authors of [85] analyzed the impacts of RTRI on a training–based MIMO system with different linear receivers, and then determined the optimal training matrix for each receiver. Specifically, the authors of [86] studied the joint impact of hardware impairment and CCI on a dual–hop DF relaying scheme.

Most studies regarding to the RRI focused on non–WEH systems. Motivated by these observations, in this Chapter we study the effects of the RRI on the performance of a WEH–CC system by expanding our investigation in Chapter 2 to the scenario that the transmit hardwares of the devices contain the RTRI. However, we only consider the two special cases of the PRS scheme, i.e., Best First–Hop–based Partial Relay Selection (PRS–1), where the relay possessing the best fist–hop channel assists the source's transmission, and Best Second–Hop–based Partial Relay Selection (PRS–2), where the relay possessing the best second–hop channel assists the source's transmission. To evaluate the system performance, we derive the analytical expressions for the OP, the DLT throughput and the DTT throughput of both TSR and PSR protocols. Finally, we use the Monte Carlo simulation to verify our analytical results.

The rest of this Chapter is organized as follows. The system model and preliminary results are presented in Section 3.2. The analytical expressions for the OP and throughput are derived in Section 3.3. The results and discussion are given in Section 3.4. Finally, the conclusions are presented in Section 3.5.

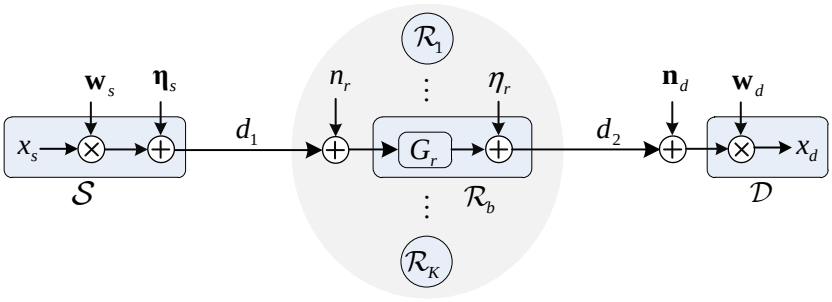

Figure 3.1: System model.

3.2 System Model and Preliminary Results

3.2.1 System Model

We consider an AF relaying WEH–CC system illustrated in Figure 3.1. As shown, the configurations of the source $\mathcal{S}$, destination $\mathcal{D}$ and WEH relay network $\mathcal{R}$ (including K nodes, $\mathcal{R}_k, 1 \leqslant k \leqslant K$) are similar to that in Chapter 2. Such as, $\mathcal{S}$ and $\mathcal{D}$ are respectively equipped with N_1 and N_2 antennas, and respectively employ MRT and MRC. $\mathcal{R}_k$ is single-antenna device and it can use the TS protocol with the TS ratio, α_T, or the PS protocol with the PS ratio, θ, to harvest energy and assist the communication. The relays are located in a cluster, and are close to each other relative to their distances d_1 to $\mathcal{S}$ and d_2 to $\mathcal{D}$. Among the K relays, only the best relay $\mathcal{R}_b$ selected using PRS is allowed to assist the communication.

Throughout this Chapter, the following assumptions are considered: 1) The direct link does not exist due to obstacles or severe fading. 2) The $\mathcal{S}$–$\mathcal{R}$ and $\mathcal{R}$–$\mathcal{D}$ links undergo i.i.d. Rayleigh block-fading channels, respectively. 3) The channel coefficients of the indirect links are constants during a block time T and are i.i.d. random variables

between two different block times. 4) The RTRI levels of the source antennas are identical [85].

3.2.2 Partial relay selection scheme

Let $\mathbf{h}_{1,k} = [h_{1,k,1}, \ldots, h_{1,k,N_1}]$ and $\mathbf{h}_{2,k} = [h_{2,k,1}, \ldots, h_{2,k,N_2}]^\top$ be the channel vectors of the $\mathcal{S}$–$\mathcal{R}_k$ and $\mathcal{R}_k$–$\mathcal{D}$ links, respectively, where $h_{m,k,i} \sim \mathcal{CN}(0, \lambda_m), m = \{1, 2\}$ and $i = 1, 2, \ldots, N_m$. According to Section 1.3.3, The strategy of the PRS-1 and PRS-2 schemes are described as follows:

$$\mathcal{R}_b = \underset{1 \leqslant k \leqslant K}{\arg\max} \{\|\mathbf{h}_{1,k}\|^2\}, \qquad \text{(for the PRS-1 scheme)}, \tag{3.1a}$$

$$\mathcal{R}_b = \underset{1 \leqslant k \leqslant K}{\arg\max} \{\|\mathbf{h}_{2,k}\|^2\}, \qquad \text{(for the PRS-2 scheme)}. \tag{3.1b}$$

According to [87, 88], the PDF and CDF of $\|\mathbf{h}_{m,k}\|^2$ are given by

$$f_{\|\mathbf{h}_{m,k}\|^2}(x) = \frac{x^{N_m-1}}{\Gamma(N_m)\lambda_m^{N_m}} e^{-\frac{x}{\lambda_m}}, \tag{3.2}$$

$$F_{\|\mathbf{h}_{m,k}\|^2}(x) = 1 - e^{-\frac{x}{\lambda_m}} \sum_{j=0}^{N_m-1} \frac{1}{j!} \left(\frac{x}{\lambda_m}\right)^j. \tag{3.3}$$

Let us define $g_{m,b} = \max\limits_{1 \leqslant k \leqslant K} \{\|\mathbf{h}_{m,k}\|^2\}$. The PDF and CDF of $g_{m,b}$ are given by

$$f_{g_{m,b}}(x) = K f_{\|\mathbf{h}_{m,k}\|^2}(x) \left(F_{\|\mathbf{h}_{m,k}\|^2}(x)\right)^{K-1}, \tag{3.4}$$

$$F_{g_{m,b}}(x) = \left(F_{\|\mathbf{h}_{m,k}\|^2}(x)\right)^K. \tag{3.5}$$

In (3.4) and (3.5), the elements containing a power of a sum can be expanded using the multinomial theorem given by (A.6).

3.2.3 Time-switching relaying protocol with RTRI

In the TS protocol, the communication of each block time T consist of three phases: energy-harvesting with a duration $\alpha_T T$, $\mathcal{S}$–$\mathcal{R}_b$ transmission with a duration $(1-\alpha_T)T/2$, and $\mathcal{S}$–$\mathcal{R}_b$ transmission with a duration $(1-\alpha_T)T/2$.

Energy harvesting and source-to-relay transmission

To perform MRT, $\mathcal{S}$ applies a transmit beamforming vector $\mathbf{w}_s = \mathbf{h}_{1,b}^{\dagger}/\left\|\mathbf{h}_{1,b}\right\|$ to its signal x_s before transmitting $\mathbf{w}_s x_s$ to $\mathcal{D}$, where $\mathbf{h}_{1,b} = [h_{1,b,1}, \ldots, h_{1,b,N_1}]$ is a channel vector of the $\mathcal{S}$–$\mathcal{R}_b$ link and $\mathbb{E}\{x_s x_s^*\} = 1$. The received signal of $\mathcal{R}_b$ is given by

$$y_r^{TS} = \sqrt{\frac{P_s}{d_1^{\tau}}}\mathbf{h}_{1,b}\left(\mathbf{w}_s x_s + \boldsymbol{\eta}_s\right) + n_r^{[a]} + n_r^{[c]}, \tag{3.6}$$

where P_s is the transmit power of $\mathcal{S}$, τ is the path loss exponent, $\boldsymbol{\eta}_s \in \mathbb{C}^{N_1 \times 1}$ and $\boldsymbol{\eta}_s \sim \mathcal{CN}(\mathbf{0}, \kappa_s^2 \mathbf{I}_{N_1})$ is the RTRI noise vector at $\mathcal{S}$ with the RTRI level κ_s^2, and $n_r^{[a]} \sim \mathcal{CN}(0, \sigma^2_{n_r^{[a]}})$ and $n_r^{[c]} \sim \mathcal{CN}(0, \sigma^2_{n_r^{[c]}})$ are antenna and conversion AWGNs at $\mathcal{R}_b$, respectively [30].

The energy harvested by $\mathcal{R}_b$ during the interval αT is given by

$$E_r^{TS} = \frac{\zeta P_s \left\|\mathbf{h}_{1,b}\right\|^2 \alpha_T T}{d_1^{\tau}}, \tag{3.7}$$

where ζ is the energy conversion efficiency.

Relay-to-destination transmission and end-to-end SNR

In this phase, a power constraint factor $G_r^{TS} = \left(\frac{P_s\left\|\mathbf{h}_{1,b}\right\|^2}{d_1^{\tau}}\left(1+\kappa_s^2\right) + \sigma^2_{n_{1,r}}\right)^{-1/2}$ is applied to the received signal of $\mathcal{R}_b$ before forwarding $G_r^{TS} y_r^{TS}$ to $\mathcal{D}$, where $n_{1,r} :=$

$n_r^{[a]} + n_r^{[c]}$, $\sigma^2_{n_{1,r}} := \sigma^2_{n_r^{[a]}} + \sigma^2_{n_r^{[c]}}$, and $\mathbb{E}\left\{\mathbf{h}_{1,b}\boldsymbol{\eta}_s(\mathbf{h}_{1,b}\boldsymbol{\eta}_s)^*\right\} = \|\mathbf{h}_{1,b}\|^2 \kappa_s^2$. The received signal of $\mathcal{D}$ can be expressed as

$$\mathbf{y}_d^{TS} = \sqrt{\frac{P_r^{TS}}{d_2^\tau}}\mathbf{h}_{2,b}\left(G_r^{TS}y_r^{TS} + \eta_r\right) + \mathbf{n}_d^{[a]} + \mathbf{n}_d^{[c]}, \tag{3.8}$$

where $P_r^{TS} = \frac{2E_r^{TS}}{(1-\alpha_T)T}$, $\mathbf{h}_{2,b} = [h_{2,b,1}, \ldots, h_{2,b,N_2}]^\top$ is the channel vector of the $\mathcal{S}$–$\mathcal{R}_b$ link, $\eta_r \sim \mathcal{CN}(0, \kappa_r^2)$ is the RTRI noise at $\mathcal{R}_b$ with the RTRI level κ_r^2, $\mathbf{n}_d^{[a]} \in \mathbb{C}^{N_2\times 1}$ and $\mathbf{n}_d^{[a]} \sim \mathcal{CN}(\mathbf{0}, \sigma^2_{\mathbf{n}_d^{[a]}}\mathbf{I}_{N_2})$ is the antenna AWGN vector at $\mathcal{D}$, and $\mathbf{n}_d^{[c]} \in \mathbb{C}^{N_2\times 1}$ and $\mathbf{n}_d^{[c]} \sim \mathcal{CN}(\mathbf{0}, \sigma^2_{\mathbf{n}_d^{[c]}}\mathbf{I}_{N_2})$ is the conversion AWGN vectors at $\mathcal{D}$.

The received signal of $\mathcal{D}$ after MRC is expressed as

$$x_d^{TS} = \mathbf{w}_d\mathbf{y}_d^{TS} = \sqrt{\frac{P_r^{TS}\|\mathbf{h}_{2,b}\|^2}{d_2^\tau}}\left(\mathcal{G}_r^{TS}y_r^{TS} + \eta_r\right) + \mathbf{w}_d\mathbf{n}_d, \tag{3.9}$$

where $\mathbf{w}_d = \mathbf{h}_{2,b}^\dagger / \|\mathbf{h}_{2,b}\|$ is the weight vector of MRC and $\mathbf{n}_d := \mathbf{n}_d^{[c]} + \mathbf{n}_d^{[c]}$.

From (3.6),(3.7), (3.8) and (3.9), the instantaneous end-to-end SNR for the TSR protocol can be evaluated as

$$\gamma_{e2e}^{TS} = \frac{\mathrm{a}^{TS}\|\mathbf{h}_{1,b}\|^4\|\mathbf{h}_{2,b}\|^2}{\mathrm{a}^{TS}\kappa_{AF}^2\|\mathbf{h}_{1,b}\|^4\|\mathbf{h}_{2,b}\|^2 + \mathbb{b}^{TS}\|\mathbf{h}_{1,b}\|^2\|\mathbf{h}_{2,b}\|^2 + \|\mathbf{h}_{1,b}\|^2 + \mathbb{c}^{TS}}, \tag{3.10}$$

where $\mathrm{a}^{TS} = \frac{2\zeta\alpha_T P_s}{d_1^\tau d_2^\tau(1-\alpha_T)\sigma^2_{\mathbf{n}_d}(1+\kappa_s^2)}$, $\mathbb{b}^{TS} = \frac{2\zeta\alpha_T\sigma^2_{n_{1,r}}\left(1+\kappa_r^2\right)}{d_2^\tau(1-\alpha_T)\sigma^2_{\mathbf{n}_d}(1+\kappa_s^2)}$, $\mathbb{c}^{TS} = \frac{d_1^\tau\sigma^2_{n_{1,r}}}{P_s(1+\kappa_s^2)}$, and $\kappa_{AF}^2 = (\kappa_s^2 + \kappa_r^2 + \kappa_s^2\kappa_r^2)$.

3.2.4 Power-splitting relaying protocol with RTRI

In the PSR protocol, each block time T is split into two equal sub-blocks $T/2$. The first sub-block is employed for the energy-harvesting and $\mathcal{S}$–$\mathcal{R}_b$ transmission phases, whereas the second sub-block is used for the $\mathcal{R}_b$–$\mathcal{D}$ transmission phase.

Energy harvesting and source-to-relay transmission

The input signal of the information receiver of $\mathcal{R}_b$ is given by

$$y_r^{PS} = \sqrt{\frac{(1-\theta)\,P_s}{d_1^\tau}}\mathbf{h}_{1,b}\left(\mathbf{w}_s x_s + \boldsymbol{\eta}_s\right) + \sqrt{(1-\theta)}n_a^{[r]} + n_c^{[r]}, \tag{3.11}$$

and the energy harvested by $\mathcal{R}_b$ during $T/2$ is given by

$$E_r^{PS} = \frac{\zeta\theta P_s \left\|\mathbf{h}_{1,b}\right\|^2 T}{2d_1^\tau}. \tag{3.12}$$

Relay-to-destination transmission and SNR at destination

Similar to the TSR protocol, y_r^{PS} is multiplied by a power constraint factor $G_r^{PS} = \left(\frac{(1-\theta)P_s\left\|\mathbf{h}_{1,b}\right\|^2}{d_1^\tau}\left(1+\kappa_s^2\right)+\sigma_{n_{2,r}}^2\right)^{-1/2}$ before forwarding $G_r^{PS}y_r^{PS}$ to $\mathcal{D}$, where $n_{2,r} := \sqrt{(1-\theta)}n_r^{[a]} + n_r^{[c]}$ and $\sigma_{n_{2,r}}^2 := (1-\theta)\,\sigma_{n_r^{[a]}}^2 + \sigma_{n_r^{[c]}}^2$. Thus, the received signal at $\mathcal{D}$ can be expressed as

$$\mathbf{y}_d^{PS} = \sqrt{\frac{P_r^{PS}}{d_2^\tau}}\mathbf{h}_{2,b}\left(G_r^{PS}y_r^{PS} + \eta_r\right) + \mathbf{n}_d, \tag{3.13}$$

where $P_r^{PS} = \frac{2E_r^{PS}}{T}$.

The received signal of $\mathcal{D}$ after MRC is expressed as

$$x_d^{PS} = \mathbf{w}_d\mathbf{y}_d^{PS} = \sqrt{\frac{P_r^{PS}\left\|\mathbf{h}_{2,b}\right\|^2}{d_2^\tau}}\left(G_r^{PS}y_r^{PS} + \eta_r\right) + \mathbf{w}_d\mathbf{n}_d. \tag{3.14}$$

From (3.11), (3.12), (3.13) and (3.14), the instantaneous end-to-end SNR for the PSR protocol can be evaluated as

$$\gamma_{e2e}^{PS} = \frac{\mathrm{a}^{PS}\left\|\mathbf{h}_{1,b}\right\|^4\left\|\mathbf{h}_{2,b}\right\|^2}{\mathrm{a}^{PS}\kappa_{AF}^2\left\|\mathbf{h}_{1,b}\right\|^4\left\|\mathbf{h}_{2,b}\right\|^2 + \mathbb{b}^{PS}\left\|\mathbf{h}_{1,b}\right\|^2\left\|\mathbf{h}_{2,b}\right\|^2 + \left\|\mathbf{h}_{1,b}\right\|^2 + \mathbb{c}^{PS}}, \tag{3.15}$$

where $\mathrm{a}^{PS} = \frac{\zeta\theta P_s}{d_1^\tau d_2^\tau\sigma_{\mathbf{n}_d}^2(1+\kappa_s^2)}$, $\mathbb{b}^{PS} = \frac{\zeta\theta\sigma_{n_{2,r}}^2\left(1+\kappa_r^2\right)}{d_2^\tau(1-\theta)\sigma_{\mathbf{n}_d}^2(1+\kappa_s^2)}$, and $\mathbb{c}^{PS} = \frac{d_1^\tau\sigma_{n_{2,r}}^2}{(1-\theta)P_s(1+\kappa_s^2)}$.

3.3 Performance Analysis

3.3.1 Outage probability

Since the exact analysis appears to be difficult, an alternative approach is deriving the tight lower bound of the OP by analyzing the upper bound of the end-to-end SNR $\gamma^w_{e2e,up}, w = \{TS, PS\}$. From (3.10) and (3.15), $\gamma^w_{e2e,up}$ can be expressed as

$$\gamma^w_{e2e,up} = \frac{\mathbb{a}^w \left\|\mathbf{h}_{1,b}\right\|^2 \left\|\mathbf{h}_{2,b}\right\|^2}{\mathbb{a}^w \kappa^2_{AF} \left\|\mathbf{h}_{1,b}\right\|^2 \left\|\mathbf{h}_{2,b}\right\|^2 + \mathbb{b}^w \left\|\mathbf{h}_{2,b}\right\|^2 + 1}. \tag{3.16}$$

As shown in (3.16) that the effect of RTRI levels on $\gamma^w_{e2e,up}$ can be represented by κ^2_{AF}. Then, the lower bound of the outage probability is evaluated as

$$\mathcal{P}^w_{out,low}(\gamma) = F_{\gamma^w_{e2e,up}}(\gamma) = \Pr\left\{\left\|\mathbf{h}_{2,b}\right\|^2 \left(\hat{\mathbb{a}}^w \left\|\mathbf{h}_{1,b}\right\|^2 - \mathbb{b}^w\right) < 1\right\}, \tag{3.17}$$

where $F_{\gamma^w_{e2e,up}}(\cdot)$ denotes the CDF of $\gamma^w_{e2e,up}$ and $\hat{\mathbb{a}}^w = \mathbb{a}^w \left(\frac{1}{\gamma} - \kappa^2_{AF}\right)$.

Proposition 3.1 If $\gamma \geqslant \kappa^{-2}_{AF}$, the tight lower bounds on the OPs for the PRS-1 scheme, $\mathcal{P}^{w,1}_{out,low}$, and PRS-2 scheme, $\mathcal{P}^{w,2}_{out,low}$, are equal to 1; and if $\gamma < \kappa^{-2}_{AF}$, $\mathcal{P}^{w,1}_{out,low}$ and $\mathcal{P}^{w,2}_{out,low}$ are as follows.

$$\mathcal{P}^{w,1}_{\text{out,low}}(\gamma) = 1 - \sum_{l=0}^{N_1-1}\sum_{j=0}^{N_2-1}\sum_{u=0}^{K-1}\sum_{(p_0^{(1)}+\ldots+p_{N_1-1}^{(1)}=u)}\sum_{q=0}^{\omega_1}\frac{2(-1)^u K(\mathbb{b}\lambda_2)^{N_1+\omega_1-l-q-1}}{j!\Gamma(N_1)(u+1)^{N_1+\omega_1}}\times$$
$$\binom{N_1-1}{l}\binom{K-1}{u}\binom{u}{p_0^{(1)},\ldots,p_{N_1-1}^{(1)}}\binom{\omega_1}{q}\left(\prod_{i=0}^{N_1-1}\left(\frac{1}{i!}\right)^{p_i^{(1)}}\right)\Xi\left(\gamma;\alpha_1,\beta_{1,w},\upsilon_1,\mu_{1,w}\right), \tag{3.18}$$

$$\mathcal{P}^{w,2}_{\text{out,low}}(\gamma) = 1 - \sum_{i=0}^{N_1-1}\sum_{u=1}^{K}\sum_{(p_0^{(2)}+\ldots+p_{N_2-1}^{(2)}=u)}\frac{2(-1)^u(\mathbb{b}\lambda_2)^{N_1-i-1}}{\Gamma(N_1)u^{N_1+\omega_2-i-1}}\binom{K}{u}\binom{N_1-1}{i}\times$$
$$\binom{u}{p_0^{(2)},\ldots,p_{N_2-1}^{(2)}}\left(\prod_{i=0}^{N_2-1}\left(\frac{1}{j!}\right)^{p_j^{(2)}}\right)\Xi\left(\gamma;\alpha_2,\beta_{2,w},\upsilon_2,\mu_{2,w}\right), \tag{3.19}$$

Table 3.1: The input parameters of $\Xi(\gamma; \alpha_\epsilon, \beta_{\epsilon,w}, \upsilon_\epsilon, \mu_{\epsilon,w})$

$\boldsymbol{\epsilon}$	$\boldsymbol{\alpha_\epsilon}$	$\boldsymbol{\beta_{\epsilon,w}}$	$\boldsymbol{\upsilon_\epsilon}$	$\boldsymbol{\mu_{\epsilon,w}}$
1	$2N_1 + 2\omega_1 + j - l - q - 1$	$\frac{(u+1)\mathbb{b}}{\lambda_1 \hat{\mathbb{a}}_w}$	$l + q - j + 1$	$\frac{(u+1)}{\lambda_1 \lambda_2 \hat{\mathbb{a}}_w}$
2	$2N_1 + \omega_2 - i - 1$	$\frac{\mathbb{b}}{\lambda_1 \hat{\mathbb{a}}_w}$	$i - \omega_2 + 1$	$\frac{u}{\lambda_1 \lambda_2 \hat{\mathbb{a}}_w}$

Note: i, j, l, u and q are the loop control variables defined in (3.18) and (3.19).

where $\omega_1 = \sum_{i=0}^{N_1-1} i p_i^{(1)}$, $\omega_2 = \sum_{j=0}^{N_2-1} j p_j^{(2)}$, and $\Xi(\gamma; \alpha_\epsilon, \beta_{\epsilon,w}, \upsilon_\epsilon, \mu_{\epsilon,w}) = \mu_{\epsilon,w}^{\frac{\alpha_\epsilon}{2}} e^{-\beta_{\epsilon,w}} K_{\upsilon_\epsilon}\left(2\sqrt{\mu_{\epsilon,w}}\right)$; $\alpha_\epsilon, \beta_{\epsilon,w}, \upsilon_\epsilon$, and $\mu_{\epsilon,w}$ are given in Table 1 for $\epsilon = 1, 2$.

Proof: See Appendix B.1.

3.3.2 Throughput analysis

Delay-limited transmission mode

In the DLT mode, $\mathcal{S}$ transmits its information at a fixed rate R so that the minimum end-to-end SNR at $\mathcal{D}$ required for successful decoding is $\gamma_{\min} = 2^R - 1$. We denote the DLT throughput by $\mathcal{T}_R$. Then, using similar steps in Section 2.3.2, the upper bound of $\mathcal{T}_R$ for the TSR protocol of the PRS-m scheme can be expressed as

$$\mathcal{T}_{R,up}^{TS,m} = \frac{1}{2} R\Big(1 - \mathcal{P}_{out,low}^{TS,m}(\gamma_{\min})\Big)(1 - \alpha_T), \tag{3.20}$$

and the upper bound of $\mathcal{T}_R$ for the PSR protocol of the PRS-m scheme can be expressed as

$$\mathcal{T}_{R,up}^{PS,m} = \frac{1}{2} R\left(1 - \mathcal{P}_{out,low}^{PS,m}(\gamma_{\min})\right). \tag{3.21}$$

Delay-tolerant transmission mode

In the DTT mode, $\mathcal{S}$ sends its information at the rate equal to the ergodic capacity at $\mathcal{D}$, which is the maximum rate for successful decoding at $\mathcal{D}$. According to [30], the ergodic capacity for the TSR and PSR protocols can be approximated using the upper bound of the end-to-end SNR at $\mathcal{D}$, $\gamma^{w}_{e2e,up}$ in (3.16), as follows.

$$\mathcal{C}^{w} = \mathbb{E}\left\{\log_2\left(1+\gamma^{w}_{e2e}\right)\right\} \approx \int_{0}^{\kappa_{AF}^{-2}} \log_2\left(1+\gamma\right) f_{\gamma^{w}_{e2e,up}}\left(\gamma\right) d\gamma. \tag{3.22}$$

From the expressions of outage probability, the calculation in (3.22) is mostly focused on solving $\Upsilon\left(\alpha_\epsilon, \beta_{\epsilon,w}, \upsilon_\epsilon, \mu_{\epsilon,w}\right) = \int_{0}^{\kappa_{AF}^{-2}} \log_2\left(1+\gamma\right)\left(\frac{d\Xi(\gamma;\alpha_\epsilon,\beta_{\epsilon,w},\upsilon_\epsilon,\mu_{\epsilon,w})}{d\gamma}\right) d\gamma$.

Proposition 3.2 $\Upsilon\left(\alpha_\epsilon, \beta_{\epsilon,w}, \upsilon_\epsilon, \mu_{\epsilon,w}\right)$ can be calculated as

$$\begin{aligned}
&\Upsilon\left(\alpha_\epsilon, \beta_{\epsilon,w}, \upsilon_\epsilon, \mu_{\epsilon,w}\right) = \tfrac{(\alpha_\epsilon-\upsilon_\epsilon)\hat{\mu}_{\epsilon,w}}{2}\Lambda\left(\alpha_\epsilon-2, \beta_{\epsilon,w}, \upsilon_\epsilon, \mu_{\epsilon,w}\right)\\
&-\hat{\mu}_{\epsilon,w}\Lambda\left(\alpha_\epsilon-1, \beta_{\epsilon,w}, \upsilon_\epsilon-1, \mu_{\epsilon,w}\right) + \left((\alpha_\epsilon-\upsilon_\epsilon)\kappa_{AF}^2 - \hat{\beta}_{\epsilon,w}\right)\Lambda\left(\alpha_\epsilon, \beta_{\epsilon,w}, \upsilon_\epsilon, \mu_{\epsilon,w}\right)\\
&-2\kappa_{AF}^2\Lambda\left(\alpha_\epsilon+1, \beta_{\epsilon,w}, \upsilon_\epsilon-1, \mu_{\epsilon,w}\right) + \tfrac{((\alpha_\epsilon-\upsilon_\epsilon)\kappa_{AF}^2-4\hat{\beta}_{\epsilon,w})\kappa_{AF}^2}{2\hat{\mu}_{\epsilon,w}}\Lambda\left(\alpha_\epsilon+2, \beta_{\epsilon,w}, \upsilon_\epsilon, \mu_{\epsilon,w}\right)\\
&-\tfrac{\kappa_{AF}^4}{\hat{\mu}_{\epsilon,w}}\Lambda\left(\alpha_\epsilon+3, \beta_{\epsilon,w}, \upsilon_\epsilon-1, \mu_{\epsilon,w}\right) - \tfrac{\hat{\beta}_{\epsilon,w}\kappa_{AF}^4}{\hat{\mu}_{\epsilon,w}^2}\Lambda\left(\alpha_\epsilon+4, \beta_{\epsilon,w}, \upsilon_\epsilon, \mu_{\epsilon,w}\right),
\end{aligned} \tag{3.23}$$

where $\Lambda\left(\alpha_\epsilon, \beta_{\epsilon,w}, \upsilon_\epsilon, \mu_{\epsilon,w}\right) = \int_{0}^{\kappa_{AF}^{-2}} \log_2(1+\gamma)\Xi\left(\gamma;\alpha_\epsilon, \beta_{\epsilon,w}, \upsilon_\epsilon, \mu_{\epsilon,w}\right) d\gamma$, $\hat{\beta}_{w,\epsilon} = \beta_{w,\epsilon}\hat{\mathrm{a}}^{w}/\mathrm{a}^{w}$, and $\hat{\mu}_{w,\epsilon} = \mu_{w,\epsilon}\hat{\mathrm{a}}^{w}/\mathrm{a}^{w}$.

Proof: See Appendix B.2.

Proposition 3.3 The ergodic capacity for the TSR and PSR protocols of the PRS-1

scheme $\mathcal{C}^{w,1}$ and PRS-2 scheme $\mathcal{C}^{w,2}$ are as follows.

$$\mathcal{C}^{w,1} \approx -\sum_{l=0}^{N_1-1}\sum_{j=0}^{N_2-1}\sum_{u=0}^{K-1}\sum_{(p_0^{(1)}+\ldots+p_{N_1-1}^{(1)}=u)}\sum_{q=0}^{\omega_1}\frac{2(-1)^u K(\mathbb{b}\lambda_2)^{N_1+\omega_1-l-q-1}}{j!\Gamma(N_1)(u+1)^{N_1+\omega_1}}\binom{N_1-1}{l}$$
$$\times\binom{K-1}{u}\binom{u}{p_0^{(1)},\ldots,p_{N_1-1}^{(1)}}\binom{\omega_1}{q}\left(\prod_{i=0}^{N_1-1}\left(\frac{1}{i!}\right)^{p_i^{(1)}}\right)\Upsilon\left(\alpha_1,\beta_{1,w},\upsilon_1,\mu_{1,w}\right), \quad (3.24)$$

$$\mathcal{C}^{w,2} \approx -\sum_{i=0}^{N_1-1}\sum_{u=1}^{K}\sum_{(p_0^{(2)}+\ldots+p_{N_2-1}^{(2)}=u)}\frac{2(-1)^u(\mathbb{b}\lambda_2)^{N_1-i-1}}{\Gamma(N_1)u^{N_1+\omega_2-i-1}}\binom{K}{u}\binom{N_1-1}{i}$$
$$\times\binom{u}{p_0^{(2)},\ldots,p_{N_2-1}^{(2)}}\left(\prod_{j=0}^{N_2-1}\left(\frac{1}{j!}\right)^{p_j^{(2)}}\right)\Upsilon\left(\alpha_2,\beta_{2,w},\upsilon_2,\mu_{2,w}\right). \quad (3.25)$$

Proof: Substituting the result of Lemma 1 into the derivative of (3.18) and (3.19), we can derive the PDF of $\gamma_{e2e,up}^{w}$ for the PRS-1 and PRS-2 schemes, respectively. Then, the ergodic capacity for these PRS schemes can be formulated.

Similar to $\mathcal{T}_R$, the throughput in the delay-tolerant mode $\mathcal{T}_{erg}$ for the TSR and PSR protocols of the PRS-m scheme can be respectively expressed as follows.

$$\mathcal{T}_{erg}^{TS,m} = \frac{1}{2}\mathcal{C}^{TS,m}(1-\alpha_T), \quad (3.26)$$

$$\mathcal{T}_{erg}^{PS,m} = \frac{1}{2}\mathcal{C}^{PS,m}. \quad (3.27)$$

3.4 Results and Discussion

In this section, we present the numerical results to validate the analytical expressions of the system performance presented in Section 3.3. Unless otherwise specified, we set $K=5, \eta=0.5, N_1=N_2=2, \alpha_T=0.2, \theta=0.5, d_1=d_2=1, \tau=3, \lambda_1=\lambda_2=1, \kappa_s^2=\kappa_r^2=\kappa_0^2$ and $\sigma_{n_r^{[a]}}^2=\sigma_{\mathbf{n}_d^{[a]}}^2=\sigma_{n_r^{[a]}}^2=\sigma_{\mathbf{n}_d^{[a]}}^2=\sigma_0^2=0.5$.

Figure 3.2 presents the OP of the proposed system versus κ_0^2. It can be observed that the OP is a decreasing function of K, N_1 and N_2, whereas it is an increasing function of κ_0^2. In the case of increasing K, N_1 and/or N_2, the OP is reduced owing to the improvement of the channel gains of $\mathcal{R}_b$; while in the case of increasing κ_0^2, the degradation of the end–to–end SNR cause the OP to increase. At a given value of γ, when the RTRI levels are high enough (i.e., $\kappa_{AF}^2 \geqslant \frac{1}{\gamma}$), a^w becomes non–positive; therefore, $\mathcal{D}$ cannot successfully decode the received signal (see equation (3.17)). It can be seen from Figure 3.2 that when κ_0^2 reaches a threshold value $\breve{\kappa}_0^2 = \sqrt{1+\frac{1}{\gamma}}-1 \approx 0.147$ (this is the valid root of $\kappa_{AF}^2 = \frac{1}{\gamma}$ in the case of Figure 3.2), the OP approaches zero. Comparing the PRS–1 and PRS–2 schemes, the outage performance of the PRS–1 scheme is better than that of the PRS–2 scheme. This is because $\mathcal{R}_b$ in the PRS–1 scheme can exploit spatial diversity in energy harvesting. Moreover, increasing N_1 gives a better performance than increasing N_2.

Figure 3.3 illustrates the effects of α_T and of θ on the DLT and DTT throughputs. Specifically, the optimal energy-harvesting time α_T^* and the optimal PS ratio θ^* that maximize the throughput are obtained using the GSS method with the tolerance $\varepsilon = 10^{-3}$. The trends of the throughput in Figure 3.3 are similar to that in Figure 2.4. The effects of α_T and θ on the trend of the throughput were explained in the discussion of Figure 2.4. For both the PSR and TSR protocols, the PRS–1 scheme always yields better throughput than the PRS–2 scheme. Moreover, as shown in Figure 3.3 that $\mathcal{T}_{erg}$ is always higher than $\mathcal{T}_R$.

Figure 3.4 illustrates the impact of κ_0^2 on the optimal DLT throughput $\mathcal{T}_R^*$ and the optimal DTT throughput $\mathcal{T}_{erg}^*$. The general trends of these optimal throughputs

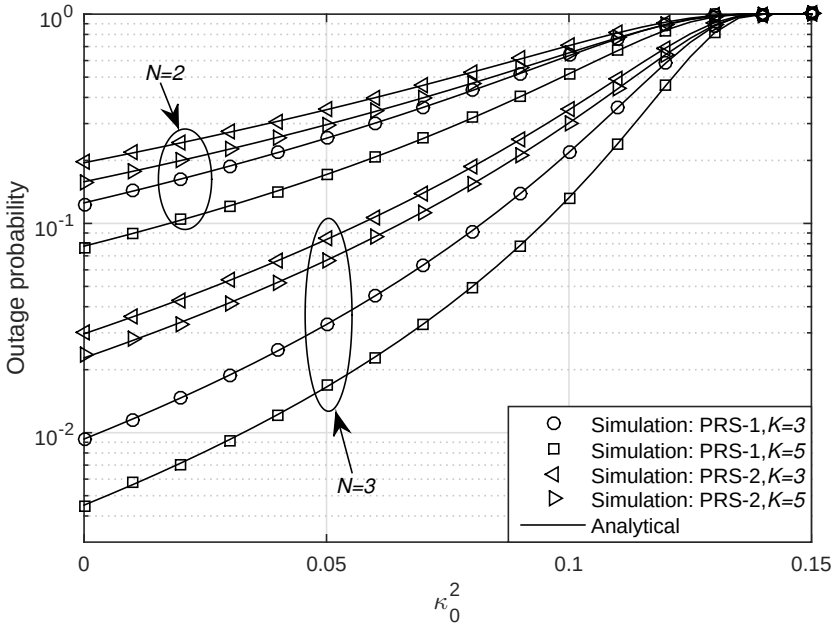

(a)

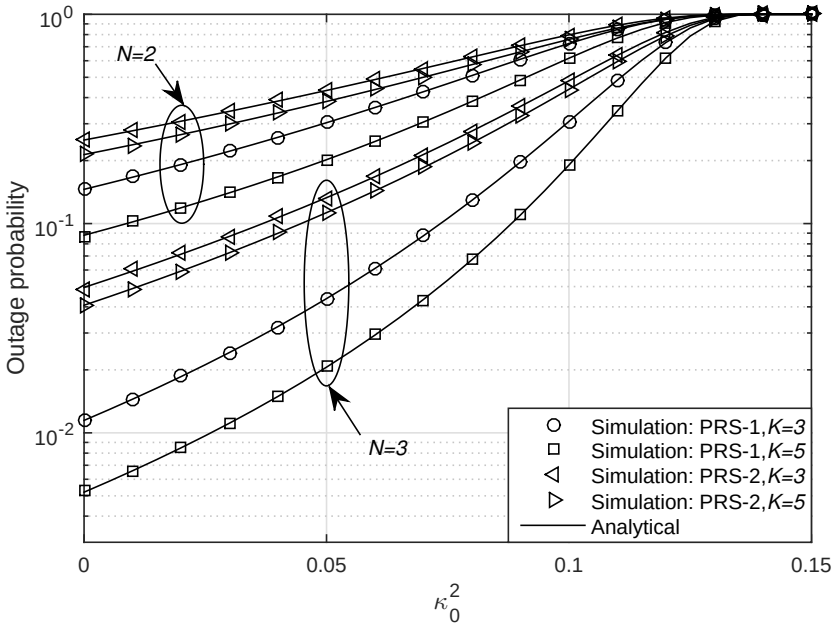

(b)

Figure 3.2: The outage probability versus κ_0^2 for the (a) TSR and (b) PSR protocols. Other parameters: $P_s/2\sigma_0^2 = 10(dB)$ and $\gamma = 5(dB)$.

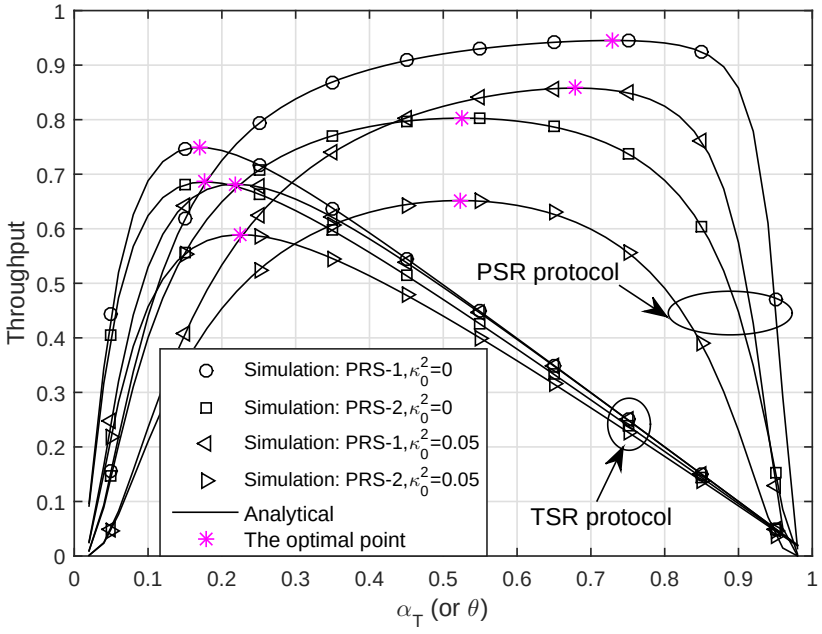

(a)

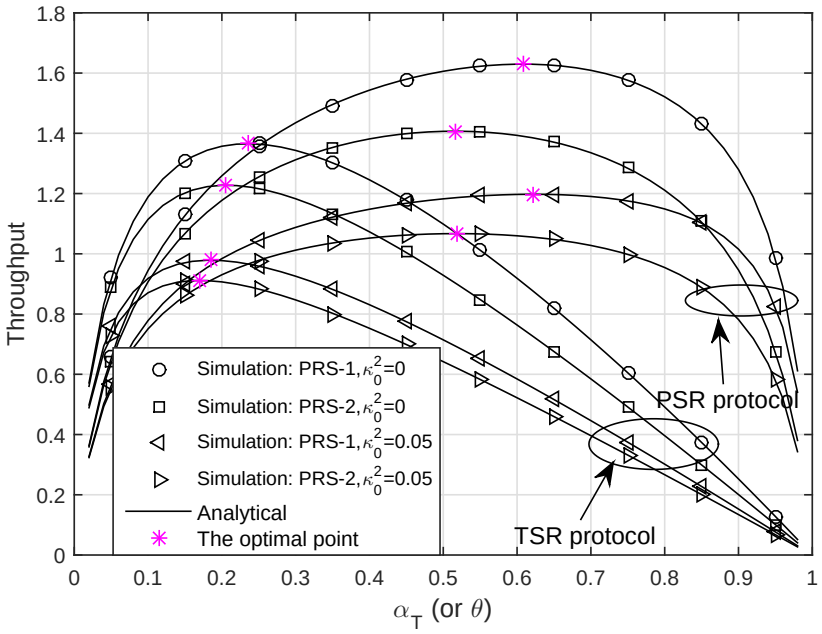

(b)

Figure 3.3: The effects of α_T (TSR protocol) and θ (PSR protocol) on the throughput in the (a) DLT and (b) DTT modes. Other parameters: $R = 2(bits/s/Hz)$ and $P_s/2\sigma_0^2 = 10(dB)$.

are decreasing trends of κ_0^2. For a given system configuration, $\mathcal{T}_{erg}^*$ is higher than $\mathcal{T}_R^*$, and the PRS–1 scheme gives greater throughput than the PRS–2 scheme. In the DLT mode, the PSR protocol performs better than the TSR protocol at low RTRI levels; however, at high RTRI levels, the TSR protocol is more efficient than the PSR protocol. This is because for the PSR protocol, a strong effect of η_r on a portion of the received signal strength of $\mathcal{R}_b$ causes a significantly decrease in the throughput performance (see Eq. (3.11) and (3.13)). Moreover, $\mathcal{T}_R^*$ approaches zero when κ_0^2 reaches a threshold value $\hat{\kappa}_0^2 = \sqrt{2^R/(2^R-1)} - 1$ (this is the valid root of $\kappa_{AF}^2 = \frac{1}{\gamma_{min}}$), and the value of $\hat{\kappa}_0^2$ becomes smaller as R increases. On the other hand, in the DTT mode, the optimal throughput for the PSR protocol is always higher than that for the TSR protocol, and the limit of $\mathcal{T}_{erg}^*$ is close but not equal to zero. In reality, the RTRI levels are fixed when the hardware is selected; therefore, these results provide valuable comprehension for hardware choosing. For example, it can be seen from Figure 3.4 that we must chose the hardware that satisfies $\kappa_0^2 < 0.155$ and $\kappa_0^2 < 0.069$ for $R = 2bits/s/Hz$ and $R = 3bits/s/Hz$, respectively, to achieve a positive DLT throughput.

Figure 3.5 presents the effect of the number of relays K on the optimal DLT throughput and optimal DTT throughputs. It can be seen that the optimal throughput is an increasing function of K. This is because when K increases, $\mathcal{R}_b$ can get better channel gains; hence, the end–to–end SNR can be improved. Moreover, the increase of the optimal throughput slows down as K increases. These results provide insight into practical design on the choice of K. In reality, using many relays causes a lot problems, such as high system complexity, high power for setup phase P_{setup} which

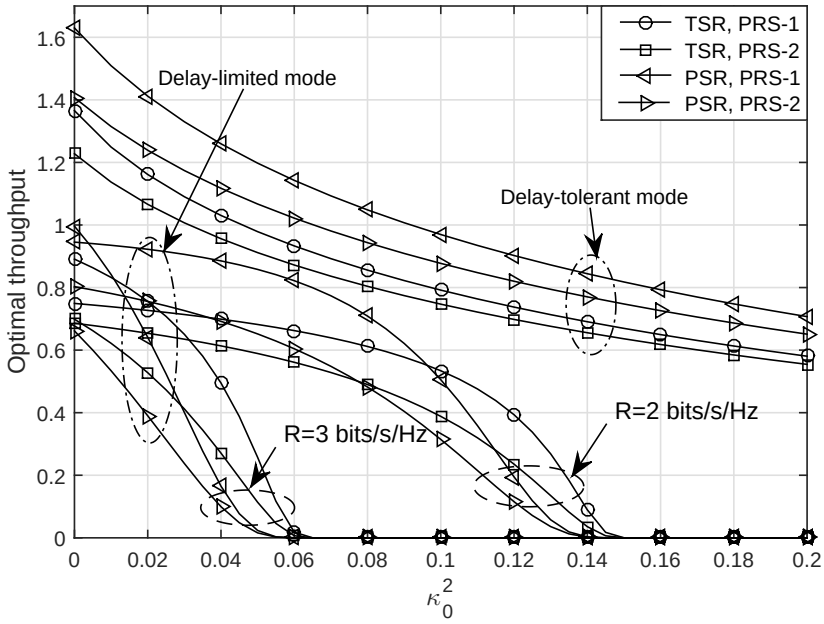

Figure 3.4: The optimal throughput versus κ_0^2. Other parameters: $P_s/2\sigma_0^2 = 10(dB)$.

uses for CSI acquisition, relay–selection process. To solve these problems, instead of using many relays, a sufficient number of relays should be chosen to achieve great advantages of using multiple relays with low system complexity and low P_{setup}. In particular, K should be set at 5 or 6 in the case of Figure 3.5; and with these settings, P_{setup} is negligible as compared to the power used for data transmission which does not change as K increases.

Figure 3.6 presents the impact of R on the DLT throughput. The analytical and simulation results shown in Figures 3.6(a) and 3.6(b) are respectively prepared by varying R from 0.1 to 7.9 (bits/s/Hz) by steps of 0.1 (bits/s/Hz) and from 1 to 7 (bits/s/Hz) by steps of 1 (bits/s/Hz). The optimal data rate R_{opt} that maximizes $\mathcal{T}_R$ was obtained by using GSS method. In both subfigures, $\mathcal{T}_R$ follows bell curves. When R is smaller than R_{opt}, due to the small effect of the OP, $\mathcal{T}_R$ is an increasing function

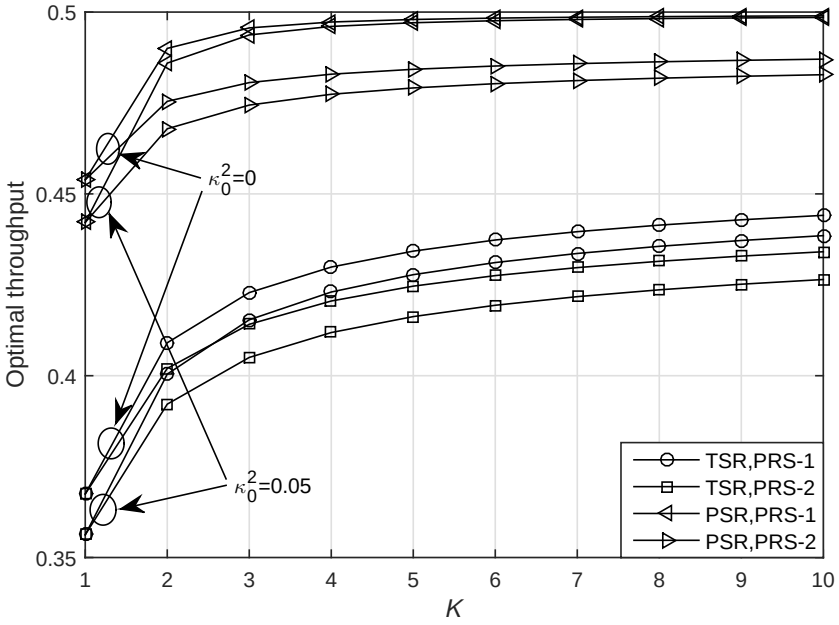

(a)

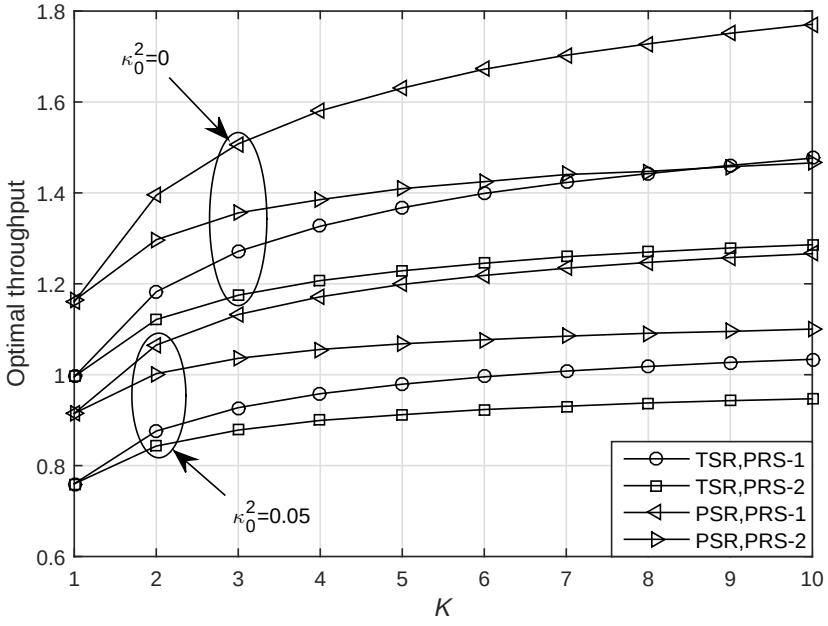

(b)

Figure 3.5: The optimal throughput versus K for the (a) DLT and (b) DTT modes. Other parameters: $P_s/2\sigma_0^2 = 10(dB)$, and $R = 1(bits/s/Hz)$.

of R. In contrast, when R is higher than R_{opt}, because the OP rapidly increase with increasing R, $\mathcal{T}_R$ becomes a decreasing function of R. Moreover, in the case of existing RTRI, if $R \geqslant \hat{R} = \log_2(1+\kappa_{AF}^{-2})$ the throughput is approximately zero. It can be seen from Figure 3.6 that, in the case of $\kappa_0^2 = 0.05$, $\mathcal{T}_R \approx 0$ as $R \to \hat{R} \approx 3.43 bits/s/Hz$.

3.5 Conclusions

In this Chapter, we studied the effects of RTRI on an AF relaying WEH–CC system with PRS. We derived the analytical expressions for the three performance metrics, i.e., the OP, DLT throughput and DTT throughput, for both TSR and PSR protocols. These analytical results allow us to understand different influences of RTRI on the system performance and provide insight into practical designs of our proposed system. The accuracy of our analysis was verified by the Monte Carlo simulations. The results showed that:

- The system performance is notably affected by RTRI; especially at high transmission rates, the throughput drastically decreases.
- The impact of RTRI can be significantly reduced by increasing the number of antennas and relays.
- The PRS–1 scheme outperforms the PRS–2 scheme, and increasing the number of source antennas is more efficient than increasing the number of destination antennas.
- In the delay–limited mode, the TSR protocol performs better than the PSR

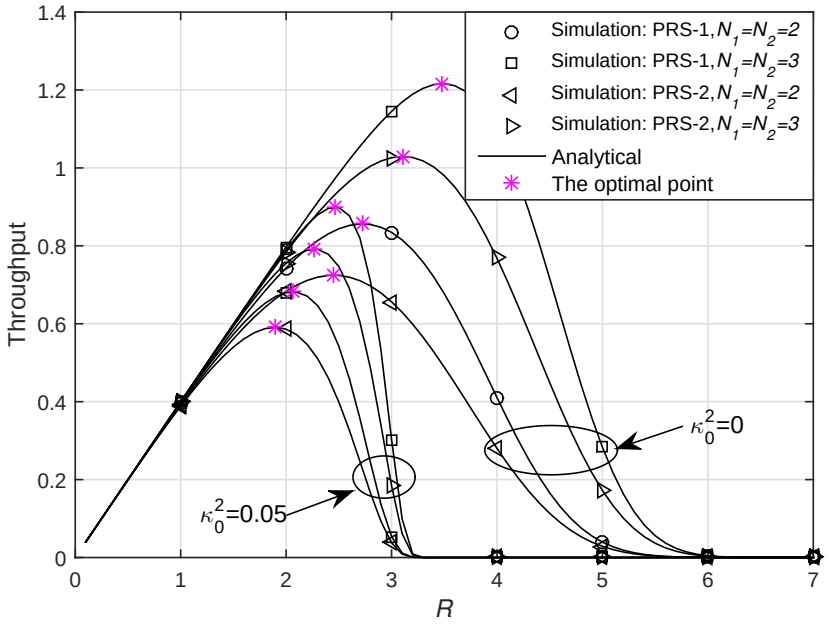

(a)

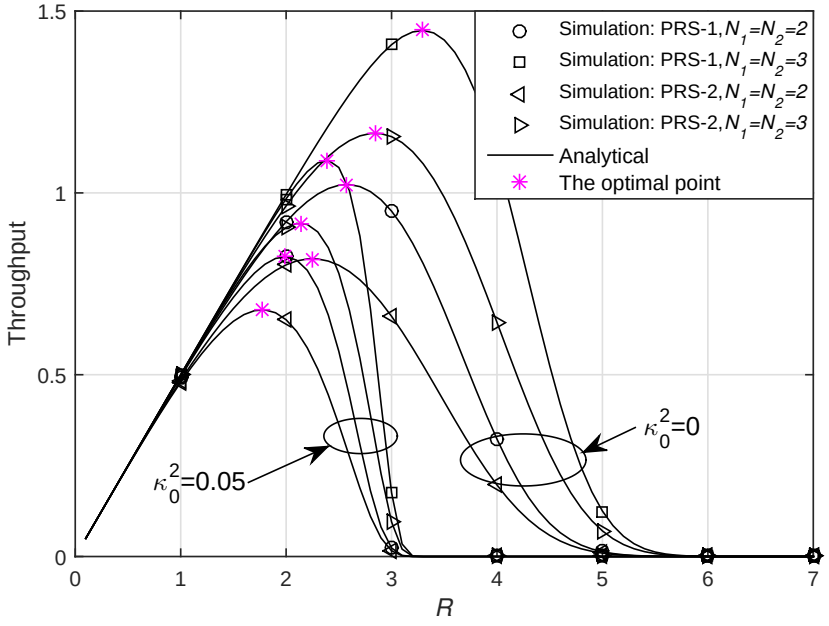

(b)

Figure 3.6: The DLT throughput versus $R(bits/s/Hz)$ for the (a) TSR and (b) PSR protocols. Other parameters: $P_s/2\sigma_0^2 = 10(dB)$.

protocol at high impairment levels, whereas in the delay–tolerant mode, the throughput of the PSR protocol is always superior to that of the TSR protocol.

Finally, the impact of various key system parameters, such as K, source rate, TS fraction and θ, were examined to provide useful designs.

Chapter 4

Secure communication via a wireless energy-harvesting untrusted relay with imperfect CSI

[1]

4.1 Introduction

The broadcast nature of wireless signal makes it become a potential energy source for prolonging the lifetime of the wireless energy–constrained network; however, it also causes the wireless medium to become insecure. For that reason, security in WEH networks has recently become an interesting research direction and received a lot attention from the researchers. The studies relevant to PLS in WEH and WEH–CC

[1]The study in this chapter was published in Annals of Telecommunications [89]

networks were discussed in Chapter 1. In this dissertation, we focus on another aspect of PLS in WEH–CC networks, namely, secure communication of Untrusted Relaying Wireless Energy Harvesting (UR–WEH) networks. Moreover, we expand our investigation to practical scenarios. Specifically, this Chapter (Chapter 3) evaluates the secure performance of the UR–WEH system with the imperfect CSI; Chapter 4 examines the secure performance of the UR–WEH system in the presence of an external eavesdropper; and Chapter 5 studies the effects of RSS on the secure performance of the UR–WEH system.

In this Chapter, we investigate an UR–WEH system including a multi–antenna source, a single–antenna destination and a single–antenna untrusted relay. The relay is an AF WEH node. To exploit the benefit of using multiple antennas at the source, two multiple–antenna schemes, TAS and MRT, are employed; moreover, a RAS scheme is considered at the source for performance comparison. Although the use of multiple antennas improves the secrecy performance, it can cause the imperfect CSI. Thus, the CSI of the soure–to–relay link is examined in two cases: perfect CSI and imperfect CSI, whereas the CSI of the relay–to–destination link is assumed to be perfect. To create positive secrecy capacity, a destination–assisted jamming signal that is completely cancelled at the destination is adopted. Moreover, the jamming signal is also exploited as an additional energy source. The PS receiver architecture is adopted. The secrecy performance is evaluated by analyzing the SOP and ASC. To accomplish this, we derive the SOP expressions involving a single integral and a tight closed–form upper bound for the ASC. Moreover, closed–form expressions for the SOP at high power levels are also derived. The accuracy of the analytical results

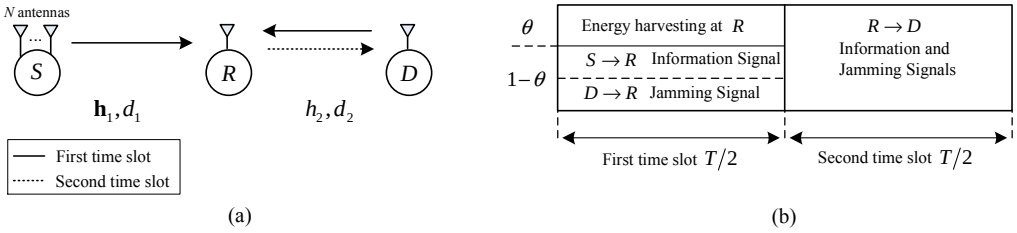

Figure 4.1: System model.

is verified by Monte Carlo simulations.

The rest of this Chapter is organized as follows. The system model is presented in Section 4.2. The analytical expressions for the SOP and ASC are derived in Section 4.3. The results and discussion are given in Section 4.4. Finally, the conclusions are presented in Section 4.5.

4.2 System Model

We consider an UR–WEH system illustrated in Figure 4.1(a). Our system consists of a multi-antenna source S, that is equipped with N antennas, a single-antenna destination D and a single-antenna untrusted relay R. R uses the PS policy shown in Figure 4.1(b) to harvest energy and uses the AF protocol to forward the source's signal. In each block time T, the entire communication consists of two time slots, $T/2$. During the first time slot, R harvests energy and decodes information with a PS ratio $0 < \theta < 1$. Then, R uses all harvested energy to forward the received signal to D during the second time slot.

Throughout this Chapter, we assume that: 1) no direct link between S and D exists; 2) the channels follow independent and identical Rayleigh distributions, hence,

the channel gains are exponential RVs; 3) the CSI of the S–R link is examined in two cases: perfect CSI and imperfect CSI (because of using N antennas at S) whereas the CSI of the R–D link is perfect; and 4) a local CSI is required at S and R, and the full CSI and the value of transmit power at R are assumed to be available at D. Because the received signal at D in the AF protocol contains both the S–R and R–D CSI [90], the full CSI at D is a necessary condition to successfully decode the source signal. Moreover, since the S–R CSI can be imperfect, R sends the value of its transmit power to D for decoding the source signal optimally.

We denote $\mathbf{h}_1 = [h_{1,1}, \ldots, h_{1,N}]$ as the channel vector between S and R during the channel estimation and feedback process. The elements of $\mathbf{h}_1$ follow i.i.d. $\mathcal{CN}(0, \lambda_1^{-1})$ where $\lambda_1 = d_1^{\tau}$, d_1 is the normalized distance between S and R, and τ is the path loss exponent. We denote $\tilde{\mathbf{h}}_1$ as the time-delayed version of $\mathbf{h}_1$. Mathematically, $\tilde{\mathbf{h}}_1$ can be modeled as

$$\tilde{\mathbf{h}}_1 = \sqrt{\zeta \mathbf{h}_1} + \sqrt{1-\zeta}\mathbf{e}, \tag{4.1}$$

where $\zeta \in [0, 1]$ is the channel correlation coefficient, and $\mathbf{e}$ is an error vector in which the elements of $\mathbf{e}$ are i.i.d. $\mathcal{CN}(0, \lambda_1^{-1})$. We also denote $h_2 \sim \mathcal{CN}(0, \lambda_2^{-1})$ as the channel between R and D where $\lambda_2 = d_2^{\tau}$ and d_2 is the normalized distance between R and D.

We investigate two transmit antenna schemes, TAS and MRT. In addition, the RAS scheme is also considered for performance comparison. In the RAS scheme, S randomly chooses an antenna to transmit its signal x_s, whereas, in the TAS scheme, S selects the best antenna, denoted by the n^*–th antenna, to transmit x_s, which

satisfies the condition given by

$$n^* = \underset{1 \leqslant n \leqslant N}{\arg\max} \left\{ |h_{1,n}|^2 \right\}. \tag{4.2}$$

In the MRT scheme, S calculates a weight vector $\mathbf{w} = \frac{\mathbf{h}^\dagger}{\|\mathbf{h}\|}$ and applies $\mathbf{w}$ to x_s before transmitting x_s on N antennas in the data transmission phase.

4.2.1 Communication in the first time slot

The received signal at R for three transmit antenna schemes in the first time slot is given by

$$y_r = \begin{cases} \tilde{h}_{1,ran}\sqrt{(1-\theta)\,P_s}x_s + h_2\sqrt{(1-\theta)\,P_d}x_d + n_r & ;\text{(RAS)} \\ \tilde{h}_{1,n*}\sqrt{(1-\theta)\,P_s}x_s + h_2\sqrt{(1-\theta)\,P_d}x_d + n_r & ;\text{(TAS)} \\ \tilde{\mathbf{h}}_1\mathbf{w}_1\sqrt{(1-\theta)\,P_s}x_s + h_2\sqrt{(1-\theta)\,P_d}x_d + n_r & ;\text{(MRT)} \end{cases}, \tag{4.3}$$

where P_s and P_d are the transmit powers of S and D, respectively, x_d is the AN of D, and $n_r \sim \mathcal{CN}(0, \sigma_0^2)$ is the AWGN at R. Using (4.1), we can rewrite (4.3) as

$$y_r = \begin{cases} h_{1,ran}\sqrt{\zeta\,(1-\theta)\,P_s}x_s + e\sqrt{(1-\zeta)\,(1-\theta)\,P_s}x_s & \\ \qquad + h_2\sqrt{(1-\theta)\,P_d}x_d + n_r & ;\text{(RAS)} \\ h_{1,n*}\sqrt{\zeta\,(1-\theta)\,P_s}x_s + e\sqrt{(1-\zeta)\,(1-\theta)\,P_s}x_s & \\ \qquad + h_2\sqrt{(1-\theta)\,P_d}x_d + n_r & ;\text{(TAS)} \\ \mathbf{h}_1\mathbf{w}_1\sqrt{\zeta\,(1-\theta)\,P_s}x_s + \mathbf{e}\mathbf{w}_1\sqrt{(1-\zeta)\,(1-\theta)\,P_s}x_s & \\ \qquad + h_2\sqrt{(1-\theta)\,P_d}x_d + n_r & ;\text{(MRT)} \end{cases}. \tag{4.4}$$

For notational convenience, we define X_1 and $\tilde{X}_1$ as follows.

$$X_1 = \begin{cases} |h_{1,\text{ran}}|^2 & ;\text{(RAS)} \\ |h_{1,n^*}|^2 & ;\text{(TAS)} \\ \|\mathbf{h}_1\mathbf{w}_1\|^2 & ;\text{(MRT)} \end{cases}, \text{ and } \tilde{X}_1 = \begin{cases} |\tilde{h}_{1,\text{ran}}|^2 & ;\text{(RAS)} \\ |\tilde{h}_{1,n^*}|^2 & ;\text{(TAS)} \\ \|\tilde{\mathbf{h}}_1\mathbf{w}_1\|^2 & ;\text{(MRT)} \end{cases}. \tag{4.5}$$

Then, the harvested energy at R is calculated as

$$E_h = \eta\theta YT/2, \tag{4.6}$$

where η is the RF–to–DC conversion efficiency, $Y = P_s\tilde{X}_1 + P_dX_2$ and $X_2 = |h_2|^2$.

From (4.4), the Signal to Interference plus Noise Ratio (SINR) at R can be expressed as

$$\gamma_r = \frac{\zeta(1-\theta)\rho_s X_1}{(1-\theta)\rho_d X_2 + \mu}, \tag{4.7}$$

where $\rho_s = P_s/\sigma_0^2, \rho_d = P_d/\sigma_0^2$, and $\mu = (1-\zeta)(1-\theta)\frac{\rho_s}{\lambda_1} + 1$.

4.2.2 Communication in the second time slot

In the second time slot, R uses all harvested energy in (4.6) to forward its received signal; therefore, the transmit power of R is $P_r = 2E_h/T = \eta\theta Y$. The received signal at D is given by

$$y_d = \sqrt{P_r}h_2Gy_r + n_d, \tag{4.8}$$

where $G = 1/\sqrt{\kappa P_r + \sigma_0^2}$ with $\kappa = (1-\theta)/\eta\theta$. Substituting (4.4) into (4.8) yields

$$y_d = \begin{cases} \underbrace{h_{1,ran} h_2 \sqrt{\zeta\,(1-\theta)\,P_s P_r} G x_s}_{\text{desired signal}} + \underbrace{h_2^2 \sqrt{(1-\theta)\,P_d P_r} G x_d}_{AN} \\ \quad + \underbrace{e h_2 \sqrt{(1-\zeta)\,(1-\theta)\,P_s P_r} G x_s + h_2 \sqrt{P_r} G n_r + n_d}_{\text{overall noise}} \quad ; \text{(RAS)} \\ \underbrace{h_{1,n*} h_2 \sqrt{\zeta\,(1-\theta)\,P_s P_r} G x_s}_{\text{desired signal}} + \underbrace{h_2^2 \sqrt{(1-\theta)\,P_d P_r} G x_d}_{AN} \\ \quad + \underbrace{e h_2 \sqrt{(1-\zeta)\,(1-\theta)\,P_s P_r} G x_s + h_2 \sqrt{P_r} G n_r + n_d}_{\text{overall noise}} \quad ; \text{(TAS)} \\ \underbrace{\mathbf{h}_1 \mathbf{w}_1 h_2 \sqrt{\zeta\,(1-\theta)\,P_s P_r} G x_s}_{\text{desired signal}} + \underbrace{h_2^2 \sqrt{(1-\theta)\,P_d P_r} G x_d}_{AN} \\ \quad + \underbrace{\mathbf{e}\mathbf{w}_1 h_2 \sqrt{(1-\zeta)\,(1-\theta)\,P_s P_r} G x_s + h_2 \sqrt{P_r} G n_r + n_d}_{\text{overall noise}} \quad ; \text{(MRT)} \end{cases} . \tag{4.9}$$

Because D can eliminate the AN in (4.9) and $\mathbb{E}\{\mathbf{e}\mathbf{w}_1 (\mathbf{e}\mathbf{w})^*\} = \lambda_1^{-1}$, the end-to-end SNR at D is calculated as

$$\gamma_d = \frac{\zeta\,(1-\theta)\,\rho_s X_1 X_2 P_r}{P_r\,(X_2\mu + \kappa) + \sigma_0^2} \approx \frac{\zeta\,(1-\theta)\,\rho_s X_1 X_2}{X_2\mu + \kappa}. \tag{4.10}$$

The approximation in (4.10) is acceptable because the noise variance term is negligible compared to the other factors in the denominator.

4.3 Performance Analysis

4.3.1 Secrecy outage probability

Using (1.14), the instantaneous secrecy rate of the proposed system is given by

$$R_{\text{sec}} = [\mathcal{C}_{\text{d}} - \mathcal{C}_{\text{r}}]^+, \tag{4.11}$$

where $\mathcal{C}_d = \log_2(1+\gamma_d)$, and $\mathcal{C}_r = \log_2(1+\gamma_r)$. Then, the SOP is given by

$$\begin{aligned}\text{SOP} &= \Pr(R_{\text{sec}} < R_{\text{th}}) = \Pr(\zeta(1-\theta)\rho_s X_1 \Xi(X_2;\beta) < \beta - 1) \\ &= 1 - \Pr\left(X_1 > \frac{\beta-1}{\zeta(1-\theta)\rho_s \Xi(X_2;\beta)} | X_2 > \bar{x}_1\right), \end{aligned} \tag{4.12}$$

where $\beta = 2^{R_{th}}$, $\Xi(x;\beta) = \frac{x}{\mu x+\kappa} - \frac{\beta}{x(1-\theta)\rho_d+\mu}$, and $\bar{x}_1 = \frac{\mu(\beta-1)+\sqrt{\mu^2(\beta-1)^2+4\beta(1-\theta)\rho_d\kappa}}{2(1-\theta)\rho_d}$ is the positive root of the equation $\Xi(x;\beta) = 0$.

Proposition 4.1 The SOPs of the RAS, TAS, and MRT schemes are expressed as

$$\text{SOP}_{\text{RAS}} = 1 - \lambda_2 \int_{\bar{x}_1}^{+\infty} e^{-\frac{\alpha}{\Xi(x;\beta)} - \lambda_2 x} dx, \tag{4.13}$$

$$\text{SOP}_{\text{TAS}} = 1 + \lambda_2 \sum_{n=1}^{N} \binom{N}{n} (-1)^n \int_{\bar{x}_1}^{+\infty} e^{-\frac{n\alpha}{\Xi(x;\beta)} - \lambda_2 x} dx, \tag{4.14}$$

$$\text{SOP}_{\text{MRT}} = 1 - \lambda_2 \sum_{n=0}^{N-1} \frac{\alpha^n}{n!} \int_{\bar{x}_1}^{\infty} \Xi(x;\beta)^{-n} e^{-\frac{\alpha}{\Xi(x;\beta)} - \lambda_2 x} dx, \tag{4.15}$$

where $\alpha = \frac{\lambda_1(\beta-1)}{\zeta(1-\theta)\rho_s}$.

Proof: See Appendix C.1.

The integrals in (4.13–4.15) do not admit closed-form expressions. Below, we derive the asymptotic functions for the SOP at high power levels, i.e., $(P_s, P_d) \to (\infty, \infty)$.

Proposition 4.2 In the case of perfect CSI ($\zeta = 1$), the asymptotic functions for the SOP of the RAS, TAS, and MRT schemes are respectively given by

$$\text{SOP}^{\infty}_{\text{RAS}} = \text{SOP}^{\infty}_{\text{TAS}} = \text{SOP}^{\infty}_{\text{MRT}} = \lambda_2 \sqrt{\frac{\beta}{\eta\theta\rho_d}}, \tag{4.16}$$

In the case of imperfect CSI ($0 < \zeta < 1$), we have the follows

$$\mathrm{SOP}_{\mathrm{RAS}}^{\infty} = 1 - 2e^{-\frac{\bar{x}_2\lambda_1}{\zeta\omega} - \lambda_2\bar{x}_2}\sqrt{\frac{\bar{x}_2\left(1-\zeta\right)\beta\lambda_2}{\zeta}}K_1\left(2\sqrt{\frac{\bar{x}_2\left(1-\zeta\right)\beta\lambda_2}{\zeta}}\right), \tag{4.17}$$

$$\begin{aligned}\mathrm{SOP}_{\mathrm{TAS}}^{\infty} = 1 + 2\sum_{n=1}^{N}\binom{N}{n}(-1)^n e^{-\frac{n\bar{x}_2\lambda_1}{\zeta\omega} - \lambda_2\bar{x}_2} \\ \times\sqrt{\frac{n\bar{x}_2\left(1-\zeta\right)\beta\lambda_2}{\zeta}}K_1\left(2\sqrt{\frac{n\bar{x}_2\left(1-\zeta\right)\beta\lambda_2}{\zeta}}\right),\end{aligned} \tag{4.18}$$

$$\begin{aligned}\mathrm{SOP}_{\mathrm{MRT}}^{\infty} = 1 - \sum_{n=0}^{N-1}\frac{2}{n!}e^{-\frac{\bar{x}_2\lambda_1}{\zeta\omega} - \lambda_2\bar{x}_2}\sum_{k=0}^{n}\binom{n}{k}(\mu_0\alpha)^{n-k} \\ \times\left(\frac{\mu_0\alpha\bar{x}_2\beta\lambda_2}{\beta-1}\right)^{\frac{k+1}{2}}K_{1-k}\left(2\sqrt{\frac{\mu_0\alpha\bar{x}_2\beta\lambda_2}{\beta-1}}\right),\end{aligned} \tag{4.19}$$

where $\omega = \rho_s/\rho_d, \mu_0 = (1-\zeta)(1-\theta)\frac{\rho_s}{\lambda_1}$, and $\bar{x}_2 = (1-\zeta)(\beta-1)\frac{\omega}{\lambda_1}$.

Proof: See Appendix C.2.

4.3.2 Average secrecy capacity

The ASC of the proposed system is given by

$$\bar{R}_{\mathrm{sec}} = \mathbb{E}\left\{\left[\mathcal{C}_{\mathrm{d}} - \mathcal{C}_{\mathrm{r}}\right]^+\right\}. \tag{4.20}$$

Using the fact that $\mathbb{E}\left\{\max\left\{x,y\right\}\right\} \geqslant \max\left\{\mathbb{E}\left\{x\right\},\mathbb{E}\left\{y\right\}\right\}$, the lower bound of the ASC can be determined as

$$\bar{R}_{\mathrm{sec,low}} = \left[\bar{\mathcal{C}}_d - \bar{\mathcal{C}}_r\right]^+, \tag{4.21}$$

where $\bar{\mathcal{C}}_d = \mathbb{E}\left\{\log_2\left(1+\gamma_d\right)\right\}$, and $\bar{\mathcal{C}}_r = \mathbb{E}\left\{\log_2\left(1+\gamma_r\right)\right\}$.

We first derive the closed-form expression for $\bar{\mathcal{C}}_d$. Considering the function $f\left(x\right) = \ln\left(1+e^x\right)$, it can be seen that $f(x)$ is a convex function and linearly increases for

high values of x. Then, using Jensens inequality for $f(x)$, we can approximate $\bar{\mathcal{C}}_d$ as

$$\begin{aligned}\mathcal{C}_d &= \mathbb{E}\left\{\log_2\left(1+e^{\ln(\gamma_d)}\right)\right\} \approx \log_2\left(1+e^{\mathbb{E}\{\ln(\gamma_d)\}}\right)\\ &\approx \log_2\left(1+e^{\ln(\zeta(1-\theta)\rho_s)+\mathcal{J}_1+\mathcal{J}_2-\mathcal{J}_3}\right),\end{aligned} \tag{4.22}$$

where $\mathcal{J}_1 = \mathbb{E}\{\ln(X_1)\}$, $\mathcal{J}_2 = \mathbb{E}\{\ln(X_2)\}$, and $\mathcal{J}_3 = \mathbb{E}\{\ln(X_2\mu+\kappa)\}$.

Proposition 4.3 $\bar{\mathcal{C}}_d$ of the RAS, TAS, and MRT schemes can be approximated as

$$\mathcal{C}_d^{\mathrm{RAS}} \approx \log_2\left(1+\exp\left(\ln\left(\tfrac{\zeta(1-\theta)\rho_s}{\kappa\lambda_1\lambda_2}\right)+2\Psi(1)+e^{\frac{\lambda_2\kappa}{\mu}}Ei\left(-\tfrac{\lambda_2\kappa}{\mu}\right)\right)\right), \tag{4.23}$$

$$\begin{aligned}\mathcal{C}_d^{\mathrm{TAS}} \approx \log_2\Bigg(1+\exp\Bigg(&\ln\left(\tfrac{\zeta(1-\theta)\rho_s}{\kappa\lambda_2}\right)+2\Psi(1)+e^{\frac{\lambda_2\kappa}{\mu}}Ei\left(-\tfrac{\lambda_2\kappa}{\mu}\right)\\ &-N\sum_{n=0}^{N-1}\binom{N-1}{n}\frac{(-1)^n}{(n+1)}\ln\left((n+1)\lambda_1\right)\Bigg)\Bigg),\end{aligned} \tag{4.24}$$

$$\mathcal{C}_d^{\mathrm{MRT}} \approx \log_2\left(1+\exp\left(\ln\left(\tfrac{\zeta(1-\theta)\rho_s}{\kappa\lambda_1\lambda_2}\right)+\psi(N)+\Psi(1)+e^{\frac{\lambda_2\kappa}{\mu}}Ei\left(-\tfrac{\lambda_2\kappa}{\mu}\right)\right)\right). \tag{4.25}$$

where $Ei(\cdot)$ is the exponential integral function [53, Eq. (8.310.1)].

Proof: See Appendix C.3.

Next, we derive the closed-form expression for $\bar{\mathcal{C}}_r$. According to [91], $\bar{\mathcal{C}}_r$ is calculated as

$$\bar{\mathcal{C}}_r = \mathbb{E}\{\log_2(1+\gamma_r)\} = \frac{1}{\ln(2)}\int_0^\infty \frac{1-F_{\gamma_r}(\gamma)}{1+\gamma}. \tag{4.26}$$

Proposition 4.4 $\bar{\mathcal{C}}_r$ of the RAS scheme is calculated as follows.

- For $\lambda_1 \neq \lambda_2\zeta\omega$:

$$\bar{\mathcal{C}}_r^{\mathrm{RAS}} \approx \frac{1}{\ln(2)\left(1-\frac{\lambda_1}{\lambda_2\zeta\omega}\right)}\left(e^{\frac{\mu\lambda_2\zeta\omega}{\zeta(1-\theta)\rho_s}}Ei\left(\tfrac{-\mu\lambda_2\omega}{(1-\theta)\rho_s}\right)-e^{\frac{\lambda_1\mu}{\zeta(1-\theta)\rho_s}}Ei\left(\tfrac{-\lambda_1\mu}{\zeta(1-\theta)\rho_s}\right)\right). \tag{4.27}$$

- For $\lambda_1 = \lambda_2\zeta\omega$:

$$\bar{\mathcal{C}}_r^{\mathrm{RAS}} \approx \frac{1}{\ln(2)}\left(1 + \frac{\lambda_1\mu}{\zeta(1-\theta)\rho_s} e^{\frac{\lambda_1\mu}{\zeta(1-\theta)\rho_s}} Ei\left(\frac{-\lambda_1\mu}{\zeta(1-\theta)\rho_s}\right)\right). \tag{4.28}$$

$\bar{\mathcal{C}}_r$ of the TAS scheme is calculated as follows.

- For $n\lambda_1 \neq \lambda_2\zeta\omega$:

$$\begin{aligned}\bar{\mathcal{C}}_r^{\mathrm{TAS}} \approx & \sum_{n=1}^{N}\binom{N}{n}\frac{(-1)^{n+1}}{\ln(2)\left(1-\frac{n\lambda_1}{\lambda_2\zeta\omega}\right)} \\ & \times\left(e^{\frac{\mu\lambda_2\zeta\omega}{\zeta(1-\theta)\rho_s}} Ei\left(\frac{-\mu\lambda_2\omega}{(1-\theta)\rho_s}\right) - e^{\frac{n\lambda_1\mu}{\zeta(1-\theta)\rho_s}} Ei\left(\frac{-n\lambda_1\mu}{\zeta(1-\theta)\rho_s}\right)\right).\end{aligned} \tag{4.29}$$

- For $n\lambda_1 = \lambda_2\zeta\omega$:

$$\bar{\mathcal{C}}_r^{\mathrm{TAS}} \approx \sum_{n=1}^{N}\binom{N}{n}\frac{(-1)^{n+1}}{\ln(2)}\left(1 + \frac{n\lambda_1\mu}{\zeta(1-\theta)\rho_s} e^{\frac{n\lambda_1\mu}{\zeta(1-\theta)\rho_s}} Ei\left(\frac{-n\lambda_1\mu}{\zeta(1-\theta)\rho_s}\right)\right). \tag{4.30}$$

$\bar{\mathcal{C}}_r$ of the MRT scheme is calculated as follows.

- For $\lambda_1 \neq \lambda_2\zeta\omega$:

$$\begin{aligned}\bar{\mathcal{C}}_r^{\mathrm{MRT}} \approx & \frac{\lambda_2}{\ln(2)}\sum_{n=0}^{N-1}\frac{1}{n!}\left(\frac{\lambda_1}{\zeta\omega}\right)^n \sum_{k=0}^{n}\binom{n}{k}\left(\frac{\mu}{(1-\theta)\rho_d}\right)^{n-k}\Gamma(k+1) \\ & \times\left(A_0 e^{\frac{\lambda_1\mu}{\zeta(1-\theta)\rho_s}}\Gamma(n+1)\Gamma\left(-n, \frac{\lambda_1\mu}{\zeta(1-\theta)\rho_s}\right)\right. \\ & \left. + \sum_{i=1}^{k+1}\frac{A_i}{\lambda_2^i}\left(\frac{\zeta\omega\lambda_2}{\lambda_1}\right)^{n+1}\Gamma(n+1)\,U\left(n+1, n-i+2; \frac{\omega\lambda_2\mu}{(1-\theta)\rho_s}\right)\right).\end{aligned} \tag{4.31}$$

- For $\lambda_1 = \lambda_2\zeta\omega$:

$$\begin{aligned}\bar{\mathcal{C}}_r^{\mathrm{MRT}} \approx & \frac{\lambda_2}{\ln(2)}\sum_{n=0}^{N-1}\frac{1}{n!}\left(\frac{\lambda_1}{\zeta\omega}\right)^n \sum_{k=0}^{n}\binom{n}{k}\left(\frac{\mu}{(1-\theta)\rho_d}\right)^{n-k} \\ & \times\left(\frac{\zeta\omega}{\lambda_1}\right)^{k+1}\Gamma(k+1)\Gamma(n+1)\,U\left(n+1, n-k; \frac{\omega\lambda_2\mu}{(1-\theta)\rho_s}\right).\end{aligned} \tag{4.32}$$

where $U(a,b;x)$ is the confluent hypergeometric function of the second kind [53, Eq. (9.211.4)], $A_0 = \left(\lambda_2 - \frac{\lambda_1}{\zeta\omega}\right)^{-k-1}$ and $A_i = \frac{-\lambda_1}{\zeta\omega}\left(\lambda_2 - \frac{\lambda_1}{\zeta\omega}\right)^{-k-2+i}$.

Proof: See Appendix C.4.

4.4 Results and Discussion

In this section, we present numerical results to validate the analytical expressions presented in Section 4.3. Unless otherwise specified, we set $\eta = 0.5, \theta = 0.5, \tau = 3, R_{\text{th}} = 1$ (bits/s/Hz), $N = 3$, and $\sigma_0^2 = 1$. The coordinates in the two-dimensional plane of S, D, and R are set to $(0, 0), (2, 0)$, and $(d, 0.2)$, respectively.

In Figure 4.2, we show the SOP and its asymptote when both S and D increase their transmit powers, i.e., $\rho_s = \rho_d = \rho$. As can be seen, when ρ increases, the SOP for perfect CSI remarkably improves while that in the case of imperfect CSI converges to a determined value. These results can be explained using the effect of the noise caused by imperfect CSI on the SOP. Particularly, in the case of imperfect CSI, the strength of this noise linearly increases with the signal strength; hence, the SOP converges at high ρ values. Comparing the three antenna schemes, we observe that the MRT provides a better SOP than the TAS scheme, and both the MRT and TAS schemes outperform the RAS scheme; especially in the case of imperfect CSI, these trends become even clearer. Moreover, as shown in Figure 4.2, the asymptote agrees well with the exact SOP at high ρ values.

In Figure 4.3, we investigate the effect of θ on the SOP and ASC. The value of θ is varied from 0 to 1. As shown, the SOP and ASC improve as θ increases from 0 to the corresponding optimal PS ratios, at which point the SOP or ASC achieve the best values, and they rapidly become worse with further increases in θ. The trends of the SOP and ASC are respectively similar to the trends of the OP and throughput in Chapter 2 and Chapter 3. This is because the same effect of θ on the harvested energy and the signal strength portion used for information decoding at the relay

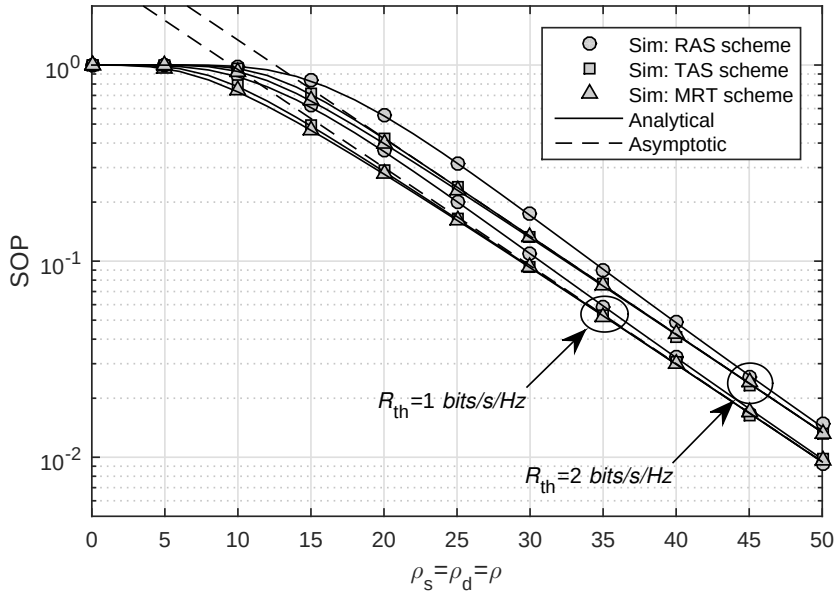

(a)

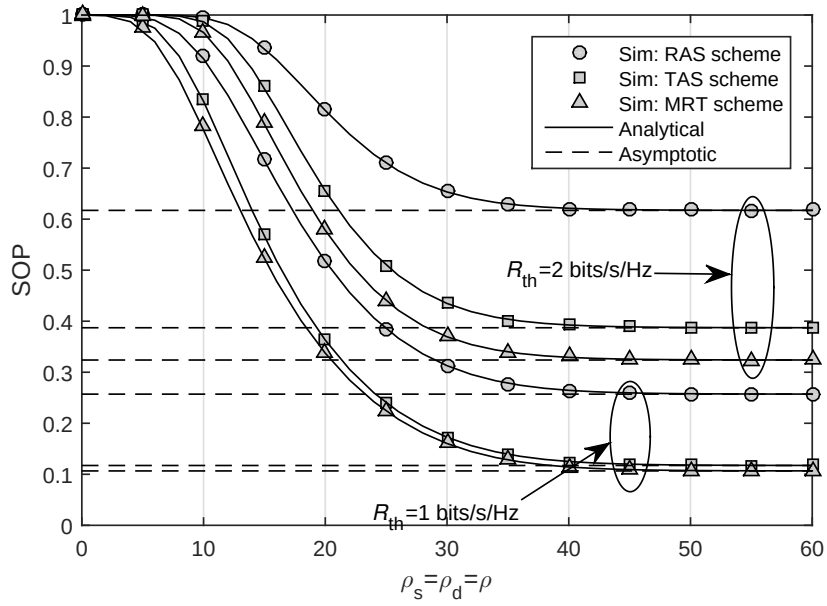

(b)

Figure 4.2: The effect of ρ on the SOP and its asymptote in the cases of a) $\zeta = 1$ and b) $\zeta = 0.9$. Other parameters: $d = 1$ and $\rho_s = \rho_d = \rho$.

that were explained in the discussion of Figure 2.4. Moreover, the effects of η on the SOP and ASC are also examined. It can be observed that the secrecy performance is enhanced as η increases.

In Figure 4.4, we investigate the effects of ρ_s and ρ_d on the optimal SOP and optimal ASC in different scenarios: S_1, S_2, and S_3. We fix ρ_s and ρ_d in scenarios S_1 and S_2, respectively, while we vary their values in scenario S_3. Comparing the three antenna schemes, it can be observed that the MRT scheme provide the best secrecy performance, whereas the RAS scheme yields the poorest secrecy performance. Moreover, we consider the secrecy performance in two cases, perfect CSI (see Figure 4.4(a,b)) and imperfect CSI with $\zeta = 0.9$ (see Figure 4.4(c,d)).

In the case of perfect CSI, the optimal SOP is an increasing function of ρ, and the optimal ASC is a decreasing function of ρ. Moreover, as ρ increases, the secrecy performance in scenarios S_1 and S_2 converges whereas it linearly increases in scenario S_3. These results can be explained using the trends of $\mathcal{C}_r$ and $\mathcal{C}_d$ in the three scenarios. In scenario S_1, the fixed ρ_s value leads to a fixed $\mathcal{C}_d$, which limits the secrecy performance. In scenario S_2, the same increasing rates of $\mathcal{C}_r$ and $\mathcal{C}_d$ cause the secrecy performance to converge. In scenario S_3, the increasing trends of ρ_s and ρ_d leads to substantial growth in $\mathcal{C}_d$ and the limit in $\mathcal{C}_r$, respectively, which contribute to the remarkable increase in secrecy performance. Additionally, at low ρ values, the secrecy performance in scenario S_2 overcomes those in scenarios S_1 and S_3.

In the case of imperfect CSI, the secrecy performance in scenarios S_1 and S_3 decreases and converges whereas that in scenario S_2 improves at first and then degrades. Comparing these results with that in the perfect CSI case, we have the follows. For

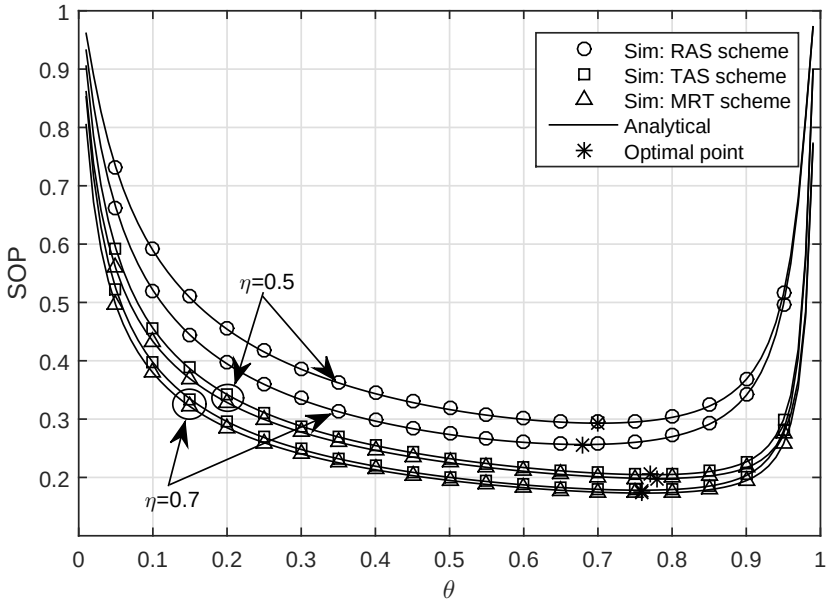

(a)

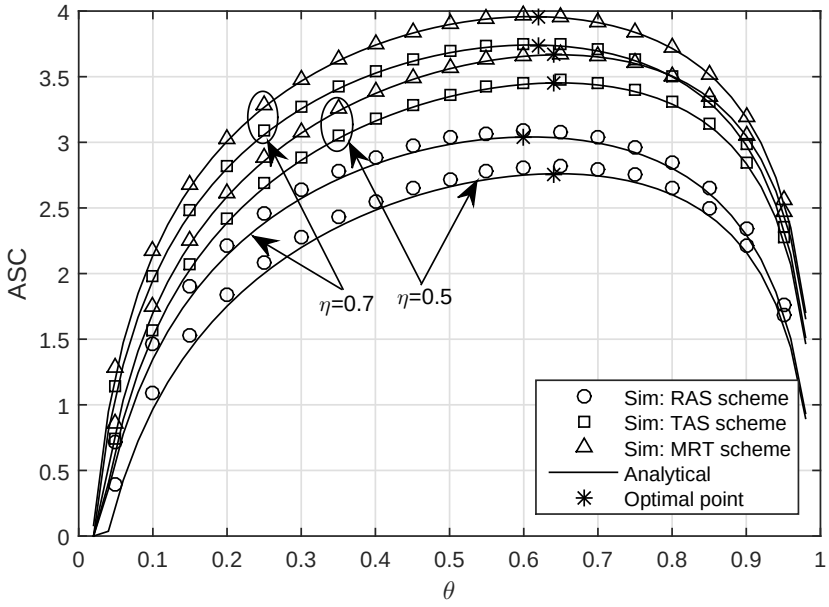

(b)

Figure 4.3: The effect of θ on the SOP and ASC. Other parameters: $d = 1, \rho_s = \rho_d = 25(dB)$ and $R_s = 2(bits/sec/Hz)$.

scenario S_1, the secrecy performance trends in both perfect CSI and imperfect CSI cases are similar, except for the limit of each case. In contrast, the secrecy performance trends in the perfect CSI and imperfect CSI cases are different for scenarios S_2 and S_3. This is because of the effect of the noise caused by imperfect CSI. Particularly, for scenario S_2, both $\mathcal{C}_r$ and $\mathcal{C}_d$ converge to a value in which the convergence rate of $\mathcal{C}_d$ is higher than that of $\mathcal{C}_r$ due to the effect of the AN; therefore, the optimal SOP and optimal ASC follow a convex function and a concave function of ρ, respectively. In scenario S_3, $\mathcal{C}_d$ converges to a higher value than $\mathcal{C}_r$ due to the effect of the AN, hence, the secrecy performance converges to a non–zero value. On the other hand, at high ρ values, the secrecy performance in scenario S_1 becomes better than that in the other scenarios, whereas at low ρ values, the secrecy performance in scenario S_2 outperforms that in the other scenarios.

In Figure 4.5, we present the optimal SOP and optimal ASC results in term of the trade-off between the transmit powers of S and D. The overall transmit power over noise power is $\rho_\Sigma = 10^3$, i.e., $\rho_s + \rho_d = \rho_\Sigma$. As shown in Figure 4.5, the highest secrecy performance is obtained as ρ_s is between 0 and ρ_Σ, and the secrecy performance rapidly decreases as ρ_s tends to 0 or ρ_Σ. These results show an important role of the destination-assisted jamming in creating the positive secrecy capacity, such as, with low destination-assisted jamming signal's powers, the secure communication between S and D does not exist. Moreover, it can be seen that the peaks of the optimal SOP and ASC curves move toward to the left (the decreasing trend of ρ_s) when ζ increases. Comparing three considered schemes, the peaks of the optimal SOP and ASC curves for the TAS scheme is located in the left side of that for the

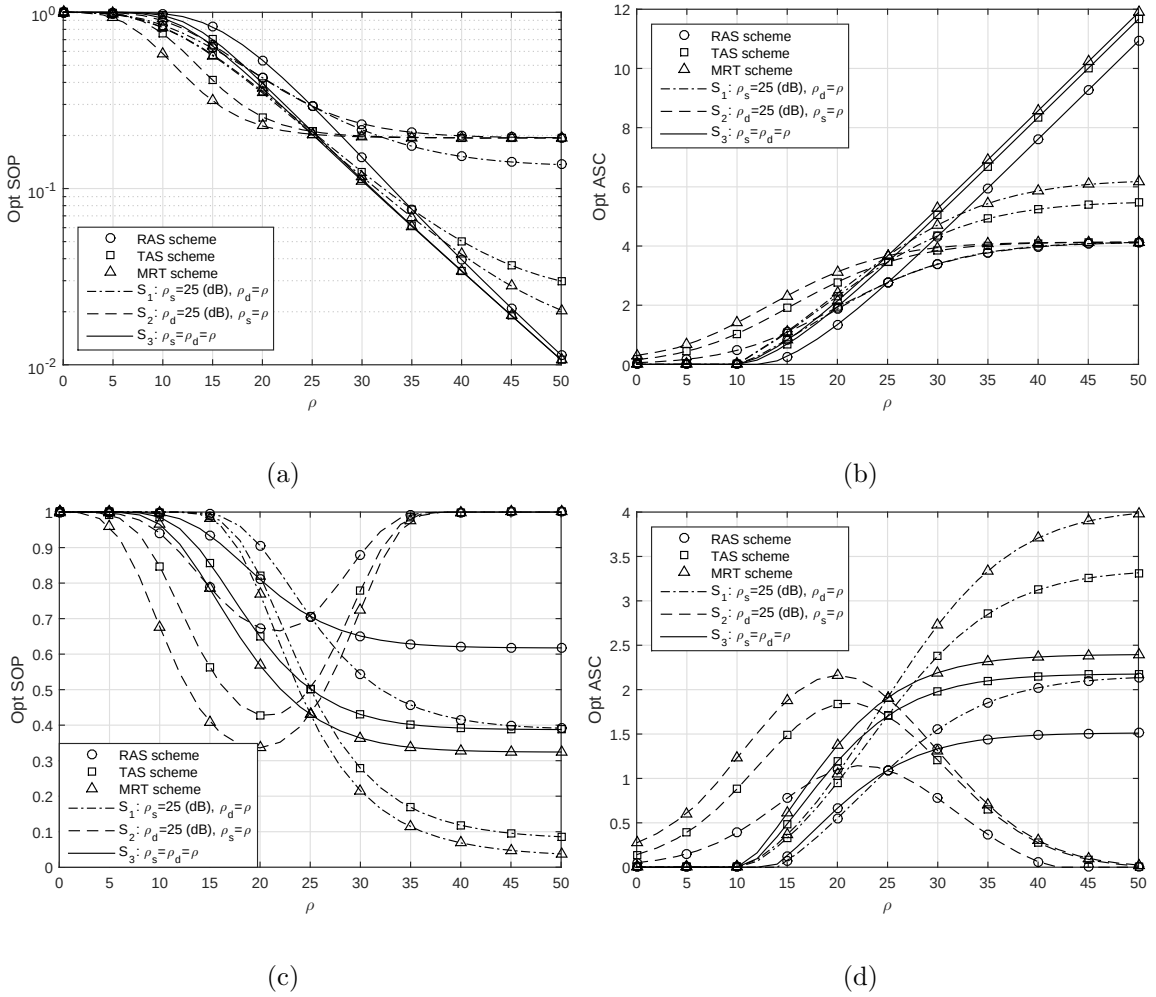

Figure 4.4: The effect of ρ_s and ρ_d on the optimal SOP and optimal ASC. Other parameters: $d = 1$ and $R_{th} = 2(bits/sec/Hz)$.

RAS scheme and in the right side of that for the MRT scheme. For all values of $\rho_s \in (0, \rho_\Sigma]$, the MRT scheme yields the best secrecy performance while the RAS scheme gives a lowest secrecy performance.

In Figure 4.6, we investigate the effects of N and ζ on the optimal SOP and optimal ASC. From (4.9), it can be seen that the signal strength that can be decoded at the receiver decreases and the noise power caused by the imperfect CSI increases as ζ decreases; therefore, the secrecy performance degrades as ζ decreases. On the

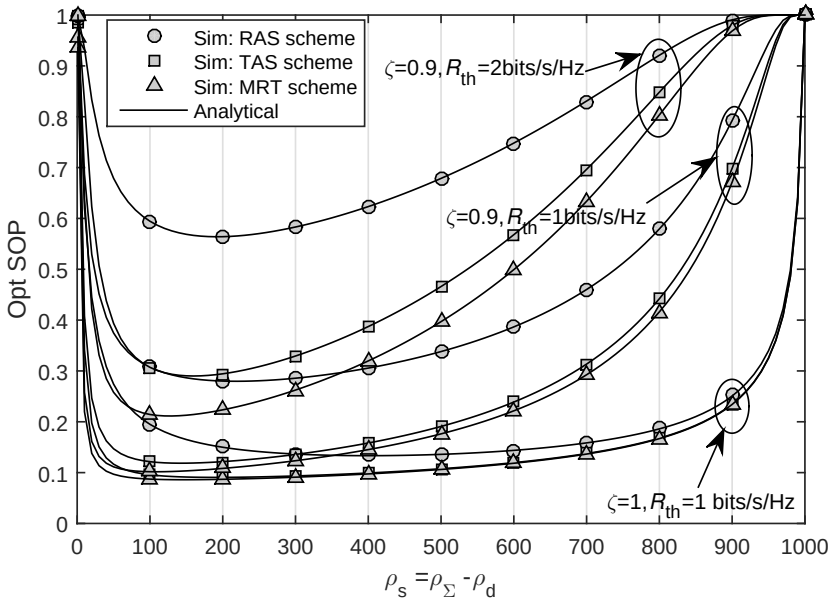

(a)

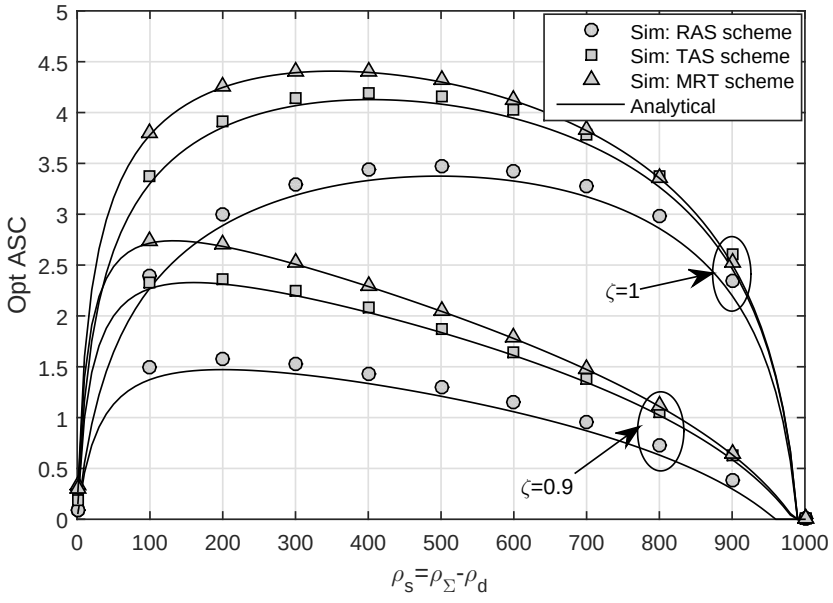

(b)

Figure 4.5: The optimal SOP and optimal ASC in term of the trade-off between ρ_s and ρ_d ($\rho_s + \rho_d = \rho_\Sigma$). Other parameter: $d = 1$ and $\rho_\Sigma = 30(dB)$.

other hand, it can be seen in (4.9) that, when S is equipped with a larger antenna, the signal strength used for information decoding at the receiver for the TAS and MRT schemes is enhanced, whereas the noise power caused by the imperfect CSI does not change. Therefore, when N increases, the secrecy performances for both the MRT and TAS schemes improves. Moreover, it can be seen in Figure 4.5 that the MRT scheme outperform the TAS scheme for all values of ζ.

In Figure 4.7, we investigate the effect of the relay's location on the optimal SOP and optimal ASC. As shown, the secrecy performance improves as d increases from 0 to an optimal distance, and then it slightly degrades with further increase in d. These results can be explained by using the effect of the R–D link on the AN at R and the overall noise at D. When R is near S, the ANs strength becomes weak due to the decreasing trend of the R–D channel gain, hence, the secrecy performance is low. In contrast, when R is near D, the overall noise at D increases because of an increasing trend in the R–D channel gain; therefore, the secrecy performance slightly degrades. Comparing with the conventional WEH–CC system (which uses the trusted relay in which a high performance is achieved when R is located near S), our proposed system achieves high performance when R is located between S and D. Moreover, it can be observed from Figure 4.7 that the optimal SOP is approximately zero if R is close to S, such as $d < 0.2$, for the case of $\zeta = 1$, and $d < 0.4$ for the case of $\zeta = 0.9$.

4.5 Conclusion

In this Chapter, we studied the secure communication of an UR–WEH system in a presence of imperfect CSI. We proposed equipping multiple antennas at the

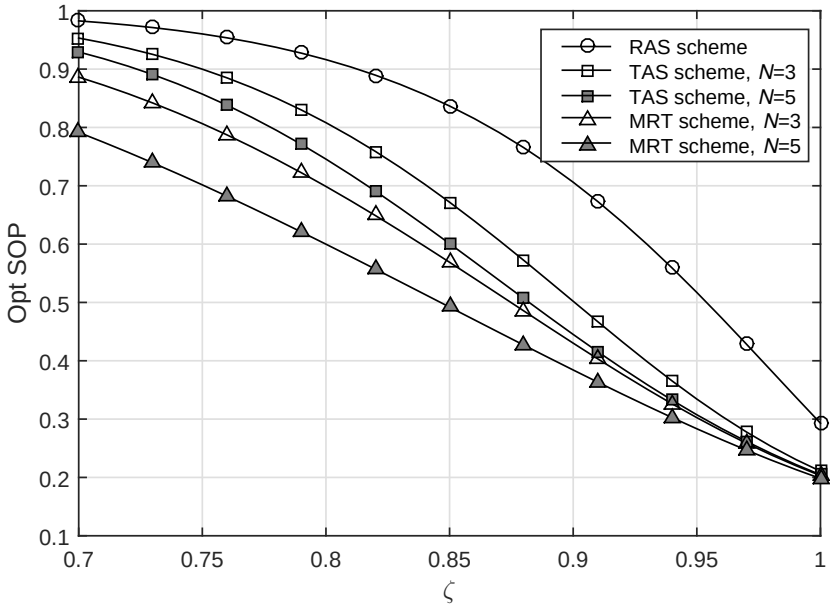

(a)

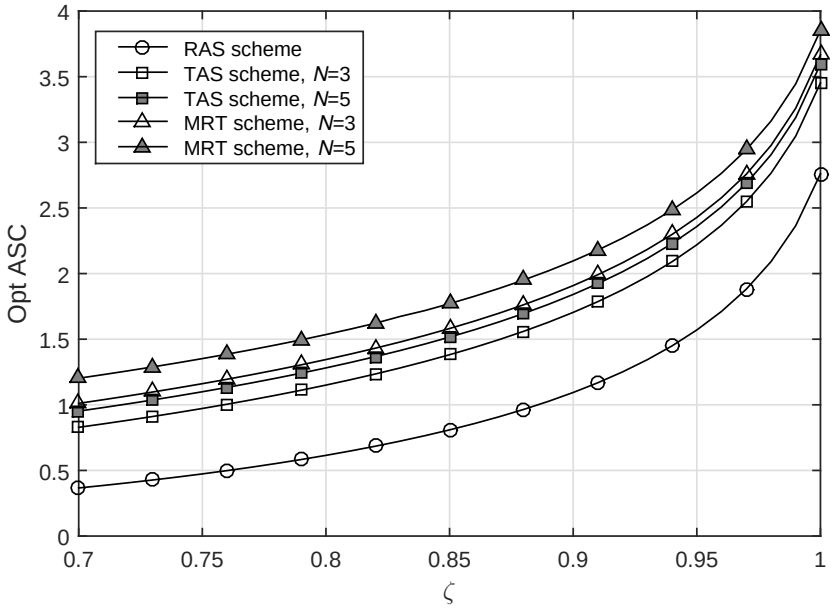

(b)

Figure 4.6: The effect of ζ on the SOP and ASC. Other parameter: $d = 1, \rho_s = \rho_d = 25(dB)$ and $R_s = 2(bits/sec/Hz)$.

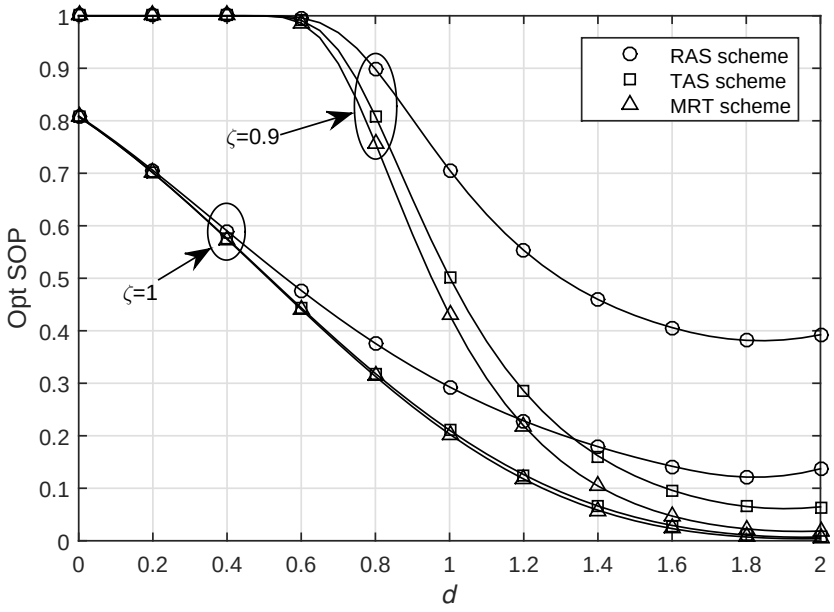

(a)

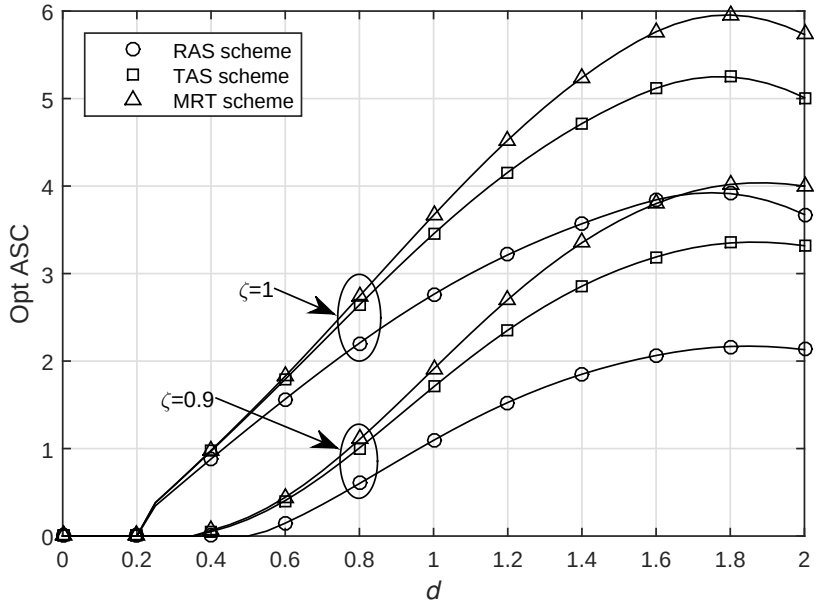

(b)

Figure 4.7: The effect of the relays location on the optimal SOP and optimal ASC. Other parameters: $\rho_s = \rho_d = 15(dB)$.

source to enhance the harvested energy at the WEH relay. Then, we employed the multi–antenna schemes, TAS and MRT, to reduce the influence of imperfect CSI caused by the multiple antennas. For secrecy performance comparison, we also examined the RAS scheme in this Chapter. We derived the analytical expressions for the two secrecy performance metrics, i.e., the SOP and ASC, for both the perfect and imperfect CSI cases; moreover, the closed–form expression for the SOP at high–power levels was also presented. We used the Monte Carlo simulations to verify the accuracy of the analytical results. The results showed that:

- The secrecy performance in both the perfect CSI case and imperfect CSI is improved as the source's antennas increases.
- The MRT scheme performs better than the TAS scheme; and both the MRT and TAS schemes provide a significant improvement in secrecy performance compared with the RAS scheme. Especially in the imperfect CSI case, these trends has shown clearer.
- The best location for the untrusted relay is between the source and the destination.

Moreover, the effects of various system parameters, such as the channel correlation coefficient, energy–harvesting efficiency, secrecy rate threshold, PS ratio, and transmit powers on secrecy performance were studied. These results provide valuable insights into system design.

Chapter 5

Secure communication via a wireless energy-harvesting untrusted relay in the presence of an eavesdropper [1]

5.1 Introduction

In this Chapter, we study the problem of secure communication in an UR–WEH system in the presence of an external eavesdropper. We use the destination–assisted jamming to create the positive secrecy rate and provide an additional energy at the relay. The PS receiver architecture proposed is adopted. We evaluate the secrecy performance by analyzing the two secrecy performance metrics, i.e., SOP and ASC.

[1] The study in this chapter was published in International Journal of Electronics [92]

For that purpose, we derive the SOP expressions involving a single integral and a tight closed–form upper bound for the ASC; moreover, the closed–form expressions for the SOP at high-power scenarios are also derived. The accuracy of the analytical results is verified by Monte Carlo simulations.

The rest of this Chapter is organized as follows. The system model is presented in Section 5.2. The analytical expressions for the SOP and ASC are derived in Section 5.3. The results and discussion are given in Section 5.4. Finally, the conclusions are presented in Section 5.5.

5.2 System Model

We consider an UR–WEH system illustrated in Figure 5.1(a). Our system consists of a source S, a destination D, an untrusted WEH relay R and an external eavesdropper E. The entire communication of each block time T is shown in 5.1(b). The block time T consists of two time slots, $T/2$. In the first time slot, S and D simultaneously send the information signal and the jamming signal to R, respectively; in the second time slot, R uses all harvested energy and the AF protocol to forward the received signal to D. R uses the PS policy with the PS ratio $0 \leqslant \theta \leqslant 1$ to harvest energy. In this proposed system, the source's information can be overheard by both R and E.

Throughout this paper, we assume that 1) the direct link between S and D does not exist; 2) the channels follow independent and identical Rayleigh distributions; hence, the channel gains are exponential RVs; 3) no CSI is required at S, the local CSI is assumed at R and E, and the full CSI of the S–R–D route is assumed at D; 4) the duration for the setup phase is negligible as compared to the block time T and

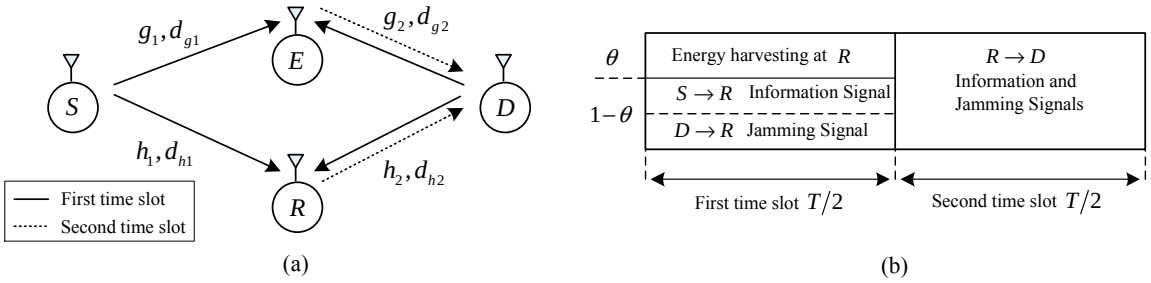

Figure 5.1: System model.

5) R and E overhear the source information separately.

Let us denote (h_1, d_{h1}), (h_2, d_{h2}), (g_1, d_{g1}), and (g_2, d_{g2}) as the Rayleigh fading channel coefficients and the distances of the S–R, R–D, S–E, and E–D links, respectively, and $X_1 = |h_1|^2, X_2 = |h_2|^2, Y_1 = |g_1|^2$ and $Y_2 = |g_2|^2$ are exponential RVs with parameters $\lambda_{X_1} = d_{h1}^{\tau}, \lambda_{X_2} = d_{h2}^{\tau}, \lambda_{Y_1} = d_{g1}^{\tau}$ and $\lambda_{Y_2} = d_{g2}^{\tau}$ where τ is the path loss exponent.

5.2.1 Communication in the first time slot

The signal component used for information decoding of R is given by

$$y_r = \sqrt{(1-\theta)\, P_s} h_1 x_s + \sqrt{(1-\theta)\, P_d} h_2 x_d + n_r, \tag{5.1}$$

where P_s and P_d are the transmit powers of S and D, respectively, x_s is the unit power information signal sent by S, x_d is the unit power jamming signal sent by D, and $n_r \sim \mathcal{CN}(0, \sigma_0^2)$ is the AWGN at R.

The overall energy harvested at R during $T/2$ is given by

$$E_h = \eta\theta \left(P_s X_1 + P_d X_2\right) T/2, \tag{5.2}$$

where η is the RF-to-DC conversion efficiency.

From (5.1), the SINR at R can be expressed as

$$\gamma_r = \frac{(1-\theta)\,\rho_s X_1}{(1-\theta)\,\rho_d X_2 + 1}, \tag{5.3}$$

where $\rho_s = P_s/\sigma_0^2$ and $\rho_d = P_d/\sigma_0^2$.

The received signal at E is given by

$$y_e = \sqrt{P_s} g_1 x_s + \sqrt{P_d} g_2 x_d + n_e, \tag{5.4}$$

where $n_e \sim \mathcal{CN}(0, \sigma_0^2)$ is the AWGN at E. Therefore, the SINR at E is given by

$$\gamma_e = \frac{\rho_s Y_1}{\rho_d Y_2 + 1}. \tag{5.5}$$

5.2.2 Communication in the second time slot

In the second time slot, R uses all of the harvested energy given by (5.2) to forward its received signal to D; hence, the received signal at D is given by

$$y_d = \sqrt{P_r} h_2 G y_r + n_d, \tag{5.6}$$

where $P_r = \frac{2E_h}{T} = \eta\theta Z, G = \sqrt{(1-\theta)\,Z + \sigma_0^2}$ and $Z = P_s X_1 + P_d X_2$. Substituting (5.1) into (5.6) yields

$$y_d = \underbrace{\sqrt{(1-\theta)\,P_s P_r} h_1 h_2 G x_s}_{\text{desired signal}} + \underbrace{\sqrt{(1-\theta)\,P_d P_r} h_2 h_2 G x_d}_{\text{artificial noise}} + \underbrace{\sqrt{P_r} h_2 G n_r + n_d}_{\text{overall noise}}. \tag{5.7}$$

Because D knows exactly the value of x_d, the influence of the artificial noise part in (5.7) on the end-to-end SNR at D can eliminate. Therefore, the end-to-end SNR

at D can be expressed as

$$\begin{aligned}\gamma_d &= \frac{\eta\theta\left(1-\theta\right)Z\rho_s X_1 X_2}{\eta\theta Z X_2 + \left(1-\theta\right)Z + \sigma_0^2} \\ &\approx \frac{\left(1-\theta\right)\rho_s X_1 X_2}{X_2 + \kappa},\end{aligned} \tag{5.8}$$

where $\kappa = (1-\theta)/\eta\theta$.

The approximation in (5.8) is acceptable because the noise variance term is negligible compared to the other factors in the denominator. Then, the instantaneous secrecy capacity can be calculated as

$$R_{\text{sec}} = \left[\min\left\{R_{\text{sec},1}, R_{\text{sec},2}\right\}\right]^+, \tag{5.9}$$

where $R_{\text{sec},1} = \mathcal{C}_d - \mathcal{C}_r$ and $R_{\text{sec},2} = \mathcal{C}_d - \mathcal{C}_e$ with $\mathcal{C}_d = \log_2\left(1+\gamma_d\right), \mathcal{C}_r = \log_2\left(1+\gamma_r\right)$ and $\mathcal{C}_e = \log_2\left(1+\gamma_e\right)$.

5.3 Performance analysis

5.3.1 Secrecy outage probability

The SOP is given by

$$\begin{aligned}P_{\text{out}} &= \Pr\left(\min\left\{R_{\text{sec},1}, R_{\text{sec},2}\right\} < R_{\text{th}}\right) \\ &= \underbrace{\Pr\left(R_{\text{sec},1} < R_{\text{th}}\right)}_{P_{\text{out},1}} + \underbrace{\Pr\left(R_{\text{sec},2} < R_{\text{th}}, R_{\text{sec},1} \geqslant R_{\text{th}}\right)}_{P_{\text{out},2}}.\end{aligned} \tag{5.10}$$

Thanks to the author of [46], $P_{\text{sec},1}$ was given by

$$P_{\text{sec},1} = 1 - \lambda_{X_2}\int_{\bar{x}_1}^{+\infty} e^{-x_2\lambda_{X_2} - \lambda_{X_1}\frac{\beta-1}{(1-\theta)\rho_s\Xi_1(x_2)}}dx_2, \tag{5.11}$$

where $\beta = 2^{R_{\text{th}}}, \Xi_1(x) = \frac{x}{x+\kappa} - \frac{\beta}{(1-\theta)\rho_d x+1}$ and $\bar{x}_1 = \frac{\beta-1+\sqrt{(\beta-1)^2+4(1-\theta)\rho_d\beta\kappa}}{2(1-\theta)\rho_d}$, which is the positive root of the equation $\Xi_1(x) = 0$.

After some manipulation, we can rewrite $P_{\text{sec},2}$ as

$$P_{\text{sec},2} = \Pr\left(X_1 < \frac{\beta\gamma_e+\beta-1}{(1-\theta)\rho_s}\left(1+\frac{\kappa}{X_2}\right), X_1 > \frac{\beta-1}{(1-\theta)\rho_s\Xi_1(X_2)}, \gamma_e > \Xi_2(X_2), X_2 > \bar{x}_1\right), \tag{5.12}$$

where $\Xi_2(x) = \frac{(\beta-1)(x+\kappa)}{(1-\theta)\rho_d(x-\bar{x}_1)(x-\bar{x}_2)}$ and $\gamma_e > \Xi_2(X_2)$ is a condition for the inequality $\frac{\beta-1}{(1-\theta)\rho_s\Xi_1(X_2)} < \frac{\beta y+\beta-1}{(1-\theta)\rho_s}\left(1+\frac{\kappa}{X_2}\right)$ to be true.

Proposition 5.1 P_{sec} can be computed by

$$\begin{aligned} P_{\text{sec},2} = -\int_{\bar{x}_1}^{+\infty} \lambda_{X_2} e^{-\lambda_{X_2}x} \frac{\beta\lambda_{X_1}}{\beta_Y(1-\theta)\rho_s}\left(1+\frac{\kappa}{x}\right) e^{\frac{\lambda_{Y_1}}{\rho_s\beta_Y}+\left(\frac{\beta}{\beta_Y}-\beta+1\right)\frac{\lambda_{X_1}}{(1-\theta)\rho_s}\left(1+\frac{\kappa}{x}\right)} \\ \times Ei\left(-\frac{\beta_Y\Xi_2(x)+1}{\beta_Y\rho_s}\left(\lambda_{Y_1}+\frac{\beta\lambda_{X_1}}{(1-\theta)}\left(1+\frac{\kappa}{x}\right)\right)\right)dx, \end{aligned} \tag{5.13}$$

where $\beta_Y = \frac{\rho_d\lambda_{Y_1}}{\rho_s\lambda_{Y_2}}$ and $\bar{x}_2 = \frac{\beta-1-\sqrt{(\beta-1)^2+4(1-\theta)\rho_d\beta\kappa}}{2(1-\theta)\rho_d}$ is the negative root of the equation $\Xi_1(x) = 0$.

Proof: See Appendix D.1.

5.3.2 High-power secrecy outage probability approximation

To the best of the authors' knowledge, the integrals in (5.11) and (5.13) do not admit closed-form expressions. Below, we derive the closed-form expressions for the SOP at high-power levels, i.e., $(\rho_s, \rho_d) \to (\infty, \infty)$.

Proposition 5.2 $P_{\text{sec,2}}$ can be computed by

$$\begin{aligned} P_{\text{sec,HP}} =& 1 - e^{-\lambda_{X_2}\bar{x}_0} + \frac{\lambda_{X_1}(\beta-1)}{(1-\theta)\rho_s}\left(e^{-\lambda_{X_2}\bar{x}_0} - \lambda_{X_2}\kappa Ei\left(-\lambda_{X_2}\bar{x}_0\right)\right) \\ &+ \frac{\beta\lambda_{X_1}\lambda_{X_2}}{(1-\theta)\rho_s\beta_Y} e^{\frac{\lambda_{Y_1}}{\rho_s\beta_Y}+\frac{\lambda_{X_1}}{(1-\theta)\rho_s}\left(\frac{\beta}{\beta_Y}-\beta+1\right)}\Bigg(\kappa G_{2,3}^{3,0}\left(\lambda_{X_2}\bar{x}_0\big|_{0,0,0}^{1,1}\right) \\ &+ \frac{e^{-\lambda_{X_2}\bar{x}_0}\ln\left(\rho_s\bar{x}_0\right) - Ei\left(-\lambda_{X_2}\bar{x}_0\right)}{\lambda_{X_2}} - \kappa Ei\left(-\lambda_{X_2}\bar{x}_0\right)\ln\left(\rho_s\bar{x}_0\right)\Bigg), \end{aligned} \tag{5.14}$$

where $\bar{x}_0 = \sqrt{\frac{\beta\kappa}{(1-\theta)\rho_d}}$.

Proof: See Appendix D.2.

5.3.3 Average secrecy capacity

Using (5.10), the ASC of the proposed system is given by

$$\bar{R}_{\text{sec}} = \mathbb{E}\left\{\min\left[\left\{\log_2\left(\frac{1+\gamma_d}{1+\gamma_r}\right), \log_2\left(\frac{1+\gamma_d}{1+\gamma_e}\right)\right\}\right]^+\right\} \tag{5.15a}$$

$$= \mathbb{E}\left\{\left[\log_2\left(\frac{1+\gamma_d}{1+\max\{\gamma_e,\gamma_r\}}\right)\right]^+\right\}. \tag{5.15b}$$

Using the fact that $\mathbb{E}\{\max\{x,y\}\} \geqslant \max\{\mathbb{E}\{x\}, \mathbb{E}\{y\}\}$, the lower bound of the ASC can be determined as

$$\bar{R}_{\text{sec,low}} = [\mathcal{C}_d^{erg} - \mathcal{C}_T^{erg}]^+, \tag{5.16}$$

where $\mathcal{C}_d^{\text{erg}} = \mathbb{E}\{\log_2(1+\gamma_d)\}$, $\mathcal{C}_T^{\text{erg}} = \mathbb{E}\{\log_2(1+T)\}$ and $T = \max\{\gamma_e, \gamma_r\}$.

We first derive the closed-form expression for $\mathcal{C}_d^{\text{erg}}$.

Proposition 5.3 $\mathcal{C}_d^{\text{erg}}$ can be approximated as

$$\mathcal{C}_d^{\text{erg}} \approx \log_2\left(1 + e^{2\psi(1)+\ln\left(\frac{(1-\theta)\rho_s}{\kappa\lambda_{X_1}\lambda_{X_2}}\right)+e^{\lambda_{X_2}\kappa}Ei\left(-\lambda_{X_2}\kappa\right)}\right). \tag{5.17}$$

Proof: See Appendix D.3.

Next, we derive the closed-form expression for $\mathcal{C}_T^{\text{erg}}$. According to [91], $\mathcal{C}_T^{\text{erg}}$ is calculated as

$$C_T^{erg} = \frac{1}{\ln(2)} \int_0^{+\infty} \frac{1 - F_{\gamma_e}(\gamma) F_{\gamma_r}(\gamma)}{1+\gamma} d\gamma \tag{5.18}$$

Substituting the CDF of γ_e and γ_r into (18) yields

$$C_T^{\text{erg}} = C_{T,1}^{\text{erg}} + C_{T,2}^{\text{erg}} - C_{T,3}^{\text{erg}}, \tag{5.19}$$

where $C_{T,1}^{\text{erg}} = \frac{1}{\ln(2)\beta_X} \int_0^{+\infty} \frac{e^{-\frac{\gamma\lambda_{X_1}}{(1-\theta)\rho_s}}}{(\gamma+1)\left(\gamma+\beta_X^{-1}\right)} d\gamma$, $C_{T,2}^{\text{erg}} = \frac{1}{\ln(2)\beta_Y} \int_0^{+\infty} \frac{e^{-\frac{\lambda_{y_1}}{\rho_s}\gamma}}{(1+\gamma)\left(\gamma+\beta_Y^{-1}\right)} d\gamma$, $C_{T,3}^{\text{erg}} = \frac{1}{\ln(2)} \int_0^{+\infty} \frac{e^{-\mu\gamma}}{\beta_X\beta_Y(1+\gamma)\left(\gamma+\beta_X^{-1}\right)\left(\gamma+\beta_Y^{-1}\right)} d\gamma$, $\beta_X = \frac{\rho_d\lambda_{X_1}}{\rho_s\lambda_{X_2}}$, $\beta_Y = \frac{\rho_d\lambda_{Y_1}}{\rho_s\lambda_{Y_2}}$ and $\mu = \frac{\lambda_{Y_1}}{\rho_s} + \frac{\lambda_{X_1}}{\rho_s(1-\theta)}$.

Proposition 5.4 $\mathcal{C}_{T,1}^{\text{erg}}$ can be approximated as

$$\mathcal{C}_{T,1}^{\text{erg}} \approx \begin{cases} \frac{1}{\ln(2)(1-\beta_X)} \left(e^{\frac{\lambda_{X_2}}{(1-\theta)\rho_d}} Ei\left(-\frac{\lambda_{X_2}}{(1-\theta)\rho_d}\right) - e^{\frac{\lambda_{X_1}}{(1-\theta)\rho_s}} Ei\left(-\frac{\lambda_{X_1}}{(1-\theta)\rho_s}\right) \right); & (\text{for } \beta_X \neq 1) \\ \frac{1}{\ln(2)} \left(\frac{\lambda_{X_1}}{(1-\theta)\rho_s} e^{\frac{\lambda_{X_1}}{(1-\theta)\rho_s}} Ei\left(-\frac{\lambda_{X_1}}{(1-\theta)\rho_s}\right) + 1 \right); & (\text{for } \beta_X = 1) \end{cases}, \tag{5.20}$$

$\mathcal{C}_{T,2}^{\text{erg}}$ can be approximated as

$$\mathcal{C}_{T,2}^{\text{erg}} \approx \begin{cases} \frac{1}{\ln(2)(1-\beta_Y)} \left(e^{\frac{\lambda_{Y_2}}{\rho_d}} Ei\left(-\frac{\lambda_{Y_2}}{\rho_d}\right) - e^{\frac{\lambda_{Y_1}}{\rho_s}} Ei\left(-\frac{\lambda_{Y_1}}{\rho_s}\right) \right); & (\text{for } \beta_Y \neq 1) \\ \frac{1}{\ln(2)} \left(\frac{\lambda_{Y_1}}{\rho_s} e^{\frac{\lambda_{Y_1}}{\rho_s}} Ei\left(-\frac{\lambda_{Y_1}}{\rho_s}\right) + 1 \right); & (\text{for } \beta_Y = 1) \end{cases}, \tag{5.21}$$

$\mathcal{C}_{T,3}^{\text{erg}}$ can be approximated as

$$\mathcal{C}_{T,3}^{\text{erg}} \approx \begin{cases} \frac{-A_1}{\ln(2)} e^{\mu} Ei\left(-\mu\right) - \frac{B_1}{\ln(2)} e^{\frac{\mu}{\beta_X}} Ei\left(\frac{-\mu}{\beta_X}\right) & \\ \qquad - \frac{C_1}{\ln(2)} e^{\frac{\mu}{\beta_Y}} Ei\left(\frac{-\mu}{\beta_Y}\right); & (\text{for } \beta_X \neq 1, \beta_Y \neq 1, \beta_X \neq \beta_Y) \\ \frac{-A_2}{\ln(2)} e^{\mu} Ei\left(-\mu\right) + \frac{B_2\mu + A_2}{\ln(2)} e^{\frac{\mu}{\beta_0}} Ei\left(\frac{-\mu}{\beta_0}\right) + \frac{B_2\beta_0}{\ln(2)}; & (\text{for } \beta_X = \beta_Y = \beta_0; \beta_0 \neq 1) \\ \frac{B_3\mu - A_3}{\ln(2)} e^{\mu} Ei\left(-\mu\right) + \frac{B_3}{\ln(2)} + \frac{A_3}{\ln(2)} e^{\frac{\mu}{\beta_Y}} Ei\left(\frac{-\mu}{\beta_Y}\right); & (\text{for } \beta_X = 1; \beta_Y \neq 1) \\ \frac{B_4\mu - A_4}{\ln(2)} e^{\mu} Ei\left(-\mu\right) + \frac{B_4}{\ln(2)} + \frac{A_4}{\ln(2)} e^{\frac{\mu}{\beta_X}} Ei\left(\frac{-\mu}{\beta_X}\right); & (\text{for } \beta_X \neq 1; \beta_Y = 1) \\ \frac{1}{2\ln(2)} \left(1 - \mu - \mu^2 e^{\mu} Ei\left(-\mu\right)\right); & (\text{for } \beta_X = \beta_Y = 1) \end{cases}, \tag{5.22}$$

where $A_1 = \frac{1}{(\beta_X - 1)(\beta_Y - 1)}$, $B_1 = \frac{1}{(\beta_X - 1)\left(1 - \beta_Y \beta_X^{-1}\right)}$, $C_1 = \frac{1}{(\beta_Y - 1)\left(1 - \beta_X \beta_Y^{-1}\right)}$, $A_2 = \frac{1}{(\beta_0 - 1)^2}$, $B_2 = \frac{1}{\beta_0(\beta_0 - 1)}$, $A_3 = \frac{-\beta_Y}{(\beta_Y - 1)^2}$, $B_3 = \frac{1}{1 - \beta_Y}$, $A_4 = \frac{-\beta_X}{(\beta_X - 1)^2}$ and $B_4 = \frac{1}{1 - \beta_X}$.

Proof: Following the same steps for the calculation of $F_{\gamma_e}(\gamma)$ given in Appendix A, $F_{\gamma_r}(\gamma)$ is calculated as

$$F_{\gamma_r}\left(\gamma\right) = 1 - \frac{1}{\gamma\beta_X + 1} e^{-\frac{\gamma\lambda_{X_1}}{(1-\theta)\rho_s}} \tag{5.23}$$

Then, using partial fraction decomposition and applying [53, Eq. (3.353.2)], we can obtain the desired results.

5.4 Simulation results

In this section, we present numerical results to validate the analytical expressions presented in Section 3. Unless otherwise specified, we set $\rho_s = \rho_d = 25$ dB, $\eta = 0.5$, $\theta = 0.5$, $\tau = 3$, and $R_{th} = 1$ (bits/s/Hz). Any change in the values of these parameters is described at the captions and legends of the figures. The coordinates in the two-

dimensional plane of $S, D, R,$ and E are set at $(0,0), (2,0), (d_r, 0.2)$, and $(d_e, 0.2)$, respectively.

In Figure 5.2, we investigate the SOP and its approximation when both S and D increase their transmit powers, i.e., $\rho_s = \rho_d = \rho$. As can be seen, the SOP slightly improves as ρ increases from 0 to 10 dB and remarkably improves with further increases in ρ. This is because the AN efficiently degrades the SNRs of R and E at high ρ values, whereas it does not interfere with the signal quality at D. Additionally, the SOP increases as R_{th} increases. Moreover, as shown in Figure 5.2, the analytical result matches well with the exact SOP, and the high-power approximation for the SOP can be considered as the upper bound. The high-power curves are quite close to the exact SOPs at moderate ρ values (from 20 to 30 dB), and they are very tight to the exact SOPs at higher ρ values.

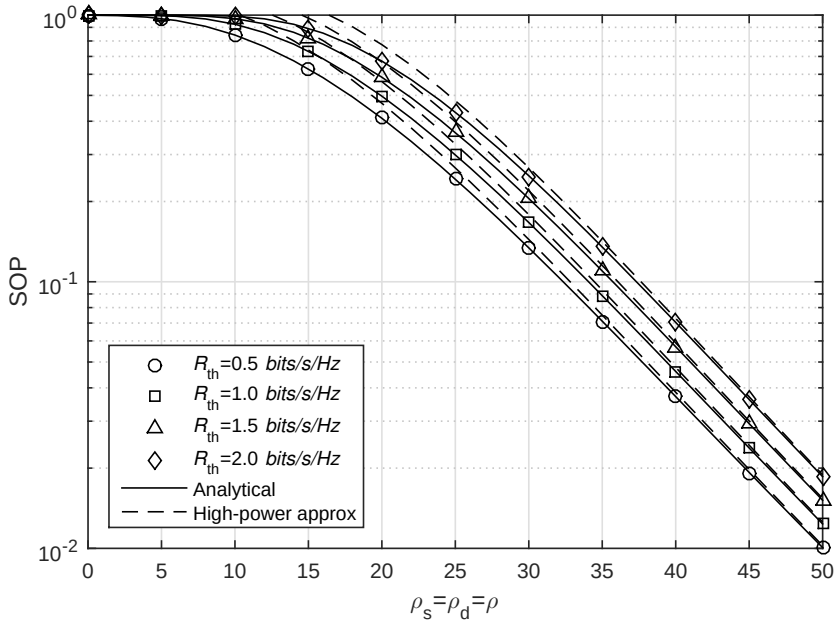

Figure 5.2: The effect of ρ on the SOP and its approximation. Other parameters: $d_r = d_e = 1$ and $\rho_s = \rho_d = \rho$.

In Figure 5.3, we investigate the effect of θ on the SOP and ASC. θ is varied from 0 to 1. As can be seen, the trends of the SOP and ASC in this figure are similar to them in Figure 4.3. The explanation of these trends was given in the discussion of the Figure 4.3. The SOP and ASC improve as θ increases and reach their optimal values at their corresponding optimal PS ratios, θ^*. Then, the SOP and ASC degrade with further increase in θ. Additionally, the SOP and ASC are examined with different values of η. As η increases, R is capable of harvesting more energy; hence, better performance can be achieved. It can also be observed that the value of θ^* decreases with increasing values of η.

In Figure 5.4, we investigate the effect of ρ_s and ρ_d on the optimal SOP and optimal ASC in different scenarios: $\mathrm{S}_1, \mathrm{S}_2$, and S_3. We fix ρ_s and ρ_d in S_1 and S_2, respectively, while we vary their values in S_3. As shown in Figure 5.4(a), the optimal SOP shows similar trends in the three scenarios, i.e., decreasing with increasing ρ. Moreover, at high ρ values, the optimal SOPs in scenarios S_1 and S_2 converge to non-zero numbers, whereas they are nearly zero in scenario S_3. As shown in Figure 5.4(b), the optimal ASCs in scenarios S_1 and S_2 increase and converge to the determined throughputs as ρ increases. In contrast, the optimal ASCs in scenario S_3 linearly increase as ρ increases. Because the results of the optimal SOP can be explained by using the trends of the optimal ASC, we focus on understanding the effects of ρ on the optimal ASC. In scenario S_1, the fixed value of ρ_s leads to a fixed $\mathcal{C}_d$, which limits the optimal ASC. In scenario S_2, the optimal ASCs converge because $\mathcal{C}_r, \mathcal{C}_e$ and $\mathcal{C}_d$ grow at the same rate at high ρ_d values. In scenario S_3, the increasing trend of ρ_s leads to substantial growth in $\mathcal{C}_d$. Additionally, the increasing trend of ρ_d limits the values of $\mathcal{C}_r$ and $\mathcal{C}_e$. These

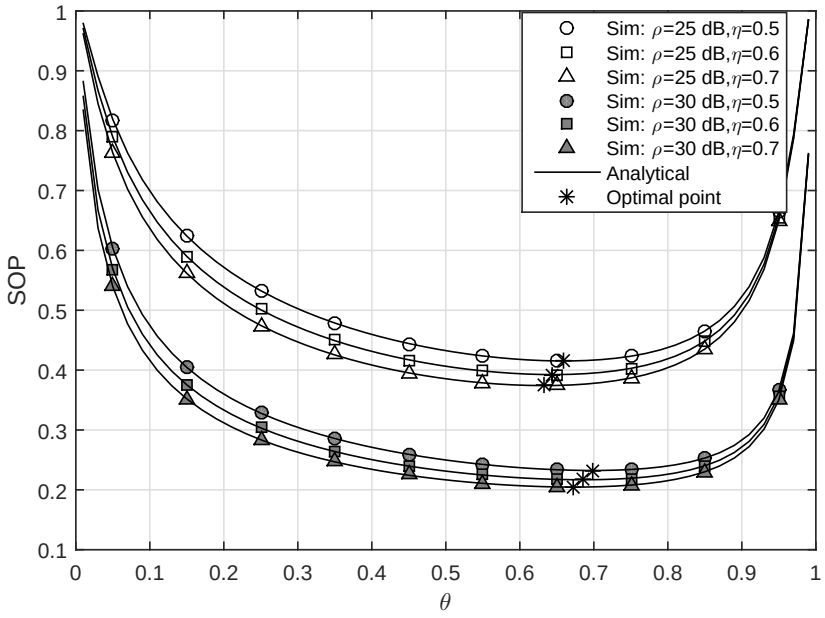

(a)

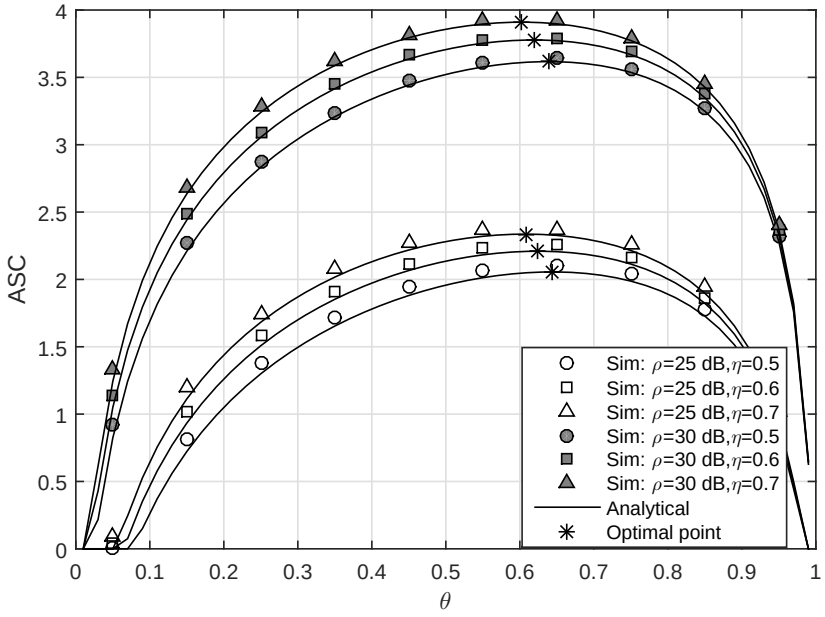

(b)

Figure 5.3: The effect of θ on a) the SOP and b) the ASC. Other parameters: $d_r = d_e = 1$, $\rho_s = \rho_d = \rho$, and $R_{th} = 2$ bits/s/Hz.

factors combine to yield a significant increase in the optimal ASC. Moreover, Figure 5.4 also shows that a sufficient strength of the AN is necessary to yield a positive ASC at D with relatively low source's transmit powers. In particular, the optimal ASC in scenarios S_1 and S_3 are nearly zero as ρ_d is less than $16dB$, whereas it in scenario S_2 can be approximately 0.5 (bits/s/Hz) for $\rho_s = 10$ dB and 1 (bits/s/Hz) for $\rho_s = 15$ (dB).

In Figure 5.5, we investigate the effect of the distances on the optimal SOP and optimal ASC. This figure clearly shows that $\mathcal{C}_r, \mathcal{C}_e$ and $\mathcal{C}_d$ achieve greater values as R and E tend to S and vice versa. Therefore, the best optimal SOP and the best optimal ASC can be observed at the position where R and E are near D, at which point $\mathcal{C}_e$ and $\mathcal{C}_r$ are significantly depressed due to the strong influence of the AN. The least optimal SOP and least optimal ASC are found at the position where E is close to S and R is near D, at which point the low $\mathcal{C}_d$ value and high $\mathcal{C}_e$ value lead to low system performance. Additionally, it can be seen in Figure 5.5(b) that there is a region at which the optimal ASC is approximately zero. It is reasonable to conclude that choosing the location of R can help improve the secure performance. In particular, when E is close to S, R should be located near S, and when E is near D, R should be located near D.

5.5 Conclusions

In this Chapter, we proposed and analyzed an UR–WEH system where the secure communication was attacked by both the untrusted relay and external eavesdropper. We employed the destination–assisted jamming signal to prevent the untrusted relay

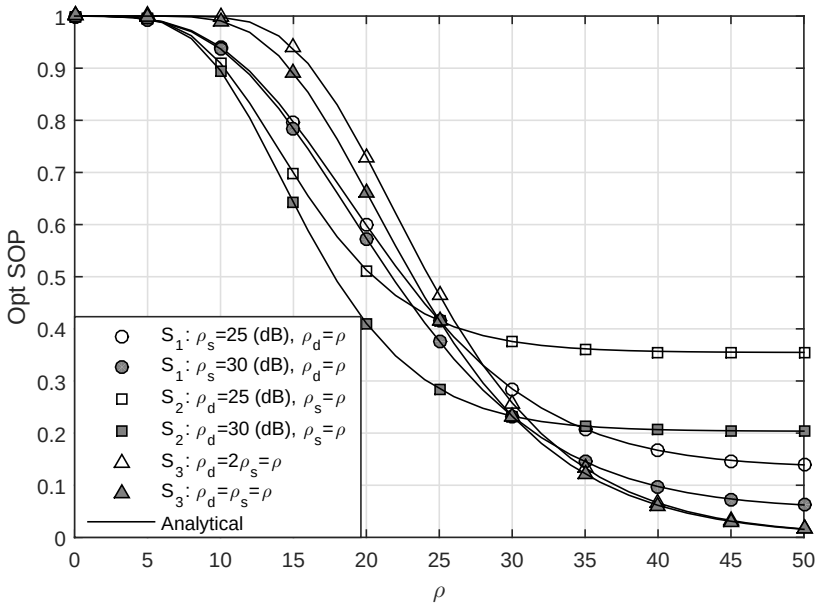

(a)

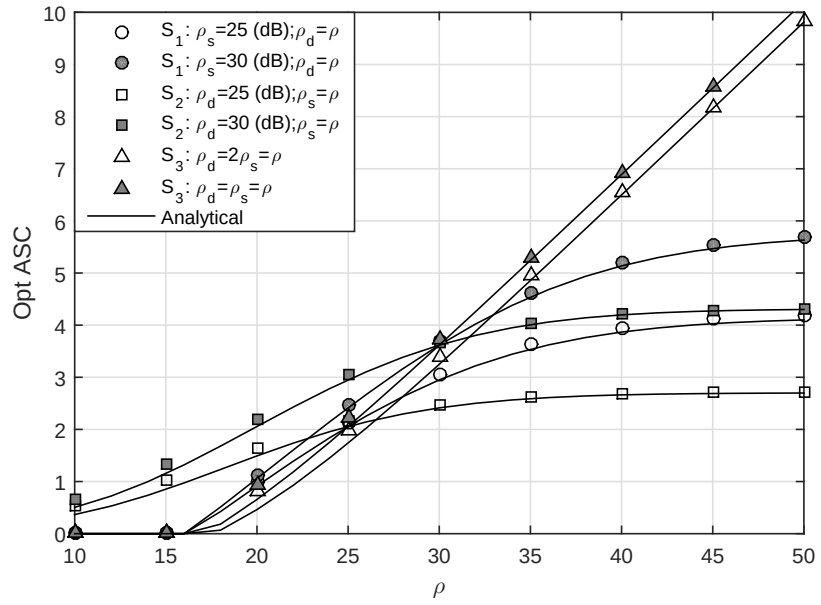

(b)

Figure 5.4: The effect of ρ_s and ρ_d on a) the optimal SOP and b) the optimal ASC. Other parameters: $d_r = d_e = 1$ and $R_{th} = 2$ bits/s/Hz.

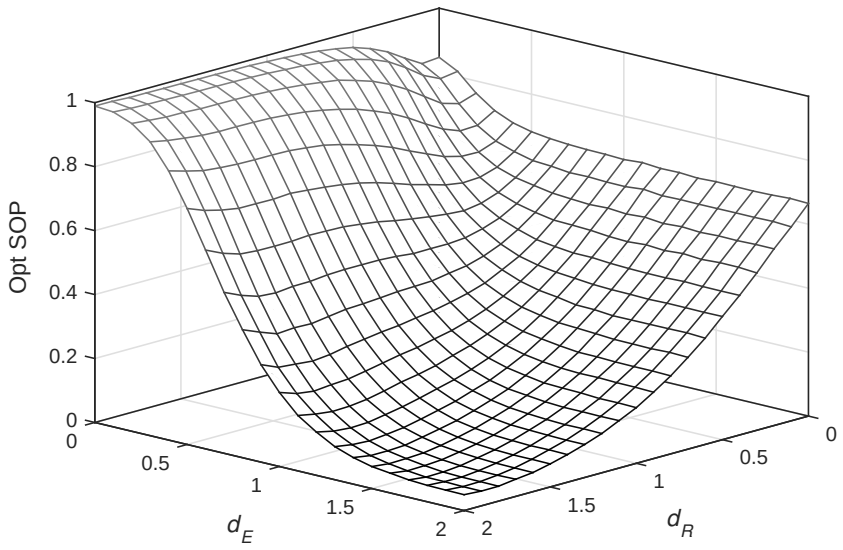

(a)

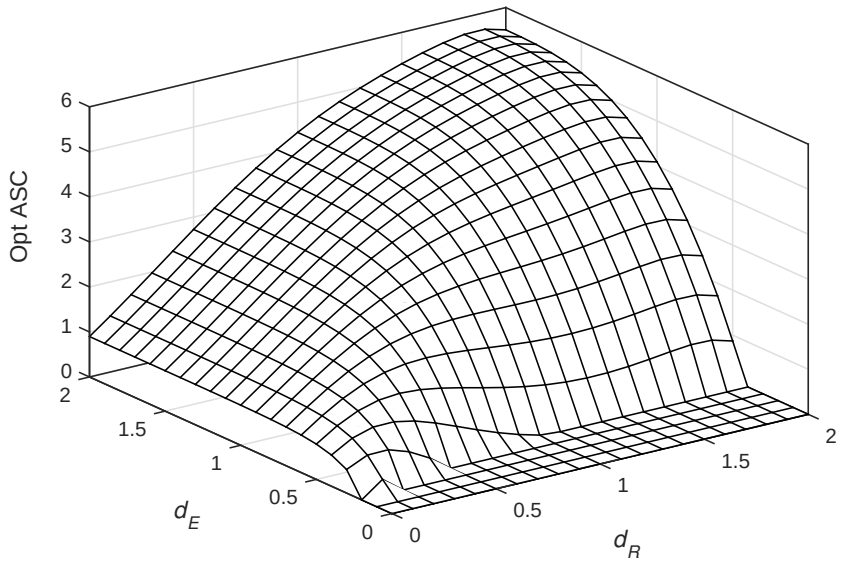

(b)

Figure 5.5: The effect of distances on a) the optimal SOP and b) the optimal ASC.

and eavesdropper from overhearing the source's confidential information. To evaluate the secrecy performance, we derived the analytical expressions for the SOP and ASC; moreover, the high–power approximation for the SOP was also presented in this Chapter. We used the Monte Carlo simulations to verify the accuracy of the analytical results. The results showed that:

- In the presence of the external eavesdropper, an reasonable location of the untrusted relay can yield a higher secrecy performance. In particular, the relay should be located near the source as the eavesdropper is close to the source and vice versa.

- At high–power scenario, the proposed system provides high secrecy performances only if the information signal power and jamming signal power linearly increase.

- The simulation results also allow detailed studies into the effects of different system parameters, such as, η, R_{th}, θ, transmit powers, and locations of the relay and eavesdropper, on the secrecy performance, which provide useful design insights.

Chapter 6

Secure communication in untrusted relay-selection network with wireless energy-harvesting [1]

6.1 Introduction

In this Chapter, we study the problem of secure communication in a relay–selection UR–WEH system. Our system consists of a multi–antenna source–destination pair and L single–antenna untrusted relays. We use the KBFC and KBSC schemes to choose the K–th best relay to assist the source–to–destination communication and use transmit beamforming technique known as MRT to eliminate the security risks from the non–selected relays. Then, we use the destination–assisted jamming to interfere the selected relay for archiving the positive secrecy rate. The PS receiver architecture

[1] The study in this chapter was published in Wireless Networks [93]

is adopted. For performance evaluation, we derive the SOP expressions involving a single integral and a tight closed–form upper bound for the ASC; moreover, the closed–form expressions for the SOP at high–power scenarios are also derived. The accuracy of the analytical results is verified by Monte Carlo simulations.

The rest of this Chapter is organized as follows. The system model is presented in Section 6.2. The analytical expressions for the SOP and ASC are derived in Section 6.3. The results and discussion are given in Section 6.4. Finally, the conclusions are presented in Section 6.5.

6.2 System Model and Preliminary Results

6.2.1 System Model

We consider an UR–WEH system illustrated in Figure 6.1(a). Our system consists of a multi–antenna source, S, equipped with N_1 antennas, a multi–antenna destination, D, equipped with N_2 antennas, and single–antenna untrusted relay network, R, including L nodes, $R_l, l = 1, \ldots, L$. The relays are located within a cluster, and are close to each other relative to the distances d_1 to $\mathcal{S}$ and d_2 to $\mathcal{D}$. We consider two relay selection schemes, KBFC and KBSC, to choose the K–th best relay, $R^{(K)}$, to assist the communication. $R^{(K)}$ uses the PS policy with a PS ratio $0 < \theta < 1$ shown in Figure 6.1(b) to harvest energy and uses the AF protocol to forward the source's signal. In each block time, T, the entire communication consists of two time slots, $T/2$. During the first time slot, S and D simultaneously send the information signal and the jamming signal to $R^{(K)}$, respectively, and $R^{(K)}$ harvests energy from these

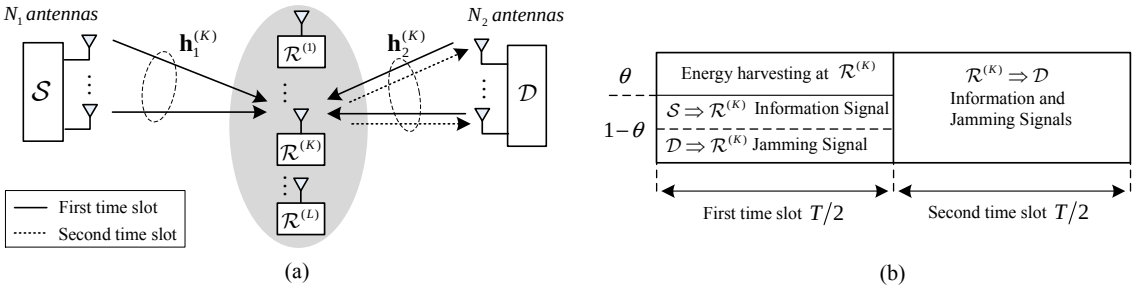

Figure 6.1: System model.

signals. Then, R uses all harvested energy to forward the received signal to D during the second time slot. The channels of wireless links undergo Nakagami-m fading; hence, the channel gains are gamma RVs.

6.2.2 Preliminary Results

The PDF and CDF of a gamma RV, $\mathcal{X}$, are given in Section 1.3.1 as

$$f_{\mathcal{X}}(x; m, \lambda) = \frac{x^{m-1}}{\Gamma(m)\lambda^m} e^{-\frac{x}{\lambda}}, \tag{6.1}$$

$$F_{\mathcal{X}}(x; m, \lambda) = \frac{1}{\Gamma(m)} \gamma\left(m, \frac{x}{\lambda}\right). \tag{6.2}$$

where m is a shape parameter and λ is a scale parameter.

Let $\mathbf{h}_{1,l} = [h_{1,l,1}, \ldots, h_{1,l,N_1}]^\top, \mathbf{h}_{2,l} = [h_{1,l,1}, \ldots, h_{1,l,N_2}]^\top$, $\mathbf{h}_1^{(K)}$ and $\mathbf{h}_2^{(K)}$ respectively represent the channel vectors of the $\mathcal{S}$–$\mathcal{R}_l, \mathcal{R}_l$–$\mathcal{D}, \mathcal{S}$–$\mathcal{R}^{(K)}$ and $\mathcal{R}^{(K)}$–$\mathcal{D}$ links, $|h_{1,l,n_1}|^2, n_1 = 1, \ldots, N_1$, and $|h_{2,l,n_2}|^2, n_2 = 1, \ldots, N_2$, are respectively gamma RVs with parameters $(m_1, \frac{\lambda_1}{m_1})$ and $(m_2, \frac{\lambda_2}{m_2})$, $\lambda_1 = d_1^{-\tau}, \lambda_2 = d_2^{-\tau}$, and τ is the path loss

exponent. The relay selection strategies are given in Section 1.3.3 as

$$\mathcal{R}^{(K)} = K\text{th} \underset{1\leqslant l\leqslant L}{\arg\max}\{\|\mathbf{h}_{1,l}\|_2^2\}, \text{ (KBFC scheme)} \tag{6.3a}$$

$$\mathcal{R}^{(K)} = K\text{th} \underset{1\leqslant l\leqslant L}{\arg\max}\{\|\mathbf{h}_{2,l}\|_2^2\}. \text{ (KBSC scheme)} \tag{6.3b}$$

According to [35], $\|\mathbf{h}_{1,l}\|_2^2$ and $\|\mathbf{h}_{2,l}\|_2^2$ are gamma RVs with parameters $\left(N_1 m_1, \frac{\lambda_1}{m_1}\right)$ and $\left(N_2 m_2, \frac{\lambda_2}{m_2}\right)$, respectively.

After selecting $\mathcal{R}^{(K)}$, the information x_s of $\mathcal{S}$ and the AN x_d of $\mathcal{D}$ are simultaneously transmitted to $\mathcal{R}^{(K)}$. We assume that each relay knows only its local CSI; therefore, by using transmit beamforming technique, security risks from the non-selected relays are eliminated; therefore, the secure communication of the proposed system is studied by analyzing the secure risk from $\mathcal{R}^{(K)}$. Let $\mathbf{w}_1 = \frac{\left(\mathbf{h}_1^{(K)}\right)^\dagger}{\|\mathbf{h}_1^{(K)}\|_2}$ and $\mathbf{w}_2 = \frac{\left(\mathbf{h}_2^{(K)}\right)^\dagger}{\|\mathbf{h}_2^{(K)}\|_2}$ be respectively the transmit beamforming vectors at $\mathcal{S}$ and $\mathcal{D}$, the signal component at the input of the information receiver of $\mathcal{R}^{(K)}$ is given by

$$y_r = \sqrt{(1-\theta)P_s}\left\|\mathbf{h}_1^{(K)}\right\|_2 x_s + \sqrt{(1-\theta)P_d}\left\|\mathbf{h}_2^{(K)}\right\|_2 x_d + n_r, \tag{6.4}$$

where P_s and P_d are respectively the transmit power of $\mathcal{S}$ and $\mathcal{D}$, $n_r \sim \mathcal{CN}(0, N_0)$ is the AWGN at $\mathcal{R}^{(K)}$, and N_0 is the noise power. The overall energy harvested at $\mathcal{R}^{(K)}$ is given by

$$E_h = \eta\theta\left(P_s X + P_d Y\right) T/2, \tag{6.5}$$

where η is the energy conversion efficiency factor; $X = \|\mathbf{h}_1^{(K)}\|_2^2$ and $Y = \|\mathbf{h}_2^{(K)}\|_2^2$.

From (6.4),the instantaneous SNR at $\mathcal{R}^{(K)}$ can be expressed as

$$\gamma_{\mathrm{r}} = \frac{\mathrm{a}X}{\mathbb{b}Y + 1}, \tag{6.6}$$

where $\mathbb{a} = (1-\theta)\,P_s/N_0$ and $\mathbb{b} = (1-\theta)\,P_d/N_0$.

During the second time slot, $\mathcal{R}^{(K)}$ forwards its received signal with transmit power $P_r = 2E_h/T$, hence, the received signal at $\mathcal{D}$ can be expressed as

$$\mathbf{y}_d = \sqrt{P_r}\mathbf{h}_2^{(K)} G_r y_r + \mathbf{n}_d, \tag{6.7}$$

where $G_r = 1/\sqrt{(1-\theta)\,(P_s X + P_d Y) + \sigma_r^2}$, and $\mathbf{n}_d \sim \mathcal{CN}\,(0, N_0\mathbf{I}_{N_2})$ is the AWGN vector at $\mathcal{D}$.

Substituting (6.4) and (6.5) into (6.7), we have the following

$$\begin{aligned} y_d = &\underbrace{\sqrt{(1-\theta)\,P_s P_r}\left\|\mathbf{h}_1^{(K)}\right\|_2 \mathbf{h}_2^{(K)} G_r x_s}_{\text{desired signal}} \\ &+ \underbrace{\sqrt{(1-\theta)\,P_r P_d}\left\|\mathbf{h}_2^{(K)}\right\|_2 \mathbf{h}_2^{(K)} G_r x_d}_{\text{artificial noise}} + \underbrace{\sqrt{P_r}\mathbf{h}_2^{(K)} G_r n_r + \mathbf{n}_d}_{\text{overall noise}}. \end{aligned} \tag{6.8}$$

Because $\mathcal{D}$ can eliminate the AN in (6.8), the instantaneous SNR at $\mathcal{D}$ can be calculated as

$$\gamma_d = \frac{\mathbb{a} XYZ}{YZ + \mathbb{c}Z + \mathbb{d}} \approx \frac{\mathbb{a} XY}{Y + \mathbb{c}}, \tag{6.9}$$

where $Z = P_s X + P_d Y$, $\mathbb{c} = \frac{(1-\theta)}{\eta\theta}$ and $\mathbb{d} = \frac{N_0}{\eta\theta}$. The approximation in (6.9) is acceptable because the noise variance term is negligible compared to the other factors in the denominator.

According to [73], the instantaneous secrecy capacity can be calculated as

$$R_{\text{sec}} = \frac{1}{2}\left[\log_2(1+\gamma_d) - \log_2(1+\gamma_r)\right]^+ \tag{6.10}$$

To evaluate the system performance, we need to study the statistical characteristics of the Kth best gamma RV. Letting $\mathcal{X}_1, \ldots, \mathcal{X}_L$ be L i.i.d. gamma RVs with

Table 6.1: The PDF and CDF of X and Y

	KBFC scheme	**KBSC scheme**
$f_X(x)$	$f_{\mathcal{X}^{(K)}}\left(x; N_1 m_1, \frac{\lambda_1}{m_1}\right)$	$f_{\mathcal{X}}\left(x; N_1 m_1, \frac{\lambda_1}{m_1}\right)$
$F_X(x)$	$F_{\mathcal{X}^{(K)}}\left(x; N_1 m_1, \frac{\lambda_1}{m_1}\right)$	$F_{\mathcal{X}}\left(x; N_1 m_1, \frac{\lambda_1}{m_1}\right)$
$f_Y(y)$	$f_{\mathcal{X}}\left(y; N_2 m_2, \frac{\lambda_2}{m_2}\right)$	$f_{\mathcal{X}^{(K)}}\left(y; N_2 m_2, \frac{\lambda_2}{m_2}\right)$
$F_Y(y)$	$F_{\mathcal{X}}\left(y; N_2 m_2, \frac{\lambda_2}{m_2}\right)$	$F_{\mathcal{X}^{(K)}}\left(y; N_2 m_2, \frac{\lambda_2}{m_2}\right)$

parameters (m, λ). According to [94], the PDF and CDF of the Kth best order RV $\mathcal{X}^{(K)} \triangleq K\text{th} \underset{1 \leqslant l \leqslant L}{\arg\max}\{\mathcal{X}_l\}$ are respectively given by

$$f_{\mathcal{X}^{(K)}}(x; m, \lambda) = \frac{L! f_{\mathcal{X}}(x; m, \lambda)}{(K-1)!\,(L-K)!\Gamma(m)^{L-1}} \gamma\left(m, \tfrac{x}{\lambda}\right)^{L-K} \Gamma\left(m, \tfrac{x}{\lambda}\right)^{K-1}, \tag{6.11}$$

and

$$F_{\mathcal{X}^{(K)}}(x; m, \lambda) = \sum_{k=0}^{K-1} \binom{L}{k} \frac{1}{\Gamma(m)^L} \gamma\left(m, \tfrac{x}{\lambda}\right)^{L-k} \Gamma\left(m, \tfrac{x}{\lambda}\right)^{k}. \tag{6.12}$$

Then, the PDF of X, $f_X(x)$, CDF of X, $F_X(x)$, PDF of Y, $f_Y(y)$ and CDF of Y, $F_Y(y)$, for the KBFC and KBSC schemes are determined in Table 6.1.

6.3 Performance Analysis

In this section, we derive the analytical expressions for the SOP and ASC, and the high–power approximation for the SOP.

6.3.1 Secrecy outage probability

The SOP is calculated by

$$P_{\text{out}} = \Pr\left(R_{\text{sec}} < R_{\text{th}}\right). \tag{6.13}$$

Substituting (6.6), (6.9) and (6.10) into (6.13), the SOP is bounded below by

$$P_{\text{out,low}} = \Pr\left(\mathbb{a}X\Xi\left(Y;\gamma_{\text{th}}\right) < \gamma_{\text{th}} - 1\right), \tag{6.14}$$

where $\gamma_{\text{th}} = 2^{2R_{\text{th}}}$, R_{th} is the target secrecy rate and $\Xi\left(y;\gamma_{\text{th}}\right) = \frac{y}{y+\mathbb{c}} - \frac{\gamma_{\text{th}}}{\mathbb{b}y+1}$.

Proposition 6.1 The SOPs for the KBFC and KBSC schemes are respectively bounded below by

$$P_{\text{out,low}}^{\text{KBFC}} = 1 + \sum_{k=0}^{K-1}\sum_{\substack{n=0\\k+n\neq 0}}^{L-k}\sum_{\left\|\mathbf{p}^{(1)}\right\|_1=k+n} \frac{(-1)^n m_2^{N_2m_2}}{\Gamma\left(N_2m_2\right)\lambda_2^{N_2m_2}}\binom{L}{k}\binom{L-k}{n}\binom{k+n}{\mathbf{p}^{(1)}}$$
$$\times\left(\prod_{i=0}^{N_1m_1-1}(i!)^{-p_i^{(1)}}\right)\left(\frac{m_1\left(\gamma_{\text{th}}-1\right)}{\mathbb{a}\lambda_1}\right)^{\omega_1}\int_{y_1}^{\infty}\frac{y^{N_2m_2-1}}{\Xi(y;\gamma_{\text{th}})^{\omega_1}}e^{-\frac{m_1(k+n)(\gamma_{\text{th}}-1)}{\mathbb{a}\lambda_1\Xi(y;\gamma_{\text{th}})}-\frac{m_2}{\lambda_2}y}dy, \tag{6.15}$$

$$P_{\text{out,low}}^{\text{KBSC}} = 1 - \sum_{j=0}^{N_1m_1-1}\sum_{n=0}^{L-K}\sum_{\left\|\mathbf{p}^{(2)}\right\|_1=K+n-1}\frac{L!(-1)^n}{j!\left(K-1\right)!\left(L-K\right)!\Gamma\left(N_2m_2\right)}$$
$$\times\left(\frac{m_1\left(\gamma_{\text{th}}-1\right)}{\mathbb{a}\lambda_1}\right)^{j}\binom{L-K}{n}\binom{K+n-1}{\mathbf{p}^{(2)}}\left(\frac{m_2}{\lambda_2}\right)^{N_2m_2+\omega_2}\left(\prod_{j=0}^{N_2m_2-1}(j!)^{-p_j^{(2)}}\right)$$
$$\times\int_{y_1}^{+\infty}\frac{y^{N_2m_2+\omega_2-1}}{\Xi\left(y;\gamma_{\text{th}}\right)^{j}}e^{-\frac{m_1\left(\gamma_{\text{th}}-1\right)}{\mathbb{a}\lambda_1\Xi\left(y;\gamma_{\text{th}}\right)}-\frac{m_2(K+n)y}{\lambda_2}}dy, \tag{6.16}$$

where $\mathbf{p}^{(1)} = \left[p_0^{(1)},\ldots,p_{N_1m_1-1}^{(1)}\right]$, $\mathbf{p}^{(2)} = \left[p_0^{(2)},\ldots,p_{N_2m_2-1}^{(2)}\right]$, $\omega_1 = \sum_{i=0}^{N_1m_1-1} ip_i^{(1)}$, $\omega_2 = \sum_{j=0}^{N_2m_2-1} jp_j^{(2)}$, and $y_1 = \frac{\gamma_{\text{th}}-1+\sqrt{\left(\gamma_{\text{th}}-1\right)^2+4\gamma_{\text{th}}\mathbb{bc}}}{2\mathbb{b}}$ is the positive root of the equation $\Xi(y,\gamma_{\text{th}}) = 0$.

Proof: See Appendix E.1.

6.3.2 High-power secrecy outage probability approximation

At high–power scenario, i.e., $(P_s, P_d) \to (\infty, \infty)$, (6.14) is rewritten as

$$\begin{aligned} P_{\text{out,low}} &= \Pr\left(\frac{\mathbb{a}\mathbb{b}X\left(Y-y_1\right)\left(Y-y_2\right)}{\left(Y+\mathbb{c}\right)\left(\mathbb{b}Y+1\right)} < \gamma_{\text{th}}-1\right) \\ &= \Pr\left(Y<y_1\right)+\Pr\left(X<x_0|Y>y_1\right)\Pr(Y>y_1), \end{aligned} \tag{6.17}$$

where $y_2 = \frac{\gamma_{\text{th}}-1-\sqrt{(\gamma_{\text{th}}-1)^2+4\gamma_{\text{th}}\mathbb{b}\mathbb{c}}}{2\mathbb{b}}$ is the negative root of the equation $\Xi(y,\gamma_{\text{th}})=0$, and $x_0 = \frac{(\gamma_{\text{th}}-1)(Y+\mathbb{c})(\mathbb{b}Y+1)}{\mathbb{a}\mathbb{b}(Y-y_1)(Y-y_2)}$.

Without loss of generality, we assume that $\mathbb{a} = \zeta\mathbb{b}$ and $(\mathbb{a},\mathbb{b}) \to (\infty,\infty)$ where ζ is constant; therefore, we can simplify x_0, y_1, and y_2 by evaluating the leading-order terms in the numerators and denominators as follows: $y_1 \approx y_0, y_2 \approx -y_0$ and $x_0 \approx \frac{\gamma_{\text{th}}-1}{\mathbb{a}}\left(1+\frac{\mathbb{c}}{Y}\right)$ where $y_0 \triangleq \sqrt{\frac{\gamma_{\text{th}}\mathbb{c}}{\mathbb{b}}}$. Then, (6.17) at high-power scenario can be approximated by

$$P_{\text{out,HPL}} \approx \underbrace{F_Y\left(y_0\right)}_{\mathcal{J}_1} + \underbrace{\int_{y_0}^{\infty} F_X\left(\frac{\gamma_{\text{th}}-1}{\mathbb{a}}\left(1+\frac{\mathbb{c}}{y}\right)\right) f_Y\left(y\right) dy}_{\mathcal{J}_2}. \tag{6.18}$$

Proposition 6.2 The SOPs for the KBFC and KBSC schemes at high-power scenario are respectively approximated by (6.19) and (6.20) shown on the top of the next page.

where $Ei(\cdot)$ is the exponential integral function [53, Eq. (8.310.1)], $\mu_1 = \frac{m_1(\gamma_{\text{th}}-1)}{\zeta\gamma_{\text{th}}\mathbb{c}\lambda_1}$ and $\mu_2 = \frac{m_2(K+n)y_0}{\lambda_2}$.

Proof: See Appendix E.2.

$$P_{\text{out,HPL}}^{\text{KBFC}} \approx \frac{1}{(N_2m_2)!}\left(\frac{m_2y_0}{\lambda_2}\right)^{N_2m_2} + \binom{L}{K-1}\frac{\left(\mu_1y_0^2\right)^{N_1m_1(L-K+1)}}{\Gamma\left(N_2m_2\right)\Gamma(N_1m_1+1)^{L-K+1}}$$
$$\times \sum_{n=0}^{N_1m_1(L-K+1)}\left(\frac{m_2\mathbb{C}}{\lambda_2}\right)^n\binom{N_1m_1(L-K+1)}{n}\Bigg(\mathbb{1}(n<N_2m_2)\Gamma\left(N_2m_2-n\right)$$
$$+\,\mathbb{1}(n\geqslant N_2m_2)\left(\frac{(-1)^{n-N_2m_2+1}}{(n-N_2m_2)!}\,Ei\left(-\frac{m_2y_0}{\lambda_2}\right)+e^{-\frac{m_2y_0}{\lambda_2}}\sum_{u=0}^{n-N_2m_2-1}(-1)^u\right.$$
$$\left.\times\,\frac{(n-N_2m_2-u-1)!}{(n-N_2m_2)!}\left(\frac{\lambda_2}{m_2y_0}\right)^{n-N_2m_2-u}\right)\Bigg), \tag{6.19}$$

$$P_{\text{out,HPL}}^{\text{KBSC}} \approx \binom{L}{K-1}\frac{1}{\Gamma(N_2m_2+1)^{L-K+1}}\left(\frac{m_2y_0}{\lambda_2}\right)^{N_2m_2(L-K+1)} + \frac{L!}{(N_1m_1)!}$$
$$\times\,\frac{\left(\mu_1y_0^2\right)^{N_1m_1}}{(K-1)!\,(L-K)!\Gamma(N_2m_2)}\sum_{n=0}^{L-K}(-1)^n\binom{L-K}{n}\sum_{\left\|\mathbf{p}^{(2)}\right\|_1=K+n-1}\binom{K+n-1}{\mathbf{p}^{(2)}}$$
$$\times\left(\prod_{j=0}^{N_2m_2-1}\left(\frac{1}{j!}\right)^{p_j^{(2)}}\right)\sum_{i=0}^{N_1m_1}\binom{N_1m_1}{i}\left(\frac{m_2\mathbb{C}}{\lambda_2}\right)^i\frac{1}{(K+n)^{N_2m_2+\omega_2-i}}$$
$$\times\left(\mathbb{1}(i<N_2m_2+\omega_2)\Gamma(N_2m_2+\omega_2-i)+\mathbb{1}(i\geqslant N_2m_2+\omega_2)\left(\frac{(-1)^{i-N_2m_2-\omega_2+1}}{(i-N_2m_2-\omega_2)!}\right.\right.$$
$$\left.\left.\times\,Ei(-\mu_2)+e^{-\mu_2}\sum_{u=0}^{i-N_2m_2-\omega_2-1}\frac{(-1)^u\,(i-N_2m_2-\omega_2-u-1)!}{(i-N_2m_2-\omega_2)!}\mu_2^{N_2m_2+\omega_2+u-i}\right)\right), \tag{6.20}$$

6.3.3 Average secrecy capacity

The ASC of the proposed system is given by

$$\bar{R}_{\text{sec}} = \frac{1}{2}\mathbb{E}\left\{\left[\log_2\left(1+\gamma_{\text{d}}\right)-\log_2\left(1+\gamma_{\text{r}}\right)\right]^+\right\}. \tag{6.21}$$

From (6.6) and (6.9), the ASC can be approximated by

$$\bar{R}_{\text{sec}} \approx \frac{1}{2}\mathbb{E}\left\{\left[\log_2\left(1+\tfrac{\mathbb{a}X}{\mathbb{c}Y^{-1}+1}\right)-\log_2\left(1+\tfrac{\mathbb{a}X}{\mathbb{b}Y+1}\right)\right]^+\right\}, \tag{6.22a}$$

$$= \frac{1}{2}\mathbb{E}\left\{\log_2\left(1+\tfrac{\mathbb{a}X}{\mathbb{c}Y^{-1}+1}\right)-\log_2\left(1+\tfrac{\mathbb{a}X}{\mathbb{b}Y+1}\right)\middle| Y>y_3\right\}\Pr\left(Y>y_3\right), \tag{6.22b}$$

$$= \frac{1}{2}\mathbb{E}\left\{\log_2\left(\tfrac{\mathbb{b}Y+1}{\mathbb{c}Y^{-1}+1}\right)+\log_2\left(1+\tfrac{\mathbb{c}Y^{-1}-\mathbb{b}Y}{\mathbb{b}Y+1+\mathbb{a}X}\right)\middle| Y>y_3\right\}\Pr\left(Y>y_3\right), \tag{6.22c}$$

where $y_3=\sqrt{\mathbb{c}/\mathbb{b}}$ is the double root of the equation $\Xi\left(y;1\right)=0$.

Because (6.22) does not admit a closed form expression, the ASC can be evaluated using its lower bound. Using the fact that $\mathbb{E}\left\{\max\left\{x,y\right\}\right\}\geqslant\max\left\{\mathbb{E}\left\{x\right\},\mathbb{E}\left\{y\right\}\right\}$, the lower bound of the ASC can be determined as

$$\bar{R}_{\text{sec},\text{low}}=\frac{1}{2}[\mathcal{C}_{\text{erg,d}}-\mathcal{C}_{\text{erg,r}}]^+, \tag{6.23}$$

where $\mathcal{C}_{\text{erg,d}}=\mathbb{E}\left\{\log_2\left(1+\gamma_{\text{d}}\right)\right\}$ and $\mathcal{C}_{\text{erg,r}}=\mathbb{E}\left\{\log_2\left(1+\gamma_{\text{r}}\right)\right\}$.

Proposition 6.3 The ASC for the KBFC scheme can be bounded below as

$$\bar{R}^{\text{KBFC}}_{\text{sec},\text{low}}=\frac{1}{2}\left[\log_2\left(1+e^{\ln(\mathbb{a})+\mathcal{J}_{3,\text{a}}+\mathcal{J}_{4,\text{a}}-\mathcal{J}_{5,\text{a}}}\right)-\mathcal{C}^{\text{KBFC}}_{\text{erg,r}}\right]^+, \tag{6.24}$$

where

$$\mathcal{C}^{\text{KBFC}}_{\text{erg,r}}=-\sum_{k=0}^{K-1}\sum_{\substack{n=0\\k+n\neq 0}}^{L-k}\sum_{\left\|\mathbf{p}^{(1)}\right\|_1=k+n}\sum_{u=0}^{\omega_1}\frac{\mathcal{I}_1\left(k,n,\mathbf{p}^{(1)},u\right)\Gamma\left(\omega_1+1\right)}{\ln\left(2\right)}\Bigg(\mathcal{A}_0 e^{\frac{m_1(k+n)}{\mathbb{a}\lambda_1}}$$

$$\times\,\Gamma\left(-\omega_1,\tfrac{m_1(k+n)}{\mathbb{a}\lambda_1}\right)+\sum_{j=1}^{N_2m_2+u}\mathcal{A}_j\mu_3^{\omega_1-j+1}U\left(\omega_1+1,\omega_1-j+2;\tfrac{m_2}{\mathbb{b}\lambda_2}\right)\Bigg), \tag{6.25}$$

$U(a,b;x)$ is the confluent hypergeometric function of the second kind [53, Eq. (9.211.4)], $\mu_3=\frac{\mathbb{a}\lambda_1 m_2}{\mathbb{b}\lambda_2 m_1(k+n)}$, $\mathcal{A}_0=(\mu_3-1)^{-N_2m_2-u}$, $\mathcal{A}_j=-(\mu_3-1)^{-N_2m_2-u+j-1}$, and $\mathcal{J}_{3,a},\mathcal{J}_{4,a},\mathcal{J}_{5,a}$

and $\mathcal{I}_1\left(k,n,\mathbf{p}^{(1)},u\right)$ are respectively defined as

$$\mathcal{J}_{3,a}=\sum_{n=0}^{L-K}\frac{L!(-1)^n}{(K-1)!\,(L-K)!\Gamma\left(N_1m_1\right)}\binom{L-K}{n}\sum_{\left\|\mathbf{p}^{(1)}\right\|_1=K+n-1}\binom{K+n-1}{\mathbf{p}^{(1)}}$$
$$\times\frac{\Gamma\left(N_1m_1+\omega_1\right)}{(K+n)^{N_1m_1+\omega_1}}\left(\psi\left(N_1m_1+\omega_1\right)-\ln\left(\tfrac{m_1(K+n)}{\lambda_1}\right)\right)\prod_{i=0}^{N_1m_1-1}\left(\frac{1}{i!}\right)^{p_i^{(1)}}, \tag{6.26}$$

$$\mathcal{J}_{4,\mathrm{a}}=\psi\left(N_2m_2\right)-\ln\left(\frac{m_2}{\lambda_2}\right), \tag{6.27}$$

$$\mathcal{J}_{5,\mathrm{a}}=\ln(\mathbb{c})+\sum_{u=0}^{N_2m_2-1}\frac{1}{(N_2m_2-u-1)!}\left(-\frac{\mathbb{c}m_2}{\lambda_2}\right)^{N_2m_2-u-1}$$
$$\times\left(-e^{\frac{\mathbb{c}m_2}{\lambda_2}}Ei\left(-\frac{\mathbb{c}m_2}{\lambda_2}\right)+\sum_{q=1}^{N_2m_2-u-1}(q-1)!\left(-\frac{\lambda_2}{\mathbb{c}m_2}\right)^q\right), \tag{6.28}$$

$$\mathcal{I}_1\left(k,n,\mathbf{p}^{(1)},u\right)=\frac{(-1)^n\left(N_2m_2+u-1\right)!}{\Gamma\left(N_2m_2\right)(k+n)^{N_2m_2+u}}\left(\frac{m_2}{\mathbb{b}\lambda_2}\right)^{N_2m_2}\left(\frac{\mathrm{a}\lambda_1}{m_1}\right)^{N_2m_2+u-\omega_1}$$
$$\times\binom{L}{k}\binom{L-k}{n}\binom{k+n}{\mathbf{p}^{(1)}}\binom{\omega_1}{u}\prod_{i=0}^{N_1m_1-1}\left(\frac{1}{i!}\right)^{p_i^{(1)}}. \tag{6.29}$$

with $\psi(x)$ is the Digamma function [53, Eq. (8.360.1)].

Proof: See Appendix E.3.

Proposition 6.4 The ASC for the KBSC scheme can be bounded below as

$$\bar{R}_{\mathrm{sec,low}}^{\mathrm{KBSC}}=\Bigg[\frac{\log_2\left(1+e^{\ln(\mathrm{a})+\mathcal{J}_{3,\mathrm{b}}+\mathcal{J}_{4,\mathrm{b}}-\mathcal{J}_{5,\mathrm{b}}}\right)}{2}+\sum_{i=0}^{N_1m_1-1}\frac{\Gamma(i+1)}{2\ln(2)}$$
$$\times\sum_{n=0}^{L-K}\sum_{\left\|\mathbf{p}^{(2)}\right\|_1=K+n-1}\sum_{u=0}^{i}\mathcal{I}_2(i,n,\mathbf{p}^{(2)},u)\Bigg(\mathcal{B}_0e^{\frac{m_1}{\mathrm{a}\lambda_1}}\Gamma\left(-i,\frac{m_1}{\mathrm{a}\lambda_1}\right)$$
$$+\sum_{q=1}^{N_2m_2+\omega_2+u}\mathcal{B}_q\mu_4^{i-q+1}U\left(i+1,i-q+2;\frac{m_1\mu_4}{\mathrm{a}\lambda_1}\right)\Bigg)\Bigg]^+, \tag{6.30}$$

where $\mu_4=\frac{\mathrm{a}\lambda_1m_2(K+n)}{\mathbb{b}\lambda_2m_1},\mathcal{B}_0=\left(\mu_4-1\right)^{-N_2m_2-\omega_2-u},\mathcal{B}_q=-\left(\mu_4-1\right)^{-N_2m_2-\omega_2-u+q-1}$,

and $\mathcal{J}_{3,b}, \mathcal{J}_{4,b}, \mathcal{J}_{5,b}$ and $\mathcal{I}_2\left(i, n, \mathbf{p}^{(2)}, u\right)$ are respectively defined as

$$\mathcal{J}_{3,b} = \psi\left(N_1 m_1\right) - \ln\left(\frac{m_1}{\lambda_1}\right), \tag{6.31}$$

$$\mathcal{J}_{4,\mathrm{b}} = \sum_{n=0}^{L-K} \sum_{\left\|\mathbf{p}^{(2)}\right\|_1 = K+n-1} \frac{L!(-1)^n \Gamma\left(N_2 m_2 + \omega_2\right)}{(K-1)!\,(L-K)!\Gamma\left(N_2 m_2\right)(K+n)^{N_2 m_2+\omega_2}} \binom{L-K}{n}$$
$$\times \binom{K+n-1}{\mathbf{p}^{(2)}} \left(\prod_{j=0}^{N_2 m_2 - 1} \left(\frac{1}{j!}\right)^{p_j^{(2)}}\right) \left(\psi\left(N_2 m_2 + \omega_2\right) - \ln\left(\tfrac{m_2(K+n)}{\lambda_2}\right)\right), \tag{6.32}$$

$$\mathcal{J}_{5,\mathrm{a}} = \ln\left(\mathbb{c}\right) + \sum_{n=0}^{L-K} \sum_{\left\|\mathbf{p}^{(2)}\right\|_1 = K+n-1} \sum_{u=0}^{N_2 m_2+\omega_2-1} \frac{L!(-1)^n \left(N_2 m_2 + \omega_2 - 1\right)!}{(K-1)!\,(L-K)!\Gamma\left(N_2 m_2\right)}$$
$$\times \frac{\left(-\mu_5\right)^{N_2 m_2+\omega_2-u-1}}{(K+n)^{N_2 m_2+\omega_2}(N_2 m_2 + \omega_2 - u - 1)!} \binom{L-K}{n} \left(\prod_{j=0}^{N_2 m_2 - 1} \left(\frac{1}{j!}\right)^{p_j^{(2)}}\right)$$
$$\times \binom{K+n-1}{\mathbf{p}^{(2)}} \left(-e^{\mu_5} Ei\left(-\mu_5\right) + \sum_{q=1}^{N_2 m_2+\omega_2-u-1} \frac{(q-1)!}{\left(-\mu_5\right)^q}\right), \tag{6.33}$$

with $\mu_5 = \frac{\mathbb{c} m_2(K+n)}{\lambda_2}$,

$$\mathcal{I}_2\left(i, n, \mathbf{p}^{(2)}, u\right) = \frac{(-1)^n L!\left(N_2 m_2 + \omega_2 + u - 1\right)!}{(K-1)!\,(L-K)!i!\Gamma\left(N_2 m_2\right)} \left(\frac{\mathbb{a}\lambda_1}{m_1}\right)^{N_2 m_2+\omega_2+u-i}$$
$$\times \left(\frac{m_2}{\mathbb{b}\lambda_2}\right)^{N_2 m_2+\omega_2} \binom{L-K}{n} \binom{K+n-1}{\mathbf{p}^{(2)}} \binom{i}{u} \left(\prod_{j=0}^{N_2 m_2 - 1} \left(\frac{1}{j!}\right)^{p_j^{(2)}}\right). \tag{6.34}$$

Proof: Using $f_X(x), F_X(x)$ and $f_Y(y)$ for the KBSC scheme, the results can be derived by following the same steps as in the proof of Proposition 6.3.

6.4 Simulation results

In this section, we use the Monte Carlo simulation to validate the analytical expressions presented in Section 6.3. Unless otherwise specified, we set $L = 4, N_1 =$

$N_2 = 2, m_1 = m_2 = 2, N_0 = 1, \eta = 0.5, \theta = 0.5, d_1 = d_2 = 1, \tau = 3, \lambda_1 = \lambda_2 = 1, R_{\text{th}} =$ 1 (bits/s/Hz), $\zeta = 1, \rho = P_s/N_0$, and $\rho_0 = 10$ (dB).

In Figure 6.2, the SOP is presented as a function of ρ. As shown, the SOP is a decreasing function of ρ, and is an increasing function of K. The analytical expressions match well with the simulation results that confirms the validity of the approximation in (6.9). Additionally, the high power-level approximations in Proposition 6.2 work quite well even at moderate values of ρ. As shown from the results of the KBFC scheme, the SOPs for different K values yield the similar SOP at high values of ρ. This assessment provides a design insight on the choice of K for the KBFC scheme. In particular, at low ρ values, the proposed system should be configured at low K values for achieving better SOPs; however, at high ρ values, we can use higher values of K to avoid overload at relay but achieve the similar SOP. In case of the KBSC scheme, the SOP is significantly enhanced as K decreases.

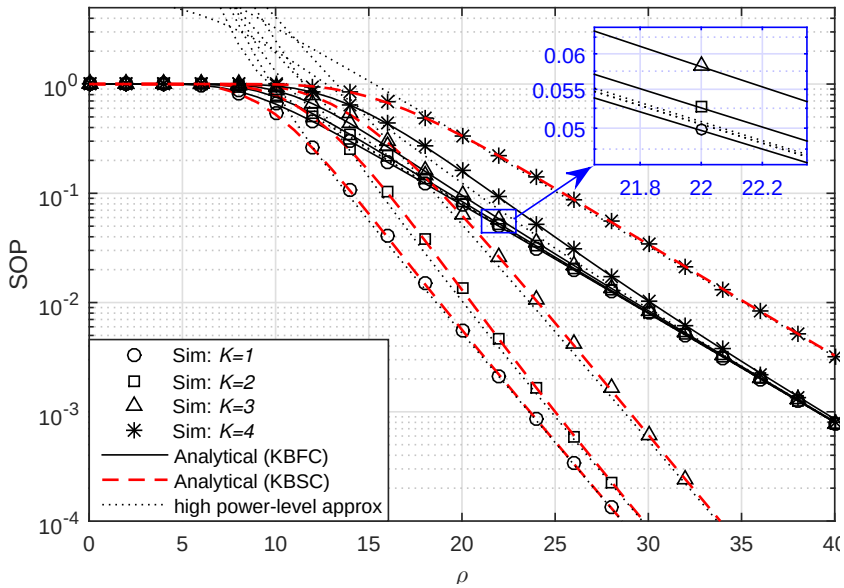

Figure 6.2: The secrecy outage probability versus ρ. Other parameters: $m_1 = m_2 = 1$.

In Figure 6.3, the ASC is presented as a function of θ. The ASC increases as θ increases from zero to an optimal value θ^*, and the ASC decreases with further increases of θ. This result agrees with previous results in Figure 4.3 and Figure 5.3. Moreover, the ASC approximates to zero if θ is below a threshold θ_{th}. The values of θ_{th} for the KBFC scheme with respect to different K values are the same whereas they for the KBSC scheme with respect to different K values are different. Specifically, θ_{th} for the KBSC scheme becomes higher as K increases.

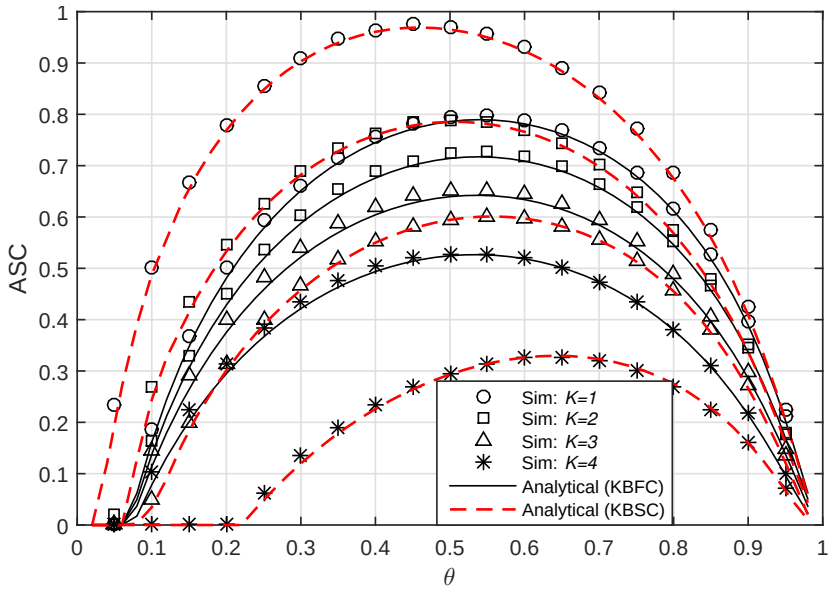

Figure 6.3: The average secrecy capacity versus θ. Other parameters: $P_s = P_d = N_0\rho_0$.

In Figure 6.4, the effect of the relay locations on the optimal ASC is investigated. For the conventional WEH–CC systems (which use trusted–relay nodes), the optimal location of the relay is close to the source; whereas, that of the UR–WEH system is between the source and destination. If $\mathcal{R}$ moves toward $\mathcal{S}$, the optimal ASC decreases because $\mathcal{C}_{\text{erg,r}}$ increases more significantly than $\mathcal{C}_{\text{erg,d}}$; and if $\mathcal{R}$ moves toward $\mathcal{D}$, the

optimal ASC decreases due to the decreasing trend of $\mathcal{C}_{\text{erg,d}}$. Therefore,an optimal distance, d^*, that balance the effects of AN on $\mathcal{C}_{\text{erg,r}}$ and $\mathcal{C}_{\text{erg,d}}$, gives the maximum ASC. Moreover, as shown in Figure 6.4 that when d_2 is sufficiently high, the optimal ASC approximates to zero. On the other hand, as $\mathcal{R}$ is close to $\mathcal{D}$, i.e., $d_2 \to 0^+$, the optimal ASCs for the KBSC scheme tend to a particular value, whereas the optimal ASCs for the KBFC scheme with respect to different values of K tend to different values. Additionally, for the best–relay selection strategy, i.e., K=1, the KBSC scheme outperforms the KBFC scheme when $\mathcal{R}$ is near $\mathcal{S}$, while the KBFC scheme performs better than the KBSC scheme when $\mathcal{R}$ is near $\mathcal{D}$.

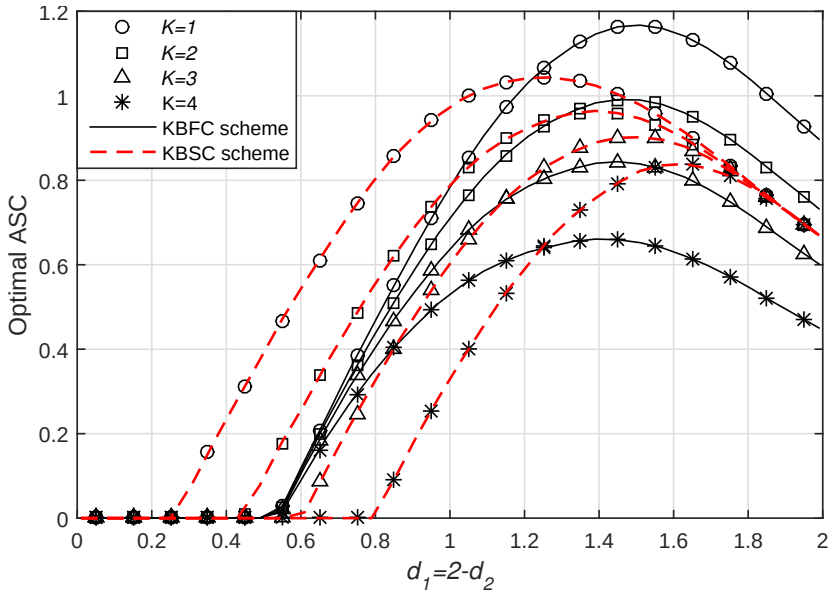

Figure 6.4: The effect of the relay locations on the optimal ASC. Other parameters: $P_s = P_d = N_0\rho_0$.

In Figure 6.5, the effect of the number of relays L on the optimal ASC is investigated for the best–relay selection strategy, i.e., $K = 1$. It can be seen that the optimal ASC is an increasing function of L, and as L progressively becomes higher,

the increase in the optimal ASC slows down. Moreover, as can be seen in this figure, the KBSC scheme outperforms the KBFC scheme. Examining the effect of the shape parameters m on the optimal ASC, we have the following: the KBFC scheme performs better as m increases; the KBSC scheme with respect to high L values achieves better ASC at lower m values, whereas that with respect to low L values achieves better ASC at higher m values.

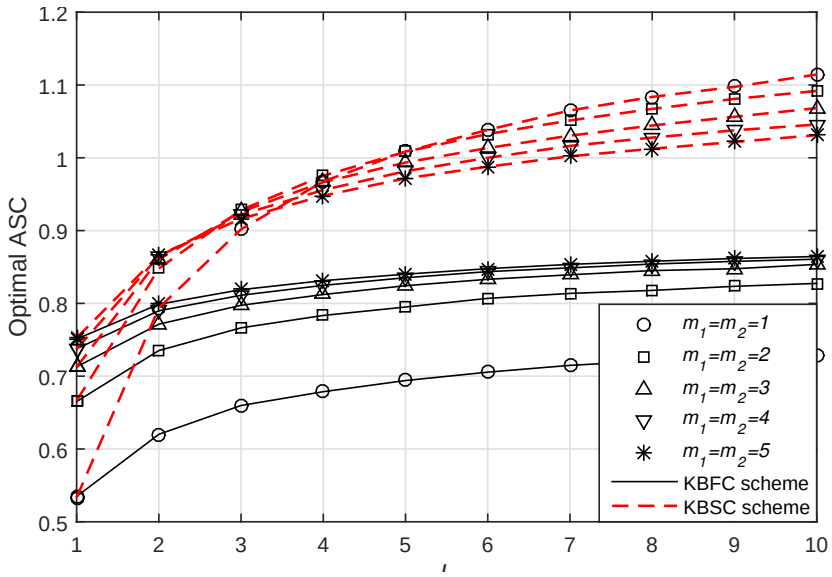

Figure 6.5: The effect of the number of relays on the optimal ASC. Other parameters: $P_s = P_d = N_0\rho_0$ and $K = 1$.

6.5 Conclusions

In this chapter, we studied the secure communication of an relay–selection UR–WEH system. We used the KBFC and KBSC schemes to choose the K–th best relay to assist the source–to–destination communication. Moreover, we applied the MRT technique to eliminate the security risks from the non–selected relays, and the des-

tination–assisted jamming to interfere the selected relay. The main contributions of this paper are summarized as follows:

- We derived the analytical expression involving a single integral for the SOP and the closed–form expression for the ASC; moreover, the and closed–form expression for the SOP at the high–power scenario was also derived.

- The results shows the advantage of using the relay–selection technique in improving the secrecy performance. In particular, the secrecy performance is enhanced as the number of the relays increases. The KBSC scheme can outperform the KBFC scheme as the relay is placed near the source while the KBFC scheme can perform better than the KBSC scheme as the relay is placed near the destination.

- Finally, the effect of various system parameters, such as transmit powers, target secrecy rate, PS ratio, shape parameter of the Nakagami–m fading, and K, on the secrecy performance, was examined which provides useful design insights.

Chapter 7

Summary of Contributions and Further Works

7.1 Introduction

In this final chapter, we summarize the main contributions of this dissertation and discuss several possible direction for further works.

7.2 Summary of Contributions

WEH is currently a hot topic in research community and is a future technique for powering small–size energy–constrained wireless networks. The feasible of WEH in different wireless networks, such as wireless sensor networks, cognitive radio networks, relaying networks, etc., was demonstrated in various scientific publications. In this dissertation, we investigated the WEH relaying networks with advanced issues in

wireless communication, such as relay selection, hardware impairment, imperfect CSI and PLS. The main contributions of this dissertation can be listed as follows.

- First, we solved problem of Simultaneous Wireless Information and Power Transfer (SWIPT) in Multiple Input Multiple Output (MIMO) systems via AF relays by proposing a novel method that allows energy beamforming technique, relay selection technique and diversity combining technique to collaborate effectively; hence, the (secrecy) performance of our proposed system is significantly improved.

- Second, we extended our investigation to practical scenarios, e.g., the devices suffer from RF impairments, the obtained CSI are imperfect, the best relay is unavailable due to its service and the relays are untrusted nodes, to make the results more practical and useful.

- Third, we solved the extension problems of the secure communication in the untrusted relaying WEH systems with the presence of an external eavesdropper or with the relay–selection technique.

- Fourth, the previous studies for the SOP of the untrusted relaying WEH systems did not provide any closed–form solution due to the complexity of the calculation. In this dissertation, we proposed an approximate analytical solution which allow us to obtain the closed–form expression for the SOP of these systems.

- Fifth, we derived the mathematical expressions for all of (secrecy) performance metrics, such as OP, SOP, ergodic capacity, ASC, etc., for all proposed systems.

We used Monte Carlo simulations to verify our derivations.

- Finally, for each proposed system, we investigated the impact of various key system parameters on the (secrecy) performance, and provided useful design insights on the choice of these parameters under different system configurations.

7.3 Future Research Directions

- Although many aspects of WEH were studied in the literature, there remain interesting research topics for the WEH technology. In this dissertation, we only studied PLS for untrusted relaying systems under the assumptions of perfect hardware; hence, the effects of the imperfect transceivers on the secure communication of untrusted relaying systems will be an interesting topic.

- Due to the different propagation delays in practical networks, the multiple replications of the signal at the receiver are misaligned causing a degradation in the post–detection SNR. Therefore, studies for our proposed systems under the effects of timing synchronization errors will be our future research directions.

- Recently, the researchers have proposed some new techniques for wireless communication, such as Non–Orthogonal Multiple Access (NOMA) network that uses the power domain for multiple access whereas the previous wireless–network systems relied on the time/frequency/code domain, and Nano–Network Communication (NNC) network that enables communication among small nano–scale devices. These new techniques allow new applications of the WEH and relaying techniques, and indicate new research directions for the PLS technique.

Publications

SCI (E) Journals/Transactions

[1] V. P. Tuan and H. Y. Kong, "Impact of residual transmit RF impairments on energy harvesting relay selection systems", International Journal of Electronics, vol. 104, no. 6, pp. 928-941, June 2017. (SCI)

[2] V. P. Tuan and H. Y. Kong, "Wireless Information and Power Transfer in K–th Best Relay Selection Systems with Energy Beamforming over Nakagami-m Fading Channels", Wireless Personal Communications, vol. 97, no. 3, pp. 4229-4722, Aug. 2017. (SCIE)

[3] V. P. Tuan and H. Y. Kong, "Secure communication via an energy-harvesting untrusted relay with imperfect CSI", Annals of Telecommunications, Aug. 2017. (Accepted) (SCI)

[4] V. P. Tuan and H. Y. Kong, "Secure communication via an energy-harvesting untrusted relay in the presence of an eavesdropper", International Journal of Electronics, vol. 105, no. 2, pp. 262-273, Feb. 2018. (SCI)

[5] V. P. Tuan and H. Y. Kong, "Secure communication in untrusted relay selec-

tion networks with wireless energy harvesting ", Wireless Networks, Feb. 2018. (Accepted) (SCI)

[6] V. P. Tuan and H. Y. Kong, "Exploiting cooperative relays to enhance the performance of energy-harvesting systems over Nakagami-m fading channels", Telecommunication Systems, Apr. 2018. (Accepted) (SCIE)

International Conferences

[7] V. Phu Tuan, S. Q. Nguyen, T. W. Kim and H. Y. Kong, "Throughput analysis of dual-hop relaying energy harvesting network with TAS/MRC," 2015 15th International Symposium on Communications and Information Technologies (ISCIT), Nara, pp. 249-252, 2015.

[8] V. P. Tuan, S. Q. Nguyen and H. Y. Kong, "Performance analysis of energy-harvesting relay selection systems with multiple antennas in presence of transmit hardware impairments", 2016 International Conference on Advanced Technologies for Communications (ATC), Hanoi, pp. 126-130, 2016.

[9] P. Ngoc Son, T. Anh Le, V. Phu Tuan and H. Yun Kong, "Best relay selection with joint effects of hardware impairments and interference constraints", 2017 International Conference on Advanced Technologies for Communications (ATC), Quy Nhon, pp. 54-59, 2017.

[10] P. N. Son, V. P. Tuan, P. Sol, L. T. Anh and H. Y. Kong, "Improving the secrecy of cooperative transmissions using unshared jamming," 2017 4th NAFOSTED Conference on Information and Computer Science, Hanoi, pp. 31-36, 2017.

References

[1] Z. Hu, C. Yuan and F. Gao, "Maximizing Harvested Energy for Full-Duplex SWIPT System With Power Splitting", in IEEE Access, vol. 5, pp. 24975-24987, 2017.

[2] V. N. Vo, T. G. Nguyen, C. So-In and D. B. Ha, "Secrecy Performance Analysis of Energy Harvesting Wireless Sensor Networks With a Friendly Jammer", in IEEE Access, vol. 5, pp. 25196-25206, 2017.

[3] M. Ashraf, A. Shahid, J. W. Jang and K. G. Lee, "Energy Harvesting Non-Orthogonal Multiple Access System With Multi-Antenna Relay and Base Station", in IEEE Access, vol. 5, pp. 17660-17670, 2017.

[4] R. Morsi, D. S. Michalopoulos and R. Schober, "Multiuser Scheduling Schemes for Simultaneous Wireless Information and Power Transfer Over Fading Channels", in IEEE Transactions on Wireless Communications, vol. 14, no. 4, pp. 1967-1982, April 2015.

[5] I. Krikidis, S. Timotheou, S. Nikolaou, G. Zheng, D. W. K. Ng and R. Schober, "Simultaneous wireless information and power transfer in modern communication systems", in IEEE Communications Magazine, vol. 52, no. 11, pp. 104-110, Nov. 2014.

[6] J. M. Kang, I. M. Kim and D. I. Kim, "Wireless Information and Power Transfer: Rate-Energy Tradeoff for Nonlinear Energy Harvesting", in IEEE Transactions on Wireless Communications, vol. 17, no. 3, pp. 1966-1981, Mar. 2018.

[7] K. Xiong, B. Wang and K. J. R. Liu, "Rate-Energy Region of SWIPT for MIMO Broadcasting Under Nonlinear Energy Harvesting Model", in IEEE Transactions on Wireless Communications, vol. 16, no. 8, pp. 5147-5161, Aug. 2017.

[8] M. M. Zhao, Y. Cai, Q. Shi, B. Champagne and M. J. Zhao, "Robust Transceiver Design for MISO Interference Channel With Energy Harvesting", in IEEE Transactions on Signal Processing, vol. 64, no. 17, pp. 4618-4633, Sep. 1 2016.

[9] Y. Zhu, K. K. Wong, Y. Zhang and C. Masouros, "Geometric Power Control for Time-Switching Energy-Harvesting Two-User Interference Channel", in IEEE Transactions on Vehicular Technology, vol. 65, no. 12, pp. 9759-9772, Dec. 2016.

[10] Y. Chen, "Energy-Harvesting AF Relaying in the Presence of Interference and Nakagami-m Fading", in IEEE Transactions on Wireless Communications, vol. 15, no. 2, pp. 1008-1017, Feb. 2016.

[11] Y. Hu, N. Cao, Y. Chen, M. Mao and Y. Feng, "Energy harvesting relaying using non-ideal relaying node in Rician fading channels", in IET Communications, vol. 11, no. 14, pp. 2154-2163, Sep. 2017.

[12] D. Xie, X. Lai, X. Lei and L. Fan, "Cognitive Multiuser Energy Harvesting Decode-and-Forward Relaying System With Direct Links", in IEEE Access, vol. 6, pp. 5596-5606, 2018.

[13] Y. Hu, N. Cao, Y. Chen, M. Mao and Y. Feng, "Energy harvesting relaying using non-ideal relaying node in Rician fading channels", in IET Communications, vol. 11, no. 14, pp. 2154-2163, 9 28 2017.

[14] H. Ding, X. Wang, D. B. da Costa, Y. Chen and F. Gong, "Adaptive Time-Switching Based Energy Harvesting Relaying Protocols", in IEEE Transactions on Communications, vol. 65, no. 7, pp. 2821-2837, Jul. 2017.

[15] W. Han, J. Ge and J. Men, "Performance analysis for NOMA energy harvesting relaying networks with transmit antenna selection and maximal-ratio combining over Nakagami-m fading", in IET Communications, vol. 10, no. 18, pp. 2687-2693, Dec. 2016.

[16] J. H. Lee and W. Choi, "Multiuser Diversity for Secrecy Communications Using Opportunistic Jammer Selection: Secure DoF and Jammer Scaling Law", in IEEE Transactions on Signal Processing, vol. 62, no. 4, pp. 828-839, Feb.15, 2014.

[17] J. Li, A. P. Petropulu and S. Weber, "On Cooperative Relaying Schemes for Wireless Physical Layer Security", in IEEE Transactions on Signal Processing, vol. 59, no. 10, pp. 4985-4997, Oct. 2011.

[18] C. Y. Wu, P. C. Lan, P. C. Yeh, C. H. Lee and C. M. Cheng, "Practical Physical Layer Security Schemes for MIMO-OFDM Systems Using Precoding Matrix Indices", in IEEE Journal on Selected Areas in Communications, vol. 31, no. 9, pp. 1687-1700, September 2013.

[19] Y. Zou, J. Zhu, X. Wang and V. C. M. Leung, "Improving physical-layer security in wireless communications using diversity techniques", in IEEE Network, vol. 29, no. 1, pp. 42-48, Jan.-Feb. 2015.

[20] S. I. Kim, I. M. Kim and J. Heo, "Secure Transmission for Multiuser Relay Networks", in IEEE Transactions on Wireless Communications, vol. 14, no. 7, pp. 3724-3737, Jul. 2015.

[21] H. Wang, X. Zhou and M. C. Reed, "Physical Layer Security in Cellular Networks: A Stochastic Geometry Approach", in IEEE Transactions on Wireless Communications, vol. 12, no. 6, pp. 2776-2787, Jun. 2013.

[22] G. Pan, C. Tang, X. Zhang, T. Li, Y. Weng and Y. Chen, "Physical-Layer Security Over Non-Small-Scale Fading Channels", in IEEE Transactions on Vehicular Technology, vol. 65, no. 3, pp. 1326-1339, Mar. 2016.

[23] H. M. Wang and X. G. Xia, "Enhancing wireless secrecy via cooperation: signal design and optimization", in IEEE Communications Magazine, vol. 53, no. 12, pp. 47-53, Dec. 2015.

[24] M. Yang, D. Guo, Y. Huang, T. Q. Duong and B. Zhang, "Physical Layer Security With Threshold-Based Multiuser Scheduling in Multi-Antenna Wireless Networks", in IEEE Transactions on Communications, vol. 64, no. 12, pp. 5189-5202, Dec. 2016.

[25] X. Zhou, R. Zhang and C. K. Ho, "Wireless Information and Power Transfer:

Architecture Design and Rate-Energy Tradeoff", in IEEE Transactions on Communications, vol. 61, no. 11, pp. 4754-4767, Nov. 2013.

[26] R. Zhang and C. K. Ho, "MIMO Broadcasting for Simultaneous Wireless Information and Power Transfer", in IEEE Transactions on Wireless Communications, vol. 12, no. 5, pp. 1989-2001, May 2013.

[27] L. Liu, R. Zhang, K.-C. Chua, "Wireless information transfer with opportunistic energy harvesting", in IEEE Transactions on Wireless Communications, vol. 3, pp. 345-362, Jan. 2013.

[28] H. Ju and R. Zhang, "Optimal Resource Allocation in Full-Duplex Wireless-Powered Communication Network", in IEEE Transactions on Communications, vol. 62, no. 10, pp. 3528-3540, Oct. 2014.

[29] A. Ikhlef, "Optimal MIMO Multicast Transceiver Design for Simultaneous Information and Power Transfer", in IEEE Communications Letters, vol. 18, no. 12, pp. 2153-2156, Dec. 2014.

[30] A. A. Nasir, X. Zhou, S. Durrani and R. A. Kennedy, "Relaying Protocols for Wireless Energy Harvesting and Information Processing", in IEEE Transactions on Wireless Communications, vol. 12, no. 7, pp. 3622-3636, Jul. 2013.

[31] A. A. Nasir, X. Zhou, S. Durrani and R. A. Kennedy, "Wireless-Powered Relays in Cooperative Communications: Time-Switching Relaying Protocols and Throughput Analysis", in IEEE Transactions on Communications, vol. 63, no. 5, pp. 1607-1622, May 2015.

[32] Y. Gu and S. Aïssa, "RF-Based Energy Harvesting in Decode-and-Forward Relaying Systems: Ergodic and Outage Capacities", in IEEE Transactions on Wireless Communications, vol. 14, no. 11, pp. 6425-6434, Nov. 2015.

[33] H. Yu, D. Wang, G. Pan, R. Shi, J. Zhang and Y. Chen, "On Outage of WPC System With Relay Selection Over Nakagami–m Fading Channels", in IEEE Transactions on Vehicular Technology, vol. 66, no. 9, pp. 8590-8594, Sept. 2017.

[34] C. Zhong, H. A. Suraweera, G. Zheng, I. Krikidis and Z. Zhang, "Wireless Information and Power Transfer With Full Duplex Relaying", in IEEE Transactions on Communications, vol. 62, no. 10, pp. 3447-3461, Oct. 2014.

[35] G. Zhu, C. Zhong, H. A. Suraweera, G. K. Karagiannidis, Z. Zhang and T. A. Tsiftsis, "Wireless Information and Power Transfer in Relay Systems With Multiple Antennas and Interference", in IEEE Transactions on Communications, vol. 63, no. 4, pp. 1400-1418, April 2015.

[36] I. Krikidis, J. Thompson, S. Mclaughlin and N. Goertz, "Amplify-and-forward with partial relay selection", in IEEE Communications Letters, vol. 12, no. 4, pp. 235-237, April 2008.

[37] P. N. Son and H. Y. Kong, "Energy-harvesting relay selection schemes for decode-and-forward dual-hop networks", in IEICE Transactions on Communications, Vol. E98-B, no. 12, pp. 2485-2495, 2015.

[38] D. K. P. Asiedu, S. Mahama, S. W. Jeon and K. J. Lee, "Optimal Power Split-

ting for Simultaneous Wireless Information and Power Transfer in Amplify-and-Forward Multiple-Relay Systems", in IEEE Access, vol. 6, pp. 3459-3468, 2018.

[39] T. T. Duy, T. Q. Duong, D. B. da Costa, V. N. Q. Bao and M. Elkashlan, "Proactive Relay Selection With Joint Impact of Hardware Impairment and Co-Channel Interference", in IEEE Transactions on Communications, vol. 63, no. 5, pp. 1594-1606, May 2015.

[40] D. Wang, R. Zhang, X. Cheng, L. Yang and C. Chen, "Relay Selection in Full-Duplex Energy-Harvesting Two-Way Relay Networks", in IEEE Transactions on Green Communications and Networking, vol. 1, no. 2, pp. 182-191, Jun. 2017.

[41] Q. N. Le, V. N. Q. Bao and B. An, "Full-duplex distributed switch-and-stay energy harvesting selection relaying networks with imperfect CSI: Design and outage analysis", in Journal of Communications and Networks, vol. 20, no. 1, pp. 29-46, Feb. 2018.

[42] L. Liu, R. Zhang and K. C. Chua, "Secrecy Wireless Information and Power Transfer With MISO Beamforming", in IEEE Transactions on Signal Processing, vol. 62, no. 7, pp. 1850-1863, Apr. 2014.

[43] H. Zhang, C. Li, Y. Huang and L. Yang, "Secure Beamforming for SWIPT in Multiuser MISO Broadcast Channel With Confidential Messages", in IEEE Communications Letters, vol. 19, no. 8, pp. 1347-1350, Aug. 2015.

[44] H. Xing, L. Liu and R. Zhang, "Secrecy Wireless Information and Power Transfer

in Fading Wiretap Channel", in IEEE Transactions on Vehicular Technology, vol. 65, no. 1, pp. 180-190, Jan. 2016.

[45] X. Chen, J. Chen and T. Liu, "Secure wireless information and power transfer in large-scale MIMO relaying systems with imperfect CSI", 2014 IEEE Global Communications Conference, Austin, TX, pp. 4131-4136, 2014.

[46] S. S. Kalamkar and A. Banerjee, "Secure Communication via a Wireless Energy Harvesting Untrusted Relay", in IEEE Transactions on Vehicular Technology, vol. 66, no. 3, pp. 2199-2213, March 2017.

[47] A. Bletsas, H. Shin and M. Z. Win, "Cooperative Communications with Outage-Optimal Opportunistic Relaying", in IEEE Transactions on Wireless Communications, vol. 6, no. 9, pp. 3450-3460, Sep. 2007.

[48] B. Sirkeci-Mergen and A. Scaglione, "Randomized Space-Time Coding for Distributed Cooperative Communication", in IEEE Transactions on Signal Processing, vol. 55, no. 10, pp. 5003-5017, Oct. 2007.

[49] A. K. Sadek, W. Su and K. J. R. Liu, "Multinode Cooperative Communications in Wireless Networks", in IEEE Transactions on Signal Processing, vol. 55, no. 1, pp. 341-355, Jan. 2007.

[50] Y. Zhao, R. Adve and T. J. Lim, "Improving amplify-and-forward relay networks: optimal power allocation versus selection", in IEEE Transactions on Wireless Communications, vol. 6, no. 8, pp. 3114-3123, Aug. 2007.

[51] I. H. Lee and D. Kim, "Probability of SNR Gain by Dual-Hop Relaying over

Single-Hop Transmission in SISO Rayleigh Fading Channels," in IEEE Communications Letters, vol. 12, no. 10, pp. 734-736, Oct. 2008.

[52] S. S. Chauhan and S. Kumar, "Adaptive-transmission channel capacity of maximal-ratio combining with antenna selection in Nakagami-m fading channels", in Wireless Personal Communications, vol. 85, no. 4, pp. 22332243, Jul. 2015.

[53] I. S. Gradshteyn, I. M. Ryzhik, A. Jeffrey and D. Zwillinger, "Table of integral, series and products", 7th ed. Elsevier, Amsterdam, 2007.

[54] K. K. Gurrala and S. Das, "Hybrid decode-amplify-forward (HDAF) scheme in distributed Alamouti-coded cooperative network", in International Journal of Electronics, vol. 102, pp. 725-741, 2015.

[55] J. Laneman, D. Tse and W. G. Wornell, "Cooperative diversity in wireless networks: Efficient protocols and outage behavior", in IEEE Transactions on Information Theory, vol. 50, no. 12, pp. 3062-3080, Dec. 2004.

[56] L. Xu, H. Zhang and T. A. Gulliver, "Joint TAS and power allocation for DF relaying M2M cooperative system", in International Journal of Electronics, vol. 103, no. 9, pp. 15101523, 2016.

[57] W. Han, J. Ge and J. Men, "Performance analysis for NOMA energy harvesting relaying networks with transmit antenna selection and maximal-ratio combining over Nakagami-m fading", in IET Communications, vol. 10, no. 18, pp. 2687-2693, Dec. 2016.

[58] B. K. Chalise, Y. D. Zhang and M. G. Amin, "A novel partial relay selection method for amplify-and-forward relay systems", 2012 IEEE Global Communications Conference (GLOBECOM), Anaheim, CA, pp. 4695-4700, 2012.

[59] I. Krikidis, J. Thompson, S. Mclaughlin and N. Goertz, "Amplify-and-forward with partial relay selection", in IEEE Communications Letters, vol. 12, no. 4, pp. 235-237, Apr. 2008.

[60] C. Kundu, S. Ghose and R. Bose, "Secrecy Outage of Dual-Hop Regenerative Multi-Relay System With Relay Selection", in IEEE Transactions on Wireless Communications, vol. 14, no. 8, pp. 4614-4625, Aug. 2015.

[61] E. Costa and S. Pupolin, "M-QAM-OFDM system performance in the presence of a nonlinear amplifier and phase noise", in IEEE Transactions on Communications, vol. 50, no. 3, pp. 462-472, Mar. 2002.

[62] J. Choi, "Downlink Multiuser Beamforming With Compensation of Channel Reciprocity From RF Impairments", in IEEE Transactions on Communications, vol. 63, no. 6, pp. 2158-2169, Jun. 2015.

[63] T. Schenk, "RF imperfections in high-rate wireless systems: Impact and digital compensation", Netherlands: Springer, 2008.

[64] E. Bjornson, M. Matthaiou and M. Debbah, "A New Look at Dual-Hop Relaying: Performance Limits with Hardware Impairments", in IEEE Transactions on Communications, vol. 61, no. 11, pp. 4512-4525, Nov. 2013.

[65] T. Gucluoglu and E. Panayirci, "Performance of Transmit and Receive Antenna

Selection in the Presence of Channel Estimation Errors", in IEEE Communications Letters, vol. 12, no. 5, pp. 371-373, May 2008.

[66] G. Pan et al., "On Secrecy Performance of MISO SWIPT Systems With TAS and Imperfect CSI", in IEEE Transactions on Communications, vol. 64, no. 9, pp. 3831-3843, Sept. 2016.

[67] J. M. Moualeu, W. Hamouda and F. Takawira, "Relay Selection for Coded Cooperative Networks with Outdated CSI over Nakagami-m Fading Channels", in IEEE Transactions on Wireless Communications, vol. 13, no. 5, pp. 2362-2373, May 2014.

[68] Q. Huang, M. Lin, K. An, J. Ouyang and W. P. Zhu, "Secrecy performance of hybrid satellite-terrestrial relay networks in the presence of multiple eavesdroppers", in IET Communications, vol. 12, no. 1, pp. 26-34, May 2018.

[69] S. Leung-Yan-Cheong and M. Hellman, "The Gaussian wire-tap channel", in IEEE Transactions on Information Theory, vol. 24, no. 4, pp. 451-456, Jul 1978.

[70] S. Shafiee, N. Liu and S. Ulukus, "Towards the Secrecy Capacity of the Gaussian MIMO Wire-Tap Channel: The 2-2-1 Channel", in IEEE Transactions on Information Theory, vol. 55, no. 9, pp. 4033-4039, Sept. 2009.

[71] A. Singh, M. R. Bhatnagar and R. K. Mallik, "Physical Layer Security of a Multiantenna-Based CR Network With Single and Multiple Primary Users", in IEEE Transactions on Vehicular Technology, vol. 66, no. 12, pp. 11011-11022, Dec. 2017.

[72] N. H. Mahmood, I. S. Ansari, P. Popovski, P. Mogensen and K. A. Qaraqe, "Physical-Layer Security With Full-Duplex Transceivers and Multiuser Receiver at Eve", in IEEE Transactions on Communications, vol. 65, no. 10, pp. 4392-4405, Oct. 2017.

[73] K. S. Ahn, S. W. Choi and J. M. Ahn, "Secrecy Performance of Maximum Ratio Diversity With Channel Estimation Error", in IEEE Signal Processing Letters, vol. 22, no. 11, pp. 2167-2171, Nov. 2015.

[74] A. D. Wyner, "The wire-tap channel", in The Bell System Technical Journal, vol. 54, no. 8, pp. 1355-1387, Oct. 1975.

[75] T. T. Duy, T. Q. Duong, T. L. Thanh and V. N. Q. Bao, "Secrecy performance analysis with relay selection methods under impact of co-channel interference", in IET Communicable, vol. 9, no. 2, pp. 14271435, 2015.

[76] X. Lu, P. Wang, D. Niyato, D. I. Kim and Z. Han, "Wireless Networks With RF Energy Harvesting: A Contemporary Survey", in IEEE Communications Surveys & Tutorials, vol. 17, no. 2, pp. 757-789, Second quarter 2015.

[77] Y. Gu and S. Aïssa, "RF-Based Energy Harvesting in Decode-and-Forward Relaying Systems: Ergodic and Outage Capacities", in IEEE Transactions on Wireless Communications, vol. 14, no. 11, pp. 6425-6434, Nov. 2015.

[78] V. P. Tuan and H. Y. Kong, "Wireless Information and Power Transfer in K–th Best Relay Selection Systems with Energy Beamforming over Nakagami-m Fad-

ing Channels", in Wireless Personal Communications, vol. 97, no. 3, pp. 4229-4722, Aug. 2017.

[79] E. K. P. Chong and S. H. Zak, "An Introduction to Optimization", 2nd ed., Wiley, 2004.

[80] M. S. Aloqlah, "Performance Analysis of Dual-Hop Fixed-Gain Relay Systems over Extended Generalized-K Fading Channels", in Wireless Personal Communications, vol. 83, no. 1, pp. 619-630, 2015.

[81] V. P. Tuan and H. Y. Kong, "Impact of residual transmit RF impairments on energy harvesting relay selection systems", in International Journal of Electronics, vol. 104, no. 6, pp. 928-941, June 2017.

[82] E. Bjornson, M. Matthaiou and M. Debbah, "A New Look at Dual-Hop Relaying: Performance Limits with Hardware Impairments", in IEEE Transactions on Communications, vol. 61, no. 11, pp. 4512-4525, Nov. 2013.

[83] M. Matthaiou, A. Papadogiannis, E. Bjornson and M. Debbah, "Two-Way Relaying Under the Presence of Relay Transceiver Hardware Impairments", in IEEE Communications Letters, vol. 17, no. 6, pp. 1136-1139, June 2013.

[84] M. Mokhtar, A. A. A. Boulogeorgos, G. K. Karagiannidis and N. Al-Dhahir, "OFDM Opportunistic Relaying Under Joint Transmit/Receive I/Q Imbalance", in IEEE Transactions on Communications, vol. 62, no. 5, pp. 1458-1468, May 2014.

[85] X. Zhang, M. Matthaiou, M. Coldrey and E. Björnson, "Impact of Residual

Transmit RF Impairments on Training-Based MIMO Systems", in IEEE Transactions on Communications, vol. 63, no. 8, pp. 2899-2911, Aug. 2015.

[86] T. T. Duy, T. Q. Duong, D. B. da Costa, V. N. Q. Bao and M. Elkashlan, "Proactive Relay Selection With Joint Impact of Hardware Impairment and Co-Channel Interference", in IEEE Transactions on Communications, vol. 63, no. 5, pp. 1594-1606, May 2015.

[87] M. G. Khafagy, A. Ismail, M. S. Alouini and S. Assa, "Efficient Cooperative Protocols for Full-Duplex Relaying Over Nakagami- m Fading Channels", in IEEE Transactions on Wireless Communications, vol. 14, no. 6, pp. 3456-3470, June 2015.

[88] S. S. Ikki and M. H. Ahmed, "On the Performance of Cooperative-Diversity Networks with the Nth Best-Relay Selection Scheme", in IEEE Transactions on Communications, vol. 58, no. 11, pp. 3062-3069, Nov. 2010.

[89] V. P. Tuan and H. Y. Kong, "Secure communication via an energy-harvesting untrusted relay with imperfect CSI", in Annals of Telecommunications, Aug. 2017. (Accepted)

[90] B. K. Chalise, Y. D. Zhang and M. G. Amin, "Local CSI Based Full Diversity Achieving Relay Selection for Amplify-and-Forward Cooperative Systems", in IEEE Transactions on Signal Processing, vol. 61, no. 21, pp. 5165-5180, Nov., 2013.

[91] G. Zhu, C. Zhong, H. A. Suraweera, Z. Zhang, C. Yuen and R. Yin, "Ergodic

Capacity Comparison of Different Relay Precoding Schemes in Dual-Hop AF Systems With Co-Channel Interference", in IEEE Transactions on Communications, vol. 62, no. 7, pp. 2314-2328, July 2014.

[92] V. P. Tuan and H. Y. Kong, "Secure communication via an energy-harvesting untrusted relay in the presence of an eavesdropper", in International Journal of Electronics, vol. 105, no. 2, pp. 262-273, Feb. 2018.

[93] V. P. Tuan and H. Y. Kong, "Secure communication in untrusted relay selection networks with wireless energy harvesting ", in Wireless Networks, Feb. 2018. (Accepted)

[94] H. A. David and H. N. Nagaraja, "Order Statistics", 3rd ed. John Wiley & Sons, Inc, 2003.

[95] E. Olfat and A. Olfat, "Outage Performance of Hybrid DecodeAmplifyForward Protocol with the nth Best Relay Selection", in Wireless Personal Communications, vol. 78, no. 2, pp. 1403-1412, 2014.

[96] Wolfram Functions. [Online]. Available: http://functions.wolfram.com/PDF/MeijerG.pdf

[97] F. W. J. Olver, D. W. Lozier, R. F. Boisvert and C. W. Clark, "NIST Handbook of Mathematical Functions. Cambridge University Press", 2010.

Appendix A

Proofs in Chapter 2

A.1 Proof of Proposition 2.1

The tight lower–bound of the OP can be calculated as

$$\mathcal{P}^{\text{low}}(\gamma) = \Pr\{\gamma^{\text{up}}_{e2e,[w]} < \gamma\}. \tag{A.1}$$

Substituting (2.14) into (A.1), we have

$$\mathcal{P}^{\text{low}}(\gamma) = 1 - \int_0^{+\infty} \left(1 - F_{\left\|\mathbf{h}_2^{(K)}\right\|^2}\left(\frac{\gamma}{\mathbb{b}_{[w]} z}\right)\right) f_{\left\|\mathbf{h}_1^{(K)}\right\|^2}\left(z + \frac{\gamma}{\mathbb{a}_{[w]}}\right) dz, \tag{A.2}$$

where $z = \left(\left\|\mathbf{h}_1^{(K)}\right\|^2 - \frac{\gamma}{\mathbb{a}_{[w]}}\right)$.

Before calculating the OP, we need to study the PDF and CDF of the K–th best order of gamma RVs. Consider L gamma RVs, $\mathcal{X}_1, \ldots, \mathcal{X}_L$, with parameters (m, λ), and the K–th best RV is determined as $\mathcal{X}^{(K)} = K\text{–th} \underset{1 \leqslant l \leqslant L}{\arg\max}(\mathcal{X}_l)$. According to [95],

the PDF and CDF of $\mathcal{X}^{(K)}$ are given by

$$f_{\mathcal{X}^{(K)}}(x;m,\lambda)=\sum_{n=0}^{L-K}\binom{L-K}{n}\frac{L!(-1)^n f(x;m,\lambda)}{(K-1)!(L-K)!}\left(\frac{\Gamma\left(m,\frac{x}{\lambda}\right)}{\Gamma(m)}\right)^{K+n-1}, \tag{A.3}$$

$$F_{\mathcal{X}^{(K)}}(x;m,\lambda)=\sum_{t=0}^{K-1}\sum_{n=0}^{L-t}(-1)^n\binom{L}{t}\binom{L-t}{n}\left(\frac{\Gamma\left(m,\frac{x}{\lambda}\right)}{\Gamma(m)}\right)^{t+n}. \tag{A.4}$$

A.1.1 Outage probability for the KBFC scheme

For the KBFC scheme, the PDF and CDF of $\|\mathbf{h}_1^{(K)}\|^2$ respectively follow (A.3) and (A.4) with parameters $(N_1m_1,\frac{\lambda_1}{m_1})$, the PDF of $\|\mathbf{h}_2^{(K)}\|^2$ follows (2.1), and the CDF of $\|\mathbf{h}_2^{(K)}\|^2$ follows

$$F_g(x;m,\lambda)=\frac{\gamma\left(m,\frac{x}{\lambda}\right)}{\Gamma(m)}=1-\frac{\Gamma\left(m,\frac{x}{\lambda}\right)}{\Gamma(m)}, \tag{A.5}$$

with parameters $\left(N_2m_2,\frac{\lambda_2}{m_2}\right)$ [52].

Substituting the PDF of $\|\mathbf{h}_1^{(K)}\|^2$ and CDF of $\|\mathbf{h}_2^{(K)}\|^2$ into (A.2), and using the multinomial theorem given in [53, Eq. (26.4.9)] as

$$(x_1+\ldots+x_n)^u=\sum_{\Sigma_{\|\mathbf{p}\|_1=u}}\binom{u}{\mathbf{p}}x_1^{p_1}\ldots x_n^{p_n}, \tag{A.6}$$

the OP for the KBFC scheme can be calculated as

$$\begin{aligned}\mathcal{P}^{\text{low}}_{\text{KBSC},[w]}(\gamma)=1-&\sum_{j=0}^{N_2m_2-1}\sum_{n=0}^{L-K}\sum_{\sum_{i=0}^{N_1m_1-1}p_i^{(1)}=K+n-1}\sum_{q=0}^{N_1m_1+\omega_1-1}\frac{L!(-1)^n}{j!(K-1)!(L-K)!}\\
&\times\frac{\left(\frac{m_2\gamma}{\mathbb{b}_{[w]}\lambda_2}\right)^j\left(\frac{m_1}{\lambda_1}\right)^{N_1m_1+\omega_1}}{\Gamma(N_1m_1)}\binom{L-K}{n}\binom{K+n-1}{p_0^{(1)},\ldots,p_{N_1m_1-1}^{(1)}}\binom{N_1m_1+\omega_1-1}{q}\\
&\times\left(\prod_{i=0}^{N_1m_1-1}\left(\frac{1}{i!}\right)^{p_i^{(1)}}\right)e^{-\frac{m_1(K+n)\gamma}{\mathbb{a}_{[w]}\lambda_1}}\int_0^{+\infty}t^{q-j}e^{-\frac{m_2\gamma}{\mathbb{b}_{[w]}\lambda_2 t}-\frac{m_1(K+n)t}{\lambda_1}}dt.\end{aligned} \tag{A.7}$$

The integration in (A.7) can be solved using [53, Eq. (3.471.9)]. Then $\mathcal{P}^{\text{low}}_{\text{KBSC},[w]}(\gamma)$ can be calculated as in (2.15).

A.1.2 Outage probability for the KBSC scheme

For the KBSC scheme, the PDF and CDF of $\|\mathbf{h}_1^{(K)}\|^2$ respectively follow (2.1) and (A.5) with parameters $(N_1 m_1, \frac{\lambda_1}{m_1})$, and the PDF and CDF of $\|\mathbf{h}_2^{(K)}\|^2$ respectively follow (A.3) and (A.4) with parameters $(N_2 m_2, \frac{\lambda_2}{m_2})$. Then, the OP for the KBSC scheme is obtained with the same steps as in Appendix A.1.1.

A.2 Proof of Proposition 2.2

A.2.1 Ergodic capacity for the KBFC scheme

Calculation for $\mathcal{C}_{\gamma_{r,[w]}}$

According to [91] and using the CDF of $\|\mathbf{h}_1^{(K)}\|^2$ for the KBFC scheme, $\mathcal{C}_{\gamma_{r,[w]}}$ can be calculated as

$$\begin{aligned}\mathcal{C}_{\gamma_{r,[w]}} &= \frac{1}{2\ln 2}\int_0^{+\infty}\frac{1-F_{\left\|\mathbf{h}_1^{(K)}\right\|^2}(x)}{\mathrm{a}_{[w]}^{-1}+x}dx \\ &= \frac{-1}{2\ln 2}\sum_{t=0}^{K-1}\sum_{\substack{n=0\\ t+n\neq 0}}^{L-t}\sum_{\sum_{i=0}^{N_1m_1-1}p_i^{(1)}=t+n}(-1)^n\binom{L}{t}\binom{L-t}{n}\binom{t+n}{p_0^{(1)},\ldots,p_{N_1m_1-1}^{(1)}} \\ &\times\left(\prod_{i=0}^{N_1m_1-1}\left(\frac{1}{i!}\right)^{p_i^{(1)}}\right)\left(\frac{m_1}{\lambda_1}\right)^{\omega_1}\int_0^{+\infty}\frac{x^{\omega_1}}{(\mathrm{a}_{[w]}^{-1}+x)}e^{-\frac{m_1(t+n)x}{\lambda_1}}dx. \end{aligned} \tag{A.8}$$

Using [53, Eq. (3.383.10)], (A.8) can be rewritten as

$$\begin{aligned}\mathcal{C}_{\gamma_{r,[w]}} &= \frac{-1}{2\ln 2}\sum_{t=0}^{K-1}\sum_{\substack{n=0\\ t+n\neq 0}}^{L-t}\sum_{\sum_{i=0}^{N_1m_1-1}p_i^{(1)}=t+n}(-1)^n\binom{L}{t}\binom{L-t}{n}\binom{t+n}{p_0^{(1)},\ldots,p_{N_1m_1-1}^{(1)}} \\ &\times\left(\prod_{i=0}^{N_1m_1-1}\left(\frac{1}{i!}\right)^{p_i^{(1)}}\right)\left(\frac{m_1}{\mathrm{a}_{[w]}\lambda_1}\right)^{\omega_1}e^{\frac{m_1(t+n)}{\mathrm{a}_{[w]}\lambda_1}}\Gamma(\omega_1+1)\Gamma\left(-\omega_1,\frac{m_1(t+n)}{\mathrm{a}_{[w]}\lambda_1}\right). \end{aligned} \tag{A.9}$$

Calculation for $\mathcal{C}_{\gamma_{d,[w]}}$

Letting $Y = \|\mathbf{h}_1^{(K)}\|^2\|\mathbf{h}_2^{(K)}\|^2$, the PDF of Y for the KBFC scheme is given by

$$f_Y(y) = \int_0^{+\infty} \frac{1}{x} f_{\left\|\mathbf{h}_2^{(K)}\right\|^2}\left(\frac{y}{x}\right) f_{\left\|\mathbf{h}_1^{(K)}\right\|^2}(x)dx. \tag{A.10}$$

Substituting the PDF of $\|\mathbf{h}_1^{(K)}\|^2$ and $\|\mathbf{h}_2^{(K)}\|^2$ for the KBFC scheme into (A.10), and with the help of [53, Eq. (3.471.9)], we have

$$\begin{aligned} f_Y(y) = &\sum_{n=0}^{L-K} \sum_{\substack{N_1m_1-1 \\ \sum_{i=0} \\ p_i^{(1)}=K+n-1}} \frac{2L!(-1)^n}{(K-1)!(L-K)!\Gamma(N_1m_1)\Gamma(N_2m_2)} \binom{L-K}{n} \\ &\times \binom{K+n-1}{p_0^{(1)},\ldots,p_{N_1m_1-1}^{(1)}} \left(\prod_{i=0}^{N_1m_1-1}\left(\frac{1}{i!}\right)^{p_i^{(1)}}\right) \frac{m_1m_2}{\lambda_1\lambda_2(K+n)^{N_1m_1+\omega_1-1}} \\ &\times z^{\frac{N_1m_1+\omega_1+N_2m_2}{2}-1} K_{N_1m_1+\omega_1-N_2m_2}\left(2\sqrt{z}\right), \end{aligned} \tag{A.11}$$

where $z = \frac{m_2m_1(K+n)y}{\lambda_1\lambda_2}$.

Then, $\mathcal{C}_{\gamma_{d,[w]}}$ can be calculated as

$$\mathcal{C}_{\gamma_{d,[w]}} = \frac{1}{2}\int_0^{+\infty} \log_2(1+\mathbb{b}_{[w]}y) f_Y(y). \tag{A.12}$$

Substituting (A.11) into (A.12) and expressing $\ln(1+x) = G_{2,2}^{1,2}\left(x\big|_{1,0}^{1,1}\right)$ [96, Eq. (07.34.03.0456.01)], we have

$$\begin{aligned} \mathcal{C}_{\gamma_{d,[w]}} = &\frac{1}{\ln(2)} \sum_{n=0}^{L-K} \sum_{\substack{N_1m_1-1 \\ \sum_{i=0} \\ p_i^{(1)}=K+n-1}} \frac{L!(-1)^n}{(L-K)!(K-1)!\Gamma(N_1m_1)\Gamma(N_2m_2)} \\ &\times \frac{1}{(K+n)^{N_1m_1+\omega_1}} \binom{L-K}{n} \binom{K+n-1}{p_0^{(1)},\ldots,p_{N_1m_1-1}^{(1)}} \left(\prod_{i=0}^{N_1m_1-1}\left(\frac{1}{i!}\right)^{p_i^{(1)}}\right) \\ &\times \int_0^{+\infty} z^{\frac{N_1m_1+\omega_1+N_2m_2}{2}-1} K_{N_1m_1+\omega_1-N_2m_2}(2\sqrt{z}) G_{2,2}^{1,2}\left(\frac{\mathbb{b}_{[w]}\lambda_1\lambda_2}{m_1m_2(K+n)}z\middle|\begin{matrix}1, & 1\\ 1, & 0\end{matrix}\right) dz. \end{aligned} \tag{A.13}$$

The integration in (A.13) can be solved using [53, Eq. (7.821.3)]; thus, $\mathcal{C}_{\gamma_{d,[w]}}$ can be expressed as

$$\mathcal{C}_{\gamma_{d,[w]}} = \frac{1}{2\ln(2)} \sum_{n=0}^{L-K} \sum_{\sum_{i=0}^{N_1 m_1 - 1} p_i^{(1)} = K+n-1} \frac{L!(-1)^n}{(K-1)!(L-K)!\Gamma(N_1 m_1)\Gamma(N_2 m_2)}$$
$$\times \frac{1}{(K+n)^{N_1 m_1 + \omega_1}} \binom{L-K}{n} \binom{K+n-1}{p_0^{(1)}, \ldots, p_{N_1 m_1 - 1}^{(1)}} \left(\prod_{i=0}^{N_1 m_1 - 1} \left(\frac{1}{i!} \right)^{p_i^{(1)}} \right)$$
$$\times G_{4,2}^{1,4} \left(\frac{\mathbb{b}_{[w]} \lambda_1 \lambda_2}{m_1 m_2 (K+n)} \middle| \begin{matrix} -N_1 m_1 - \omega_1 + 1, & -N_2 m_2 + 1, & 1, & 1 \\ 1, & & 0 & \end{matrix} \right). \tag{A.14}$$

Calculation for $\mathcal{C}_{\gamma_{t,[w]}}^{\text{low}}$

For the KBFC scheme, $\mathcal{C}_{\gamma_{t,[w]}}^{\text{low}}$ can be determined by evaluating $\mathbb{E}\{\ln(\gamma_{r,[w]})\} = \ln(\mathbb{a}_{[w]}) + \mathcal{A}$ and $\mathbb{E}\{\ln(\gamma_{d,[w]})\} = \ln(\mathbb{b}_{[w]}) + \mathcal{A} + \mathcal{D}$, where $\mathcal{A} = \mathbb{E}\{\ln(\|\mathbf{h}_1^{(K)}\|^2)\}$ and $\mathcal{D} = \mathbb{E}\{\ln(\|\mathbf{h}_2^{(K)}\|^2)\}$. Using the PDF of $\|\mathbf{h}_1^{(K)}\|^2$ and $\|\mathbf{h}_2^{(K)}\|^2$ for the KBFC scheme, and with the help of [53, Eq. (4.352.1)], $\mathcal{A}$ is given by (2.26) and $\mathcal{D}$ is given by

$$\mathcal{D} = \psi(N_2 m_2) - \ln\left(\frac{m_2}{\lambda_2}\right). \tag{A.15}$$

From (2.23), $\mathcal{C}_{\gamma_{t,[w]}}^{\text{low}}$ can be calculated as

$$\mathcal{C}_{\gamma_{t,[w]}}^{\text{low}} = \frac{1}{2} \log_2 \left(1 + e^{(\ln(\mathbb{a}_{[w]}) + \mathcal{A})} + e^{\left(\ln(\mathbb{b}_{[w]}) + \mathcal{A} + \psi(N_2 m_2) - \ln\left(\frac{m_2}{\lambda_2}\right)\right)} \right). \tag{A.16}$$

Substituting (A.9), (A.14), and (A.16) into (2.22), the analytical expression for the ergodic capacity of the KBFC scheme can be obtained.

A.2.2 Ergodic capacity for the KBSC scheme

According to the similar steps as in Appendix A.2.1, and using the PDF and CDF of $\|\mathbf{h}_1^{(K)}\|^2$ and $\|\mathbf{h}_2^{(K)}\|^2$ for the KBSC scheme given in Appendix A.1.2, the analytical

expressions of $\mathcal{C}_{\gamma_{r,[w]}}$, $\mathcal{C}_{\gamma_{d,[w]}}$, and $\mathcal{C}^{\text{low}}_{\gamma_{t,[w]}}$ for the KBSC scheme can be respectively expressed as follows:

$$\mathcal{C}_{\gamma_{r,[w]}} = \frac{1}{2\ln 2}\sum_{i=0}^{N_1m_1-1}\frac{1}{i!}\left(\frac{m_1}{\mathtt{a}_{[w]}\lambda_1}\right)^i e^{\frac{m_1}{\mathtt{a}_{[w]}\lambda_1}}\Gamma(i+1)\Gamma\left(-i,\frac{m_1}{\mathtt{a}_{[w]}\lambda_1}\right), \tag{A.17}$$

$$\begin{aligned}\mathcal{C}_{\gamma_{d,[w]}} = {} & \frac{1}{2\ln 2}\sum_{n=0}^{L-K}\sum_{\sum_{j=0}^{N_2m_2-1}p_j^{(2)}=K+n-1}\frac{(-1)^nL!}{(L-K)!(K-1)!\Gamma(N_1m_1)\Gamma(N_2m_2)} \\ & \times\frac{1}{(K+n)^{N_2m_2+\omega_2}}\binom{L-K}{n}\binom{K+n-1}{p_0^{(2)},\ldots,p_{N_2m_2-1}^{(2)}}\left(\prod_{j=0}^{N_2m_2-1}\left(\frac{1}{j!}\right)^{p_j^{(2)}}\right) \\ & \times G_{4,2}^{1,4}\left(\frac{\mathtt{b}_{[w]}\lambda_1\lambda_2}{m_1m_2(K+n)}\middle|\begin{matrix}-N_1m_1+1, & -N_2m_2-\omega_2+1, & 1, & 1\\ 1, & 0 & & \end{matrix}\right),\end{aligned} \tag{A.18}$$

$$\begin{aligned}\mathcal{C}^{\text{low}}_{\gamma_{t,[w]}} = {} & \frac{1}{2}\log_2\Bigg(1+e^{\left(\ln(\mathtt{a}_{[w]})+\psi(N_1m_1)-\ln\left(\frac{m_1}{\lambda_1}\right)\right)} \\ & +e^{\left(\ln(\mathtt{b}_{[w]})+\psi(N_1m_1)-\ln\left(\frac{m_1}{\lambda_1}\right)+\mathcal{B}\right)}\Bigg),\end{aligned} \tag{A.19}$$

where $\mathcal{B} = \mathbb{E}\{\ln(\|\mathbf{h}_1^{(K)}\|^2)\}$ given by (2.27).

Substituting (A.17), (A.18), and (A.19) into (2.22), the analytical expression for the ergodic capacity of the KBSC scheme can be obtained.

Appendix B

Proofs in Chapter 3

B.1 Proof of Proposition 3.1

As shown (3.17), when $\mathbb{a}^w \leqslant 0$ (i.e., $\kappa_{AF}^2 \geqslant \frac{1}{\gamma}$), $\mathcal{P}_{out,low}^w(\gamma) = 1$; and when $\mathbb{a}^w > 0$ (i.e. $\kappa_{AF}^2 < \frac{1}{\gamma}$), $\mathcal{P}_{out,low}^w(\gamma)$ can be evaluated as

$$\mathcal{P}_{out,low}^w(\gamma) = 1 - \int_0^{+\infty} \left(1 - F_{\|\mathbf{h}_{2,b}\|^2}\left(\frac{1}{\hat{\mathbb{a}}^w t}\right)\right) f_{\|\mathbf{h}_{1,b}\|^2}\left(t + \frac{\mathbb{b}^w}{\hat{\mathbb{a}}^w}\right) dt, \tag{B.1}$$

where $t = x - \frac{\mathbb{b}^w}{\hat{\mathbb{a}}^w}$.

B.1.1 Calculation of $\mathcal{P}_{out,low}^{w,1}$

In the PRS–1 scheme, the PDF of $\|\mathbf{h}_{1,b}\|^2$ and the CDF of $\|\mathbf{h}_{2,b}\|^2$ respectively follow (3.4) and (3.3). Using (A.6), $\mathcal{P}_{\text{out,low}}^{w,1}(\gamma)$ can be calculated as

$$\mathcal{P}_{\text{out,low}}^{w,1}(\gamma) = 1 - \sum_{l=0}^{N_1-1}\sum_{j=0}^{N_2-1}\sum_{u=0}^{K-1}\sum_{(p_0^{(1)}+\ldots+p_{N_1-1}^{(1)}=u)}\sum_{q=0}^{\omega_1}\frac{(-1)^u K e^{-\frac{(u+1)\mathbb{b}^w}{\lambda_1 \mathbb{a}^w}}}{j!\Gamma(N_1)\lambda_1^{N_1+\omega_1}(\mathbb{b}^w\lambda_2)^j}$$
$$\times \binom{N_1-1}{l}\binom{K-1}{u}\binom{u}{p_0^{(1)},\ldots,p_{N_1-1}^{(1)}}\binom{\omega_1}{q}\left(\prod_{i=0}^{N_1-1}\left(\frac{1}{i!}\right)^{p_i^{(1)}}\right)$$
$$\times \left(\frac{\mathbb{b}^w}{\mathbb{a}^w}\right)^{N_1+j+\omega_1-l-q-1}\int_0^{+\infty} t^{l+q-j}e^{-\frac{1}{\lambda_2\mathbb{a}^w t}-\frac{(u+1)t}{\lambda_1}}dt. \tag{B.2}$$

Using [53, Eq. (3.471.9)], $\mathcal{P}_{\text{out,low}}^{w,1}(\gamma)$ can be formulated as given in (3.18).

B.1.2 Calculation of $\mathcal{P}_{out,low}^{w,2}$

In the PRS–2 scheme, the PDF of $\|\mathbf{h}_{1,b}\|^2$ and the CDF of $\|\mathbf{h}_{2,b}\|^2$ respectively follow (3.2) and (3.5). Following the same steps in Section B.1.1, we obtain (3.19).

B.2 Proof of Proposition 3.2

Because the calculation of the ergodic capacity involves solving the derivative of $\Xi(\gamma;\alpha_\epsilon,\beta_{\epsilon,w},\upsilon_\epsilon,\mu_{\epsilon,w})$ with respect to γ. Using [53, Eq. (8.486.14)] and some additional manipulations, we can obtain

$$\tfrac{d}{d\gamma}\Xi(\gamma;\alpha_\epsilon,\beta_{\epsilon,w},\upsilon_\epsilon,\mu_{\epsilon,w}) = \tfrac{(\alpha_\epsilon-\upsilon_\epsilon)\hat{\mu}_{\epsilon,w}}{2}\Xi(\gamma;\alpha_\epsilon-2,\beta_{\epsilon,w},\upsilon_\epsilon,\mu_{\epsilon,w})$$
$$-\hat{\mu}_{\epsilon,w}\Xi(\gamma;\alpha_\epsilon-1,\beta_{\epsilon,w},\upsilon_\epsilon-1,\mu_{\epsilon,w}) + ((\alpha_\epsilon-\upsilon_\epsilon)\kappa_{AF}^2-\hat{\beta}_{\epsilon,w})\Xi(\gamma;\alpha_\epsilon,\beta_{\epsilon,w},\upsilon_\epsilon,\mu_{\epsilon,w})$$
$$-2\kappa_{AF}^2\Xi(\gamma;\alpha_\epsilon+1,\beta_{\epsilon,w},\upsilon_\epsilon-1,\mu_{\epsilon,w}) + \tfrac{((\alpha_\epsilon-\upsilon_\epsilon)\kappa_{AF}^2-4\hat{\beta}_{\epsilon,w})\kappa_{AF}^2}{2\hat{\mu}_{\epsilon,w}}\Xi(\gamma;\alpha_\epsilon+2,\beta_{\epsilon,w},\upsilon_\epsilon,\mu_{\epsilon,w})$$
$$-\tfrac{\kappa_{AF}^4}{\hat{\mu}_{\epsilon,w}}\Xi(\gamma;\alpha_\epsilon+3,\beta_{\epsilon,w},\upsilon_\epsilon-1,\mu_{\epsilon,w}) - \tfrac{\hat{\beta}_{\epsilon,w}\kappa_{AF}^4}{\hat{\mu}_{\epsilon,w}^2}\Xi(\gamma;\alpha_\epsilon+4,\beta_{\epsilon,w},\upsilon_\epsilon,\mu_{\epsilon,w}). \tag{B.3}$$

Substituting (B.3) into $\Upsilon(\alpha_\epsilon,\beta_{\epsilon,w},\upsilon_\epsilon,\mu_{\epsilon,w})$, Lemma 3.2 can be proved.

Appendix C

Proofs in Chapter 4

C.1 Proof of Proposition 4.1

Let $x_1, \ldots, x_N$ be N exponential RVs with a rate parameter λ. The PDF, $f(x;\lambda)$, and CDF, $F(x;\lambda)$, of $x_n, 1 \leqslant n \leqslant N$, are respectively given by (1.2) and (1.3). The CDFs of $Y = \max\{x_1, \ldots, x_N\}$ and $Z = \sum_{n=1}^{N} x_n$ are respectively given by

$$F_Y(x;\lambda,N) = F(x;\lambda)^N = 1 + \sum_{n=1}^{N} \binom{N}{n} (-1)^n e^{-n\lambda x}, \tag{C.1}$$

$$F_Z(x;\lambda,N) = 1 - e^{-\lambda x} \sum_{n=0}^{N-1} \frac{(\lambda x)^n}{n!}. \tag{C.2}$$

Next, we rewrite (4.12) as

$$\text{SOP} = 1 - \int_{\bar{x}_1}^{+\infty} \left(1 - F_{X_1}\left(\tfrac{\beta-1}{\zeta(1-\theta)\rho_s \Xi(x;\beta)}; \lambda_1, N\right)\right) f_{X_2}(x;\lambda_2)\, dx. \tag{C.3}$$

where $F_{X_1}(x;\lambda_1,N)$ and $f_{X_2}(x;\lambda_2)$ are the CDF of X_1 and the PDF of X_2, respectively.

C.1.1 Calculation for $\mathbf{SOP_{RAS}}$

Replacing $F_{X_1}(x;\lambda_1,N)$ and $f_{X_2}(x;\lambda_2)$ in (C.3) with $F(x;\lambda_1)$ and $f(x;\lambda_2)$, respectively, we obtain (4.13).

C.1.2 Calculation for $\mathbf{SOP_{TAS}}$

Replacing $F_{X_1}(x;\lambda_1,N)$ and $f_{X_2}(x;\lambda_2)$ in (C.3) with $F_Y(x;\lambda_1,N)$ and $f(x;\lambda_2)$, respectively, we obtain (4.14).

C.1.3 Calculation for $\mathbf{SOP_{MRT}}$

Replacing $F_{X_1}(x;\lambda_1,N)$ and $f_{X_2}(x;\lambda_2)$ in (C.3) with $F_Z(x;\lambda_1,N)$ and $f(x;\lambda_2)$, respectively, we obtain (4.15).

Finally, Proposition 4.1 is proved.

C.2 Proof of Proposition 4.2

C.2.1 Calculation for case of perfect CSI ($\zeta = 1$)

In this case, we have $\mu = 1, \Xi(x;\beta) \approx \frac{x}{x+\kappa}$, and $\bar{x}_1 \approx \sqrt{\frac{\beta}{\eta\theta\rho_d}}$. Therefore, (4.12) can be approximated as

$$\mathrm{SOP} = 1 - \Pr\left(X_1 > \bar{x}_3 | X_2 > \bar{x}_1\right) \approx F_{X_2}\left(\bar{x}_1;\lambda_2\right), \tag{C.4}$$

where $\bar{x}_3 = \frac{(\beta-1)}{(1-\theta)\rho_s}\left(1+\frac{\kappa}{X_2}\right)$, and the approximation in (C.4) is obtained due to the fact that $\lim\limits_{(\rho_s,\rho_d)\to(\infty,\infty)} \frac{\bar{x}_3}{\bar{x}_1} = 0$.

Using the series representation of the exponential function given in [53, Eq. (1.211.1)], we can prove (4.16).

C.2.2 Calculation for case of perfect CSI ($0 < \zeta < 1$)

In this case, we have $\mu \approx \mu_0 := (1-\zeta)(1-\theta)\frac{\rho_s}{\lambda_1}$ and $\Xi(x;\beta) \approx \frac{1}{\mu} - \frac{\beta}{(1-\theta)\rho_d X_2 + \mu}$. Therefore, $\Xi(x;\beta)^{-1}$ can be approximated by

$$\frac{1}{\Xi(x;\beta)} \approx \mu\left(1 + \frac{(1-\zeta)\omega\beta}{\lambda_1(X_2 - \bar{x}_2)}\right). \tag{C.5}$$

Then, the asymptotic functions for the SOP are calculated by

$$\begin{aligned}\mathrm{SOP}^{\infty} &= 1 - \Pr\left(X_1 > \tfrac{\bar{x}_2}{\omega\zeta}\left(1 + \tfrac{(1-\zeta)\omega\beta}{\lambda_1(X_2-\bar{x}_2)}\right) | X_2 > \bar{x}_2\right) \\ &= 1 - \int_{\bar{x}_2}^{\infty}\left(1 - F_{X_1}\left(\tfrac{\bar{x}_2}{\omega\zeta}\left(1 + \tfrac{(1-\zeta)\omega\beta}{\lambda_1(x-\bar{x}_2)}\right); \lambda_1, N\right)\right) f_{X_2}(x;\lambda_2)\, dx. \end{aligned} \tag{C.6}$$

Let us define $t = x - \bar{x}_2$, (C.6) can be rewritten as

$$\mathrm{SOP}^{\infty} = 1 - \int_{0}^{\infty}\left(1 - F_{X_1}\left(\tfrac{\bar{x}_2}{\omega\zeta}\left(1 + \tfrac{(1-\zeta)\omega\beta}{\lambda_1 t}\right); \lambda_1, N\right)\right) f_{X_2}(t + \bar{x}_2;\lambda_2)\, dt. \tag{C.7}$$

Calculation for $\mathbf{SOP}^{\infty}_{\mathbf{RAS}}$

Replacing $F_{X_1}(x;\lambda_1,N)$ and $f_{X_2}(x;\lambda_2)$ in (C.7) with $F(x;\lambda_1)$ and $f(x;\lambda_2)$, respectively, we have

$$\mathrm{SOP}^{\infty} = 1 - \lambda_2 e^{-\frac{\lambda_1\bar{x}_2}{\omega\zeta} - \lambda_2\bar{x}_2}\int_{0}^{\infty} e^{-\frac{\bar{x}_2(1-\zeta)\beta}{\zeta t} - \lambda_2 t} dt. \tag{C.8}$$

With the help of [53, Eq. (3.471.9)], (C.8) can be expressed as (4.17).

Calculation for $\mathbf{SOP}_{\mathbf{TAS}}^{\infty}$

Replacing $F_{X_1}(x;\lambda_1,N)$ and $f_{X_2}(x;\lambda_2)$ in (C.7) with $F_Y(x;\lambda_1,N)$ and $f(x;\lambda_2)$, respectively, and using the same step in the calculation for $\mathrm{SOP}_{\mathrm{RAS}}^{\infty}$, we obtain (4.18).

Calculation for $\mathbf{SOP}_{\mathbf{MRT}}^{\infty}$

Replacing $F_{X_1}(x;\lambda_1,N)$ and $f_{X_2}(x;\lambda_2)$ in (C.7) with $F_Z(x;\lambda_1,N)$ and $f(x;\lambda_2)$, respectively, and using the same step in the calculation for $\mathrm{SOP}_{\mathrm{RAS}}^{\infty}$, we obtain (4.19).

Finally, Proposition 4.2 is proved.

C.3 Proof of Proposition 4.3

C.3.1 Calculation for the RAS scheme

Using the PDFs of X_1 and X_2 for the RAS scheme given by $f(x;\lambda_1)$ and $f(x;\lambda_2)$, respectively, and [53, Eq.(4.352.1)], $\mathcal{J}_1$ and $\mathcal{J}_2$ for the RAS scheme are calculated as

$$\mathcal{J}_1^{\mathrm{RAS}} = \Psi(1) - \ln(\lambda_1), \tag{C.9}$$

$$\mathcal{J}_2^{\mathrm{RAS}} = \Psi(1) - \ln(\lambda_2) \tag{C.10}$$

Moreover, using the PDFs of X_2 and [53, Eq.(4.337.1)], $\mathcal{J}_3$ for the RAS scheme is calculated as

$$\mathcal{J}_3^{\mathrm{RAS}} = \ln(\kappa) - e^{\frac{\lambda_2\kappa}{\mu}} Ei\left(-\tfrac{\lambda_2\kappa}{\mu}\right). \tag{C.11}$$

Substituting (C.9), (C.10) and (C.11) into (4.22) yields (4.23).

C.3.2 Calculation for the TAS scheme

According to [94], the PDF of Y defined in Appendix A is given by

$$f_Y(x;\lambda,N) = Nf(x;\lambda)\,F(x;\lambda)^{N-1}. \tag{C.12}$$

Using the PDF of X_1 for the TAS scheme given by $f_Y(x;\lambda_1,N)$ and [53, Eq.(4.352.1)], $\mathcal{J}_1$ for the TAS scheme is calculated as

$$\mathcal{J}_1^{\mathrm{TAS}} = N\sum_{n=0}^{N-1}\binom{N-1}{n}\frac{(-1)^n}{n+1}\left(\Psi(1) - \ln\left((n+1)\,\lambda_1\right)\right). \tag{C.13}$$

Using the fact that $N\sum_{n=0}^{N-1}\binom{N-1}{n}\frac{(-1)^n}{(n+1)} = 1$, we can rewrite (C.13) as

$$\mathcal{J}_1^{\mathrm{TAS}} = \Psi(1) - N\sum_{n=0}^{N-1}\binom{N-1}{n}\frac{(-1)^n}{n+1}\ln\left((n+1)\,\lambda_1\right). \tag{C.14}$$

Because $\mathcal{J}_2$ and $\mathcal{J}_3$ for the TAS scheme are the same as for the RAS scheme, (4.24) is obtained by substituting (C.10), (C.11), and (C.14) into (4.22).

C.3.3 Calculation for the MRT scheme

The PDF of Z is given by

$$f_Z(x;\lambda,N) = \frac{\lambda^N x^{N-1}}{\Gamma(N)}e^{-\lambda x}. \tag{C.15}$$

Using the PDF of X_1 for the MRT scheme given by $f_Z(x;\lambda_1,N)$ and [53, Eq.(4.352.1)], $\mathcal{J}_1$ for the MRT scheme is calculated as

$$\mathcal{J}_1^{\mathrm{MRT}} = \psi(N) - \ln(\lambda_1). \tag{C.16}$$

Because $\mathcal{J}_2$ and $\mathcal{J}_3$ for the MRT scheme are the same as for the RAS scheme, (4.25) is obtained by substituting (C.10), (C.11), and (C.16) into (4.22).

C.4 Proof of Proposition 4.4

From (4.7), the PDF of γ_r is calculated as

$$F_{\gamma_r}(\gamma) = \Pr(\gamma_r < \gamma) = \int_0^\infty F_{X_1}\left(\tfrac{\gamma((1-\theta)\rho_d x+\mu)}{\zeta(1-\theta)\rho_s}; \lambda_1, N\right) f_{X_2}(x;\lambda_2)\, dx. \tag{C.17}$$

C.4.1 Calculation for the RAS scheme

Replacing $F_{X_1}(x;\lambda_1,N)$ and $f_{X_2}(x;\lambda_2)$ in (C.17) with $F(x;\lambda_1)$ and $f(x;\lambda_2)$, respectively, (C.17) can be expressed as

$$F_{\gamma_r}(\gamma) = 1 - \left(\frac{\lambda_1\gamma}{\lambda_2\zeta\omega} + 1\right)^{-1} e^{-\frac{\lambda_1\gamma\mu}{\zeta(1-\theta)\rho_s}}. \tag{C.18}$$

Substituting (C.17) into (4.26), we have the following:

$$\bar{\mathcal{C}}_r = \frac{1}{\ln(2)} \int_0^\infty \left(\tfrac{\lambda_1\gamma}{\lambda_2\zeta\omega} + 1\right)^{-1} (1+\gamma)^{-1} e^{-\frac{\lambda_1\gamma\mu}{\zeta(1-\theta)\rho_s}} d\gamma. \tag{C.19}$$

In the case of $\lambda_1 \neq \lambda_2\zeta\omega$, $\left(\frac{\lambda_1\gamma}{\lambda_2\zeta\omega} + 1\right)^{-1}(1+\gamma)^{-1}$ can be expressed as $\left(1 - \frac{\lambda_1}{\lambda_2\zeta\omega}\right)^{-1} \times \left((\gamma+1)^{-1} - \left(\gamma + \frac{\lambda_2\zeta\omega}{\lambda_1}\right)^{-1}\right)$. Then, using [53, Eq.(3.383.10)], we obtain (4.27). In the case of $\lambda_1 = \lambda_2\zeta\omega$, we obtain (4.28) with the help of [53, Eq. (3.353.2)].

C.4.2 Calculation for the TAS scheme

The result for the TAS scheme can be obtained by replacing $F_{X_1}(x;\lambda_1,N)$ and $f_{X_2}(x;\lambda_2)$ in (C.17) with $F_Y(x;\lambda_1,N)$ and $f(x;\lambda_2)$, respectively, and using the same step as in Appendix C.4.1.

C.4.3 Calculation for the MRT scheme

Replacing $F_{X_1}(x;\lambda_1,N)$ and $f_{X_2}(x;\lambda_2)$ in (C.17) with $F_Z(x;\lambda_1,N)$ and $f(x;\lambda_2)$, respectively, and using [53, Eq.(8.350.2)], (C.17) can be expressed as

$$\begin{aligned} F_{\gamma_r}(\gamma) =& 1-\lambda_2 e^{-\frac{\lambda_1\mu\gamma}{\zeta(1-\theta)\rho_s}} \sum_{n=0}^{N-1} \frac{1}{n!}\left(\frac{\lambda_1\gamma}{\zeta\omega}\right)^n \\ & \times \sum_{k=0}^{n} \binom{n}{k} \left(\frac{\mu}{(1-\theta)\rho_d}\right)^{n-k} \frac{\Gamma(k+1)}{\left(\frac{\lambda_1\gamma}{\zeta\omega}+\lambda_2\right)^{k+1}}. \end{aligned} \tag{C.20}$$

Substituting (C.20) into (4.26), we have the following:

$$\begin{aligned} \bar{\mathcal{C}}_r =& \frac{\lambda_2}{\ln(2)} \sum_{n=0}^{N-1} \frac{1}{n!}\left(\frac{\lambda_1}{\zeta\omega}\right)^n \sum_{k=0}^{n} \binom{n}{k} \left(\frac{\mu}{(1-\theta)\rho_d}\right)^{n-k} \\ & \times \Gamma(k+1) \int_0^{\infty} \gamma^n \mathcal{I}(\gamma)\, e^{-\frac{\lambda_1\mu\gamma}{\zeta(1-\theta)\rho_s}} d\gamma, \end{aligned} \tag{C.21}$$

where $\mathcal{I}(\gamma) = (1+\gamma)^{-1}\left(\frac{\lambda_1}{\zeta\omega}\gamma+\lambda_2\right)^{-k-1}$.

In the case of $\lambda_1 \neq \lambda_2\zeta\omega$, $\mathcal{I}(\gamma)$ can be decomposed using partial fraction decomposition as follows.

$$\mathcal{I}(\gamma) = \frac{A_0}{(1+\gamma)} + \sum_{i=1}^{k+1} \frac{A_i}{\left(\frac{\lambda_1}{\zeta\omega}\gamma+\lambda_2\right)^i}. \tag{C.22}$$

Substituting (C.22) into (C.21) and using [53, Eq.(3.383.10) and Eq.(9.211.4)], we obtain (4.31).

In the case of $\lambda_1 = \lambda_2\zeta\omega$, $\mathcal{I}(\gamma) = \left(\frac{\zeta\omega}{\lambda_1}\right)^{k+1}(\gamma+1)^{-k-2}$. Then, with the help of [53, Eq. (9.211.4)], we obtain (4.32).

Appendix D

Proofs in Chapter 5

D.1 Proof of Proposition 5.1

We first study the CDF and PDF of γ_e. The CDF of γ_e can be computed as

$$F_{\gamma_e}(y) = \Pr\left(\frac{\rho_s Y_1}{\rho_d Y_2 + 1} < y\right) = \int_0^{+\infty} F_{Y_1}\left(\frac{y(\rho_d y_2 + 1)}{\rho_s}\right) f_{Y_2}(y_2)\, dy_2. \tag{D.1}$$

Using the PDF and CDF of the exponential distribution, (D.1) is expressed as

$$F_{\gamma_e}(y) = 1 - \frac{1}{\beta_Y\left(y + \beta_Y^{-1}\right)} e^{-\frac{y\lambda_{y_1}}{\rho_s}}. \tag{D.2}$$

Then, the PDF of γ_e can be formulated as

$$f_{\gamma_e}(y) = \left(\frac{\lambda_{Y_2}}{\rho_d\left(y + \beta_Y^{-1}\right)} + \frac{1}{\beta_Y\left(y + \beta_Y^{-1}\right)^2}\right) e^{-\frac{y\lambda_{Y_1}}{\rho_s}}. \tag{D.3}$$

Next, we rewrite (5.12) as

$$\begin{aligned} P_{\text{sec},2} &= \int_{\bar{x}_1}^{+\infty} f_{X_2}(x_2) \int_{\Xi_2(x_2)}^{+\infty} f_{\gamma_e}(y) \int_{\frac{\beta-1}{(1-\theta)\rho_s \Xi_1(x_2)}}^{\frac{\beta y+\beta-1}{(1-\theta)\rho_s}\left(1+\frac{\kappa}{x_2}\right)} f_{X_1}(x_1) dx_1 dx_2 dy \\ &= \underbrace{\int_{\bar{x}_1}^{+\infty} f_{X_2}(x_2) e^{-\frac{\lambda_{X_1}(\beta-1)}{(1-\theta)\rho_s \Xi_1(x_2)}} dx_2 \int_{\Xi_2(x_2)}^{+\infty} f_{\gamma_e}(y) dy}_{P_{\text{sec},2,1}} \\ &\quad - \underbrace{\int_{\bar{x}_1}^{+\infty} f_{X_2}(x_2) \int_{\Xi_2(x_2)}^{+\infty} f_{\gamma_e}(y) e^{-\lambda_{X_1}\frac{\beta(y+1)-1}{(1-\theta)\rho_s}\left(1+\frac{\kappa}{x_2}\right)} dy dx_2}_{P_{\text{sec},2,2}}. \end{aligned} \tag{D.4}$$

Substituting the PDF of γ_e into $P_{\text{sec},2,2}$, while letting $u = y - \Xi_2(x_2)$ and using [53, Eq. (3.352.4) and Eq. (3.353.3)], $P_{\text{sec},2,2}$ can be calculated as

$$\begin{aligned} P_{\text{sec},2,2} &= \int_{\bar{x}_1}^{+\infty} f_{X_2}(x_2) \frac{1}{\beta_Y \Xi_2(x) + 1} e^{-\frac{\lambda_{X_1}(\beta-1)}{(1-\theta)\rho_s \Xi_1(x)} - \frac{\lambda_{Y_1}\Xi_2(x)}{\rho_s}} dx_2 \\ &\quad + \int_{\bar{x}_1}^{+\infty} f_{X_2}(x_2) \frac{\beta\lambda_{X_1}}{\beta_Y(1-\theta)\rho_s} \left(1+\frac{\kappa}{x}\right) e^{\frac{\lambda_{Y_1}}{\beta_Y \rho_s} + \frac{\lambda_{X_1}}{(1-\theta)\rho_s}\left(\frac{\beta}{\beta_Y}-\beta+1\right)\left(1+\frac{\kappa}{x}\right)} \\ &\quad \times Ei\left(-\frac{\beta_Y \Xi_2(x)+1}{\beta_Y \rho_s}\left(\lambda_{Y_1} + \frac{\beta\lambda_{X_1}}{(1-\theta)}\left(1+\frac{\kappa}{x}\right)\right)\right) dx_2. \end{aligned} \tag{D.5}$$

We use the relation $\frac{\beta-1}{\Xi_1(x)} = \left(1+\frac{\kappa}{x}\right)(\beta\Xi_2(x) + \beta - 1)$ to simplify the first element of (D.5). After some manipulation, we can show that the first element of (D.5) is equal to $P_{\text{sec},2,1}$. Finally, $P_{\text{sec},2}$ can be formulated as shown in (5.13).

D.2 Proof of Proposition 5.2

In the high-power scenario, i.e., $(P_s, P_d) \to (\infty, \infty)$, we have the following approximations: $\bar{x}_1 \approx \bar{x}_0, \bar{x}_2 \approx \bar{x}_0, \Xi_1(x) \approx \frac{x}{x+\kappa}$ and $\lim_{(P_s,P_d)\to(\infty,\infty)} \bar{x}_0 \to 0^+$.

D.2.1 High–power approximation for $P_{\mathbf{sec,1}}$

$P_{\text{sec,1}}$ can be approximated as

$$P_{\text{sec,1,HP}} \approx \Pr\left(X_2 < \bar{x}_0\right) + \Pr\left(X_1 < \frac{\beta-1}{(1-\theta)\,\rho_s}\left(1+\frac{\kappa}{X_2}\right)|X_2 > \bar{x}_0\right)$$
$$\approx 1 - e^{-\lambda_{X_2}\bar{x}_0} + \int_{\bar{x}_0}^{+\infty} \gamma\left(1, \frac{\lambda_{X_1}(\beta-1)}{(1-\theta)\,\rho_s}\left(1+\frac{\kappa}{X_2}\right)\right)\lambda_{X_2} e^{-\lambda_{X_2}x_2} dx_2. \quad \text{(D.6)}$$

By substituting the asymptotic expansion of the incomplete gamma function [53, Eq. (8.354.2)] and neglecting the higher–order terms, (D.6) can approximated as

$$P_{\text{sec,1,HP}} \approx 1 - e^{-\lambda_{X_2}\bar{x}_0} + \int_{\bar{x}_0}^{+\infty} \frac{\lambda_{X_1}(\beta-1)}{(1-\theta)\,\rho_s}\left(1+\frac{\kappa}{X_2}\right)\lambda_{X_2} e^{-\lambda_{X_2}x_2} dx_2. \quad \text{(D.7)}$$

With the help of [53, Eq. (3.351.5)], (D.7) can be calculated as

$$P_{\text{sec,1,HP}} \approx 1 + \left(\frac{\lambda_{X_1}(\beta-1)}{(1-\theta)\,\rho_s} - 1\right) e^{-\lambda_{X_2}\bar{x}_0} - \frac{\lambda_{X_1}\lambda_{X_2}(\beta-1)\,\kappa}{(1-\theta)\,\rho_s} Ei\left(-\lambda_{X_2}\bar{x}_0\right). \quad \text{(D.8)}$$

D.2.2 High–power approximation for $P_{\mathbf{sec,2}}$

Using (D.4), $P_{\text{sec,2}}$ can be approximated as

$$P_{\text{sec,2,HP}} \approx \int_{\bar{x}_0}^{+\infty} f_{X_2}(x_2) \int_0^{+\infty} f_{\gamma_e}(y) \int_{\frac{\beta-1}{(1-\theta)\rho_s}\left(1+\frac{\kappa}{x_2}\right)}^{\frac{\beta y+\beta-1}{(1-\theta)\rho_s}\left(1+\frac{\kappa}{x_2}\right)} f_{X_1}(x_1) dx_1 dx_2 dy$$
$$\approx \int_{\bar{x}_0}^{+\infty} f_{X_2}(x_2)\, e^{-\lambda_{X_1}\frac{\beta-1}{(1-\theta)\rho_s}\left(1+\frac{\kappa}{x_2}\right)} \int_0^{+\infty} f_{\gamma_e}(y)\left(1 - e^{-\frac{\lambda_{X_1}\beta y}{(1-\theta)\rho_s}\left(1+\frac{\kappa}{x_2}\right)}\right) dy dx_2. \quad \text{(D.9)}$$

Substituting (D.3) into (D.9) and applying [53, Eq. (3.352.4), Eq. (3.353.3) and

Eq. (8.214.1)], (D.9) can be approximated as

$$P_{\text{sec,2,HP}} \approx \frac{-\beta\lambda_{X_1}\lambda_{X_2}}{(1-\theta)\,\rho_s\beta_Y} e^{\frac{\lambda_{Y_1}}{\rho_s\beta_Y}+\frac{1}{(1-\theta)\rho_s}\left(\frac{\beta\lambda_{X_1}}{\beta_Y}-\lambda_{X_1}(\beta-1)\right)} \int_{\bar{x}_0}^{+\infty} \left(1+\frac{\kappa}{x_2}\right) \times e^{-\lambda_{X_2}x_2} \ln\left(\underbrace{-\frac{\lambda_{Y_1}}{\rho_s\beta_Y} - \frac{\beta\lambda_{X_1}}{(1-\theta)\,\rho_s\beta_Y}}_{I_1} - \underbrace{\frac{\beta\lambda_{X_1}\kappa}{(1-\theta)\,\rho_s\beta_Y x_2}}_{I_2} \right) dx_2. \tag{D.10}$$

Because function inside the integral in (D.10) reaches very high values at low x_2 values, the approximation of $P_{\text{sec,2,HP}}$ is studied at low x_2 values. Using L'Hospital's Rule, it is easy to show that I_2 is dominant over I_1 as $x_2 \to \bar{x}_0$. Then, applying [53, Eq. (4.337.1) and Eq. (3.351.5)] to (D.10) yields

$$\begin{aligned} P_{\text{sec,2,HP}} \approx & \frac{\ln(\rho_s\bar{x}_0)\, e^{-\lambda_{X_2}\bar{x}_0} - Ei(-\lambda_{X_2}\bar{x}_0)}{\lambda_{X_2}} - \kappa \ln(\rho_s)\, Ei(-\lambda_{X_2}\bar{x}_0) \\ & + \kappa \int_{\bar{x}_0}^{+\infty} \frac{1}{x_2} e^{-\lambda_{X_2}x_2} \ln(x_2)\, dx_2. \end{aligned} \tag{D.11}$$

With the help of Mathematica, (D.11) can rewritten as

$$\begin{aligned} P_{\text{sec,2,HP}} \approx & \frac{e^{-\lambda_{X_2}\bar{x}_0}\ln(\rho_s\bar{x}_0) - Ei(-\lambda_{X_2}\bar{x}_0)}{\lambda_{X_2}} - \kappa \ln(\rho_s\bar{x}_0)\, Ei(-\lambda_{X_2}\bar{x}_0) \\ & + \kappa G_{2,3}^{3,0}\left(\lambda_{X_2}\bar{x}_0\big|_{0,0,0}^{1,1}\right). \end{aligned} \tag{D.12}$$

Using (D.8) and (D.12), we can prove Proposition 5.2.

D.3 Proof of Proposition 5.3

Using Jensen's inequality for the convex function $f(x) = \log_2(1 + e^x)$, $\mathcal{C}_d^{\text{erg}}$ can be approximated as

$$\begin{aligned}\mathcal{C}_{\text{d}}^{\text{erg}} &= \mathbb{E}\left\{\log_2\left(1 + e^{\ln(\gamma_d)}\right)\right\} \approx \log_2\left(1 + e^{\mathbb{E}\{\ln(\gamma_{\text{d}})\}}\right) \\ &\approx \log_2\left(1 + e^{\ln((1-\theta)\rho_s)+\mathbb{E}\{\ln(X_1)\}+\mathbb{E}\{\ln(X_2)\}-\mathbb{E}\{\ln(X_2+\kappa)\}}\right). \end{aligned} \tag{D.13}$$

With the help of [53, Eq.(4.352.1)], $\mathbb{E}\{\ln(X_1)\}$ and $\mathbb{E}\{\ln(X_2)\}$ is calculated as

$$\mathbb{E}\{\ln(X_1)\} = \psi(1) - \ln(\lambda_{X_1}) \tag{D.14}$$

$$\mathbb{E}\{\ln(X_2)\} = \psi(1) - \ln(\lambda_{X_2}). \tag{D.15}$$

With the help of [53, Eq. (4.337.1)], $\mathbb{E}\{\ln(X_2 + \kappa)\}$ is calculated as

$$\mathbb{E}\{\ln(X_2 + \kappa)\} = \ln(\kappa) - e^{\lambda_{X_2}\kappa} Ei(-\lambda_{X_2}\kappa). \tag{D.16}$$

Substituting (D.14), (D.15), and (D.16) into (D.13) yields the desired result.

Appendix E

Proofs in Chapter 6

E.1 Proof of Proposition 6.1

The secrecy outage probability in (15) can be rewritten as

$$P_{\text{out,low}} = 1 - \Pr\left(\mathrm{a}X\Xi(Y;\gamma_{\text{th}}) > \gamma_{\text{th}} - 1\right). \tag{E.1}$$

Because $\Xi(Y;\gamma_{\text{th}}) \geqslant 0$ if and only if $y_1 \leqslant Y < \infty$, we can rewrite (E.1) as

$$P_{\text{out,low}} = 1 - \int_{y_1}^{\infty} \left(1 - F_X\left(\frac{\gamma_{\text{th}} - 1}{\mathrm{a}\Xi(y;\gamma_{\text{th}})}\right)\right) f_Y(y)\, dy. \tag{E.2}$$

E.1.1 Calculation for $P_{\text{out,low}}^{\text{KBFC}}$

Substituting $F_X(x)$ and $f_Y(y)$ for the KBFC scheme in to (E.2), and using [53, Eq. (8.356.3)], $P_{\text{out,low}}^{\text{KBFC}}$ can be expressed as

$$P_{\text{out,low}}^{\text{KBFC}} = 1 + \sum_{k=0}^{K-1} \sum_{\substack{n=0 \\ k+n\neq 0}}^{L-k} \binom{L}{k} \binom{L-k}{n} \frac{(-1)^n m_2^{N_2 m_2}}{\Gamma(N_2 m_2) \lambda_2^{N_2 m_2}} \times \int_{y_1}^{\infty} y^{N_2 m_2 - 1} \left(\frac{1}{\Gamma(N_1 m_1)} \Gamma\left(N_1 m_1, \frac{m_1(\gamma_{\text{th}} - 1)}{\lambda_1 \mathfrak{a} \Xi(y; \gamma_{\text{th}})} \right) \right)^{k+n} e^{-\frac{m_2 y}{\lambda_2}} dy. \quad \text{(E.3)}$$

Expressing $\Gamma(\alpha, x)$ as [53, Eq. (8.352.7)] and using the multinomial theorem [97, Eq. (26.4.9)] given by

$$(x_1 + \ldots + x_n)^u = \sum_{\|\mathbf{p}\|_1 = u} \binom{u}{\mathbf{p}} x_1^{p_1} \ldots x_n^{p_n}, \quad \text{(E.4)}$$

$P_{\text{out,low}}^{\text{KBFC}}$ can be expressed as in (16).

E.1.2 Calculation for $P_{\text{out,low}}^{\text{KBSC}}$

Using $F_X(x)$ and $f_Y(y)$ for the KBSC scheme, the expression for $P_{\text{out,low}}^{\text{KBSC}}$ can be achieved using similar calculation steps for $P_{\text{out,low}}^{\text{KBFC}}$.

E.2 Proof of Proposition 6.2

Because the exact analysis for (19) appears to be difficult, the high-power SOP is approached using the asymptotic formulas of $F_{\mathcal{X}}(x; m, \lambda)$ and $F_{\mathcal{X}^{(K)}}(x; m, \lambda)$ as $x \to 0^+$. Using the series representation of the incomplete gamma function [53, Eq. (8.354.1)] and the fact that $\lim_{x \to 0^+} \Gamma(\alpha, x) = \Gamma(\alpha)$, we yield the following asymptotic formulas:

$$\lim_{x \to 0^+} F_{\mathcal{X}}(x; m, \lambda) = \frac{1}{m!} \left(\frac{x}{\lambda} \right)^m \quad \text{(E.5)}$$

$$\lim_{x \to 0^+} F_{\mathcal{X}^{(K)}}(x; m, \lambda) = \binom{L}{K-1} \left(\frac{1}{m!} \left(\frac{x}{\lambda} \right)^m \right)^{L-K-1} \quad \text{(E.6)}$$

E.2.1 Calculation for $P_{\text{out,HPL}}^{\text{KBFC}}$

Because $\lim_{\mathbb{b}\to\infty} y_0 = \lim_{(\mathbb{a},\mathbb{b})\to(\infty,\infty)} x_0 = 0$, $\mathcal{J}_1$ in (19) can be approximated using the asymptotic formula of $F_Y(y)$ for the KBFC scheme as follows.

$$\mathcal{J}_1 \approx \frac{1}{(N_2 m_2)!}\left(\frac{m_2 y_0}{\lambda_2}\right)^{N_2 m_2}. \tag{E.7}$$

Using $f_Y(y)$ and the asymptotic formula of $F_X(x)$ for the KBFC scheme, $\mathcal{J}_2$ in (19) can be approximated by

$$\begin{aligned}\mathcal{J}_2 \approx &\binom{L}{K-1}\frac{(\mu_1 y_0^2)^{N_1 m_1 (L-K+1)}}{\Gamma\left(N_2 m_2\right)\Gamma(N_1 m_1+1)^{L-K+1}}\sum_{n=0}^{N_1 m_1 (L-K+1)}\binom{N_1 m_1 (L-K+1)}{n}\\ &\times\left(\frac{m_2 \mathbb{c}}{\lambda_2}\right)^n\left(\mathbb{1}\left(n<N_2 m_2\right)\mathcal{J}_{2,\mathrm{a}}+\mathbb{1}\left(n\geqslant N_2 m_2\right)\mathcal{J}_{2,\mathrm{a}}\right),\end{aligned} \tag{E.8}$$

where $\mathcal{J}_{2,\mathrm{a}} = \int_{m_2 y_0/\lambda_2}^{\infty} z_1^{N_2 m_2 - n - 1} e^{-z_1} dz_1$ and $z_1 = \frac{m_2 y}{\lambda_2}$. It can be seen that in the case of $n < N_2 m_2$, we have

$$\lim_{y_0\to 0^+}\mathcal{J}_{2,\mathrm{a}} = \Gamma\left(N_2 m_2 - n\right), \tag{E.9}$$

and in the case of $n \geqslant N_2 m_2$, $\mathcal{J}_{2,a}$ can be solved with help from [53, Eq. (3.351.4)] as follows.

$$\begin{aligned}\mathcal{J}_{2,\mathrm{a}} =&\frac{(-1)^{n-N_2 m_2+1}}{(n-N_2 m_2)!}Ei\left(-\frac{m_2 y_0}{\lambda_2}\right)+e^{-\frac{m_2 y_0}{\lambda_2}}\\ &\times\sum_{u=0}^{n-N_2 m_2-1}\frac{(-1)^u\left(n-N_2 m_2-u-1\right)!}{(n-N_2 m_2)!}\left(\frac{\lambda_2}{m_2 y_0}\right)^{n-N_2 m_2-u}.\end{aligned} \tag{E.10}$$

Using (E.7), (E.9) and (E.10), $P_{\text{out,HPL}}^{\text{KBFC}}$ can be expressed as in (6.19).

E.2.2 Calculation for $P_{\text{out,HPL}}^{\text{KBSC}}$

Using the asymptotic formula of $F_Y(x)$ and $F_X(x)$ for the KBSC scheme, and follows the same steps of E.2.1, $P_{\text{out,HPL}}^{\text{KBSC}}$ can be expressed as in (6.20).

E.3 Proof of Proposition 6.3

We can calculate $\mathcal{C}_{\text{erg,r}}$ as

$$\mathcal{C}_{\text{erg,r}} = \frac{1}{\ln(2)} \int_0^{+\infty} \frac{1 - F_{\gamma_\text{r}}(\gamma)}{1+\gamma} d\gamma, \tag{E.11}$$

where $F_{\gamma_r}(\gamma)$ is the CDF of γ_r. From (6), $F_{\gamma_r}(\gamma)$ can be calculated as

$$F_{\gamma_\text{r}}(\gamma) = \Pr\left(\frac{\mathbb{a}X}{\mathbb{b}Y+1} < \gamma\right) = \int_0^{+\infty} F_X\left(\frac{\gamma(\mathbb{b}y+1)}{\mathbb{a}}\right) f_Y(y)\, dy \tag{E.12}$$

Because $\mathcal{C}_{\text{erg,d}}$ does not admit closed form expressions, $\mathcal{C}_{\text{erg,d}}$ can be evaluated by its lower bound obtaining by using Jensen's inequality for a convex function $f(x) = \ln(1+e^{\ln(x)})$ as follows.

$$\mathcal{C}_{\text{erg,d,low}} = \log_2\left(1 + e^{\mathbb{E}\{\ln(\gamma_d)\}}\right), \tag{E.13}$$

From (9), (E.13) can be rewritten as

$$\mathcal{C}_{\text{erg,d,low}} = \log_2\left(1 + e^{\ln(\mathbb{a})+\mathcal{J}_3+\mathcal{J}_4-\mathcal{J}_5}\right), \tag{E.14}$$

where $\mathcal{J}_3 = \mathbb{E}\{\ln(X)\}$, $\mathcal{J}_4 = \mathbb{E}\{\ln(Y)\}$ and $\mathcal{J}_5 = \ln(\mathbb{c}) + \mathbb{E}\left\{\ln\left(\frac{Y}{\mathbb{c}}+1\right)\right\}$.

E.3.1 calculation for $F_{\gamma_r}^{\mathbf{KBFC}}(\gamma)$

Substituting $F_X(x)$ and $f_Y(y)$ for the KBFC scheme into (E.12), we have

$$F_{\gamma_\text{r}}(\gamma) = \int_0^{+\infty} F_{\mathcal{X}^{(K)}}\left(\frac{\gamma(\mathbb{b}y+1)}{\mathbb{a}}; N_1 m_1, \frac{\lambda_1}{m_1}\right) f_{\mathcal{X}}\left(y; N_2 m_2, \frac{\lambda_2}{m_2}\right) dy. \tag{E.15}$$

Using (1), (12), (E.4) and [53, Eq. (3.351.3)], (E.15) can be rewritten as

$$F_{\gamma_\text{r}}(\gamma) = \sum_{k=0}^{K-1}\sum_{n=0}^{L-k} \sum_{\left\|\mathbf{p}^{(1)}\right\|_1 = k+n} \sum_{u=0}^{\omega_1} \mathcal{I}_1\left(k, n, \mathbf{p}^{(1)}, u\right) \frac{\gamma^{\omega_1}}{(\gamma+\mu_3)^{N_2 m_2 + u}} e^{-\frac{m_1(k+n)\gamma}{\mathbb{a}\lambda_1}}. \tag{E.16}$$

E.3.2 Calculation for $\mathcal{C}_{\mathbf{erg,r}}^{\mathbf{KBFC}}$

Substituting (E.16) into (E.11), $\mathcal{C}_{\mathrm{erg,r}}^{\mathrm{KBFC}}$ can be calculated as

$$\mathcal{C}_{\mathrm{erg,r}}^{\mathrm{KBFC}} = -\sum_{k=0}^{K-1}\sum_{\substack{n=0\\k+n\neq 0}}^{L-k}\sum_{\left\|\mathbf{p}^{(1)}\right\|_1=k+n}\sum_{u=0}^{\omega_1}\frac{\mathcal{I}_1\left(k,n,\mathbf{p}^{(1)},u\right)}{\ln(2)}\int_0^{+\infty}\gamma^{\omega_1}\mathcal{J}_6\left(\gamma\right)e^{-\frac{m_1(k+n)\gamma}{\mathbb{a}\lambda_1}}d\gamma, \quad \text{(E.17)}$$

where $\mathcal{J}_6\left(\gamma\right) = (1+\gamma)^{-1}(\gamma+\mu_3)^{-N_2m_2-u}$.

Using the partial fraction expansion for $\mathcal{J}_6(\gamma)$, we have $\mathcal{J}_6\left(\gamma\right) = \frac{\mathcal{A}_0}{(\gamma+1)} + \sum_{j=1}^{N_2m_2+u}\frac{\mathcal{A}_j}{(\gamma+\mu_3)^j}$; then, applying [53, Eq. (3.383.10) and Eq. (9.211.4)] on (E.17), $\mathcal{C}_{\mathrm{erg,r}}^{\mathrm{KBFC}}$ can be expressed as in (6.25).

E.3.3 Calculation for $\mathcal{C}_{\mathbf{erg,d}}^{\mathbf{KBFC}}$

Using $f_X(x)$ for the KBFC scheme, (E.4) and [53, Eq. (4.352.1)], $\mathcal{J}_3$ can be calculated as in (6.26).

Similarly, $\mathcal{J}_4$ for the KBFC scheme can be calculated as $\mathcal{J}_{4,\mathrm{a}}$ given as (6.27).

Using $f_Y(y)$ for the KBFC scheme, $\mathcal{J}_5$ can be calculated as

$$\mathcal{J}_{5,\mathrm{a}} = \ln(\mathbb{c}) + \frac{1}{\Gamma\left(N_2m_2\right)}\int_0^{+\infty}\ln\left(\frac{\lambda_2}{\mathbb{c}m_2}z_2+1\right)z_2^{N_2m_2-1}e^{-z_2}dz_2. \quad \text{(E.18)}$$

where $z_2 = m_2y/\lambda_2$. With the help of [53, Eq. (4.337.5)], (E.18) can be rewritten as in (6.28).

Finally, $\mathcal{C}_{\mathrm{erg,d}}^{\mathrm{KBFC}}$ can be bounded below as

$$\mathcal{C}_{\mathrm{erg,d,low}}^{\mathrm{KBFC}} = \log_2\left(1+e^{\ln(\mathbb{a})+\mathcal{J}_{3,\mathrm{a}}+\mathcal{J}_{4,\mathrm{a}}-\mathcal{J}_{5,\mathrm{a}}}\right), \quad \text{(E.19)}$$

To this end, substituting (6.25) and (E.19) into (24), we can obtain the desired result.